Structural and Functional Investigations of Prokaryotic Heterodimeric ABC Exporters

Dissertation

zur

Erlangung der naturwissenschaftlichen Doktorwürde

(Dr. sc. nat.)

vorgelegt der

Mathematisch-naturwissenschaftlichen Fakultät

der

Universität Zürich

von

Michael Hohl

von

Wolfhalden (AR)

Promotionskomitee:

Prof. Dr. Markus G. Grütter (Vorsitz)

Prof. Dr. Raimund Dutzler

Prof. Dr. Ulrich Baumann

Zürich, 2013

Contents

Summary

Membrane proteins connect the cytoplasm of a cell with its environment and are essential for all living organisms. Their primary role is to transduce signals and to transport solutes across the lipid bilayer. The importance of membrane proteins is underscored by the fact that over 50 % of the drugs on the market target membrane-embedded proteins. Several families of membrane transporters confer multidrug resistance (MDR) by actively extruding a broad range of drugs such as antibiotics or anticancer substances out of the bacterial or cancer cell. MDR transporters belong to five superfamilies, namely ATP binding cassette (ABC) transporters, major facilitator superfamily (MFS) transporters, multidrug and toxic-compound extrusion (MATE) transporters, small multidrug resistance (SMR) transporters and resistance nodulation division (RND) transporters. In the course of this PhD thesis we focused on structural, functional and biochemical investigations of the ABC transporter family and especially on the subclass of heterodimeric, prokaryotic ABC exporters. ABC exporters minimally consist of four domains. Two nucleotide binding domains (NBDs) dimerize upon sandwiching of two molecules of ATP at their interface and couple this motion to two transmembrane domains (TMDs), which provide alternating access to substrates.

Membrane transporters are intrinsically flexible and rather unstable proteins and usually cannot be purified from natural sources due to low expression levels. For structural studies, membrane transporters need to be overexpressed and purified at the milligram scale as stable proteins. The goal of this thesis was to solve the structure of a heterodimeric ABC exporter, because of their medical relevance and because structural information about this subclass was not available so far. In Chapter 2, a funnel approach is described to identify and purify transporters that are amenable to x-ray crystallography. Initially, crystallization attempts with LmrCD were performed, a well-characterized heterodimeric ABC exporter conferring resistance to daunomycin and other drugs in *Lactococcus lactis*. However, no crystals of LmrCD were obtained presumably due to its limited stability. Therefore the sequence of LmrCD was used to search for a set of homologues. This set was analyzed using a peptide disorder prediction program. Based on this analysis, thirteen transporters were cloned, expressed and purified in *E. coli*. Seven homologues were identified that were expressed at sufficient yields. They exhibited high protein stability in limited tryptic proteolysis, eluted as monodisperse proteins in the size exclusion chromatography analysis and gave first diffracting crystals.

Chapter 3 describes the structure determination of the heterodimeric ABC exporter TM287/288 from *Thermotoga maritima*. Crystals of wild-type TM287/288 were obtained in the presence of the ATP analog AMP-PNP and belonged to the space group C2, containing one TM287/288 heterodimer per asymmetric unit. The structure was solved at 2.9 Å resolution by single-wavelength anomalous dispersion phasing. TM287/288 was crystallized in its inward-facing state with one AMP-PNP molecule bound to the degenerate catalytic site, which deviates from the consensus sequence in the same positions as the eukaryotic homologs CFTR and TAP1/2. In contrast to previous studies, it was found that the NBDs only partially separate and remain in contact through an interface involving the D-loop and the Walker A motif connecting the two ATP hydrolysis sites. Expression of TM287/288 in *L. lactis ΔlmrCD* partially restored daunomycin resistance and transport of the MDR substrate BCECF-AM was

monitored by fluorescence spectroscopy. Purified TM287/288 exhibited high ATPase activities which were stimulated by the addition of the MDR substrate Hoechst 33342 upon reconstitution of TM287/288 in proteoliposomes. The structure for TM287/288 describes the first heterodimeric ABC exporter with nonequal ATP binding sites at a molecular level and provides unprecedented insight into the mechanism of this medically important category of ABC transporters.

In Chapter 4 the structure of TM287/288 in its apo state devoid of bound nucleotides is presented. This structure allows for a detailed analysis of the structural changes associated with nucleotide binding to the degenerate ATPase site. Crystals belonged to the same space group as those used to solve the structure of TM287/288 with bound AMP-PNP and the structural differences were mainly located at the degenerate ATP binding site. These included the A-loop, which interacts through an aromatic residue with the adenine moiety of the bound nucleotide as well as in the Walker A motif which wraps around the γ-phosphate moiety. The NBDs were found to remain in molecular contact even in the absence of nucleotides. However, the NBD-NBD interaction mediated by the D-loop at the degenerate site appears weaker in the apo state than in the AMP-PNP bound state. Moreover, AMP-PNP binding at the degenerate site is sensed by the Walker B motif and structurally communicated to the D-loop of the consensus site, which establishes two hydrogen bonds with the opposite NBD via a conserved aspartate. Removal of the nucleotide results in the disruptions of these hydrogen bonds and a remodeling of the highly flexible consensus site D-loop. Comparisons of the nucleotide-free and AMP-PNP bound structures therefore provide unprecedented insights into the molecular communication between the asymmetric ATP binding sites of heterodimeric ABC exporters.

In Chapter 5 crystal structures of the isolated NBDs of TM287/288, NBD287 and NBD288, are presented. Numerous isolated NBDs of ABC exporters have been crystallized in the past and their structures provided important mechanistic insights. However, structural comparisons of NBDs crystallized in isolation and in the full-length context of ABC exporters are lacking. In contrast to full-length TM287/288, the isolated NBDs did not show ATPase activity, neither alone nor in a mixture of NBD287 and NBD288. Dimer formation between the two NBDs was not observed even in the presence of MgATP based on size exclusion chromatography and analytical ultracentrifugation experiments. This analysis revealed that the isolated NBDs show structural flexibility in regions where interdomain contacts are established in the full-length transporter. In particular, the degenerate ATPase site appears unstructured in isolated NBD287. In addition, density for the D-loop of NBD288, which strongly interacts via an extensive hydrogen network with NBD287, is missing. This analysis also suggests that interdomain interactions which are established in the full-length transporter are important for the formation of the degenerate ATP binding site.

Zusammenfassung

Membranproteine stellen eine Verbindung zwischen dem Zytoplasma einer Zelle und seiner Umgebung her, daher sind sie lebensnotwendig. Substanzen zu transportieren und Signale über die Zellmembran zu übertragen gehören zu ihren Hauptaufgaben. Ihre Wichtigkeit wird dadurch unterstrichen, dass über 50 % aller Medikamente auf dem Markt an Membranproteine binden. Mehrere Familien von Membranproteinen verleihen durch aktives Herauspumpen einer breiten Anzahl von Medikamenten, wie Antibiotika oder Krebsmedikamenten, aus Bakterien- oder Krebszellen sogenannte multispezifische Resistenz (MDR). MDR Transporter gehören einer von fünf Superfamilien an, den „ATP binding cassette“ (ABC) Transportern, den „major facilitator superfamily“ (MFS) Transportern, den „multidrug and toxic-compound extrusion“ (MATE) Transportern, den „small multidrug resistance“ (SMR) Transportern oder den „resistance nodulation division“ (RND) Transportern. Im Rahmen dieser Doktorarbeit beschränkte ich mich auf die strukturelle, funktionelle und biochemische Untersuchung der ABC Transporter Familie und im Speziellen der heterodimeren, prokaryotischen ABC Exporter. ABC Exporter sind aus mindestens vier Domänen aufgebaut. Die Bindung von zwei ATP Molekülen am „interface“ der Nukleotid-Bindedomänen (NBDs) führt zu deren Dimerisierung. Diese Bewegung wird an die Transmembrandomänen weitergeleitet, welche alternierenden Zugang von Substraten innerhalb oder ausserhalb der Zelle gewährleisten.

Membrantransporter sind intrinsisch flexible und unstabile Proteine und können wegen niedrigen Expressionsraten selten aus natürlichen Quellen aufgereinigt werden. Für strukturelle Untersuchungen müssen Membrantransporter daher rekombinant (z.B. in *Escherichia coli*) im Milligrammmassstab hergestellt und gereinigt werden. Das Ziel dieser Doktorarbeit war die Strukturaufklärung eines heterodimeren ABC Exporters. Dies einerseits, weil bis anhin keine Struktur eines solchen gelöst wurde und anderseits wegen deren hoher medizinischer Relevanz. In Kapitel 2 wird das Vorgehen beschrieben, wie ein geeigneter Transporter für die Strukturanalyse identifiziert wurde. Der Startpunkt für die Kristallisationsbemühungen war LmrCD, ein gut untersuchter heterodimerer ABC Exporter, welcher *Lactococcus lactis* Resistenz gegen Daunomycin und andere Antibiotika verleiht. Leider konnte LmrCD nicht kristallisiert werden, dies möglicherweise wegen dessen limitierter Stabilität. Daher wurde die Aminosäuresequenz von LmrCD verwendet, um homologe Proteine zu suchen, welche mit Hilfe eines Peptid-Stabilität Programms zusätzlich analysiert wurden. Basierend auf dieser Analyse wurden dreizehn Transporter kloniert, in *E. coli* exprimiert und gereinigt. Sieben Homologe konnten so identifiziert werden, die in genügender Menge exprimiert wurden, eine hohe Stabilität gegenüber limitiertem tryptischem Verdau aufwiesen, als monodisperse Proteine von der analytischen Gelfiltration eluierten und erste diffraktierende Kristalle ergaben.

Kapitel 3 beschreibt die Strukturaufklärung des heterodimeren ABC Exporters TM287/288 aus *Thermotoga maritima*. Kristalle von Wildtyp TM287/288 konnten in der Anwesenheit von AMP-PNP, einem ATP Analog, erhalten werden. Die Kristalle gehörten der Raumgruppe C2 an, mit einem TM287/288 Heterodimer pro asymmetrischer Einheit. Die Struktur konnte mit Hilfe von „single-wavelength anomalous dispersion“ Phasierung bei einer Auflösung von 2.9 Å gelöst werden. TM287/288 wurde in der „inward-facing“ Konformation mit nur einem an die degenerierte ATP-

Bindungsstelle gebundenen AMP-PNP Molekül kristallisiert. Diese degenerierte katalytische Bindungsstelle weicht in den gleichen Positionen der Aminosäuresequenz von der Konsensussequenz ab, wie auch die eukaryotischen Homologe CFTR und Tap1/2. Im Gegensatz zu früheren Studien konnten wir beobachten, dass sich die NBDs nur teilweise trennen und durch eine starke Interaktion zwischen dem D-loop und dem Walker A zusammengehalten werden. Expression von TM287/288 in *L. lactis ΔlmrCD* führte zu partieller Resistenz gegen Daunomycin. Des Weiteren konnte der Transport des MDR Substrates BCECF-AM mit Hilfe von Fluoreszenz Spektroskopie in TM287/288 überexprimierenden *L. lactis ΔlmrCD* Zellen nachgewiesen werden. Der gereinigte Transporter TM287/288 wies eine hohe ATPase Aktivität auf. Diese wurde zusätzlich durch das MDR Substrat Hoechst 33342 stimuliert, wenn der Transporter vorher in Proteoliposomen rekonstituiert wurde. Die Struktur von TM287/288 ist die erste Struktur eines heterodimeren ABC Exporters, welcher nichtidentische ATP Bindungsstellen aufweist. Sie erlaubt neue Einblicke in den Mechanismus dieser medizinisch wichtigen Klasse von ABC Transportern.

In Kapitel 4 wird die apo Struktur von TM287/288 beschrieben. Durch die Struktur werden detaillierte Aussagen über die strukturellen Veränderungen durch Nukleotid Bindung an die degenerierte ATP Bindungsstelle ermöglicht. Die Kristalle gehörten derselben Raumgruppe an, wie diejenigen die zur AMP-PNP Struktur geführt hatten. Die strukturellen Unterschiede beschränken sich hauptsächlich auf die degenerierte Bindungsstelle. Diese schliessen Veränderungen im A-loop ein, welcher durch eine aromatische Aminosäure mit dem Adeninring des gebundenen Nukleotids interagiert. Des Weiteren sieht man Veränderungen im Walker A Motiv, welches sich um das γ-Phosphat des Nukleotids windet. Die beiden NBDs bleiben sogar in Abwesenheit eines ATP Moleküls in molekularem Kontakt miteinander, wobei die durch den D-loop vermittelte NBD-NBD Interaktion an der degenerierte Bindungsstelle in Abwesenheit eines Nukleotids schwächer wird. AMP-PNP Bindung an die degenerierte Bindungsstelle wird durch das Walker B Motiv wahrgenommen und an den D-loop der konservierten aktiven Bindungsstelle weitergeleitet. Daraufhin werden zwei Wasserstoffbrücken mit dem gegenüberliegenden NBD durch ein konserviertes Aspartat (D-loop) ausgebildet. Die Entfernung des Nukleotids zerstört die zwei Wasserstoffbrücken und führt zu starken konformationellen Veränderungen im höchst flexiblen D-loop der konservierten Bindungsstelle. Der Vergleich der beiden gelösten TM287/288 Strukturen (AMP-PNP/apo) erlaubt somit neue Einblicke in die molekulare Kommunikation zwischen den beiden asymmetrischen ATP Bindungsstellen bei heterodimeren ABC Exportern.

In Kapitel 5 werden die Kristallstrukturen der isolierten NBDs NBD287 und NBD288 von Volllängen-TM287/288 präsentiert. Eine Vielzahl von isolierten NBDs von ABC Exportern wurden in der Vergangenheit gelöst, welche wichtige mechanistische Einblicke erlaubten. Was aber fehlte ist der Vergleich von isolierten NBDs mit NBDs im Kontext ein- und desselben intakten ABC Exporters. NBD287 und NBD288 zeigten weder alleine noch als 1:1 Mischung messbare ATPase Aktivität, ganz im Gegensatz zum intakten Transporter. Dimerbildung in Anwesenheit von MgATP konnte weder in Gelfiltrations- noch in analytischen Ultrazentrifugationsexperimenten beobachtet werden. Unsere Analysen der isolierten NBDs ergaben, dass sie hohe strukturelle Flexibilität in Regionen aufweisen, die in Interdomänen Kontakten im intakten Transporter involviert sind. Im Besonderen scheint die degenerierte ATP Bindungsstelle im isolierten NBD287 unstrukturiert zu sein. Zusätzlich, war keine

Elektronendichte für den D-loop von NBD288 sichtbar, welcher im Volllängenprotein mittels eines starken Wasserstoffbrücken Netzwerks mit NBD287 interagiert. Die Interaktion zwischen den Domänen, wie man sie im Volllängentransporter sieht, ist daher Voraussetzung für die Ausbildung der degenerierten Bindungsstelle.

1 Introduction

1.1 Discovery of Microorganisms

In the late 17th century Robert Hooke and Antoni van Leeuwenhoek were amongst the first describing bacteria and other microorganisms using primitive single-lens microscopes. In the 19th century the German botanist Ferdinand Cohn founded the field of bacteriology by proposing amongst others a way to classify bacteria. Contemporaneously, the French chemist Louis Pasteur together with the German physician Robert Koch created the field of microbiology or more precisely the field of medical microbiology. These foundations were possible due to the development of oil-immersion microscopes with a higher resolution. Louis Pasteur is best known for his success in food preservation and was in addition significantly involved in the disproval of the theory of "spontaneous generation" developed by Aristotle about 400 B.C., describing the generation of living material from non-living material. Pasteur could show in experiments with swan-necked flacks (Pasteur flasks) that spontaneous generation does not exist but that the growth of microorganisms in sterilized nutrient solutions can be ascribed to air-born microbes. Pasteur also developed vaccines for the diseases anthrax and rabies. Robert Koch became famous for the so-called Koch's postulates about the "germ theory of diseases". He showed the direct connection between disease (effect) and the occurrence of pathogenic microorganisms (cause). This was possible by the isolation of a pathogen from a diseased animal and its subsequent growth in pure liquid culture or on agar plates. Reinjection into a healthy animal aroused the disease again. The work with pure cultures led to the discovery of several pathogenic bacterial strains, e.g. *Mycobacterium tuberculosis*[1].

1.2 Development of Antibiotics

The groundbreaking findings of Robert Koch that the causative agents of so-called infectious diseases are microorganisms and the observation of Louis Pasteur that some bacteria show an antagonism between each other strongly stimulated the search for antibacterials. Koch and Pasteur described a phenomenon called antibiosis, where the growth of *Bacillus anthracis* cultures was inhibited by another airborne *Bacillus* species. Antagonistic effects of fungi against bacteria were also described by John Tyndall. In 1928 Alexander Fleming observed a similar effect that a fungus from the genus *Penicillium* exhibited against certain bacteria. Fleming assigned this effect to a compound he named penicillin. In 1932, the first sulphonamide called Prontosil, from Bayer Laboratories became commercially available. Thereafter, the progress in development of antibacterial agents was stimulated dramatically. In 1939, Gramicidin from *B. brevis* was discovered, which was used to treat wounds during World War II. Ernst Chain and Howard Florey purified penicillin G procaine in 1942. For their work they received the Nobel Prize in Medicine 1945 together with Alexander Fleming[1]. The discovery of penicillin tremendously stimulated the research in the field of antibiotic development and discovery. Many more antibiotics were developed until the end of the 1960s and became commercially available. After the 1960s the progress in the development of antibiotics was slowed down severely because the majority of the infectious diseases were believed to be conquered.

1.3 Mechanisms of Antibiotic Action

The antibiotic susceptibility of different microorganisms is variable and depends on several factors. Gram-positive bacteria and Gram-negative bacteria for example often show a different susceptibility towards an individual antibiotic. Broad-spectrum antibiotics are often effective against both groups. The dose of an antibiotic and the exposure time to it is an additional, very important factor.

Figure 1 summarizes the main mechanisms of antibiotic action and the place of intervention. These mechanisms can be classified in three main groups: nucleic acid synthesis, protein synthesis and cell wall synthesis. These classes can be further subdivided. Certain antibiotics or groups of antibiotics for example precisely target the individual subunits of the prokaryotic ribosome, either 30S or 50S and influence in this way protein synthesis. Other antibiotics interfere with nucleic acid synthesis by blocking the DNA gyrase or by inhibiting the DNA dependent RNA polymerase. A third mechanism to impede with DNA synthesis is the folate synthesis pathway. Folate is a DNA precursor and therefore blockage of its synthesis pathway is lethal for an organism.

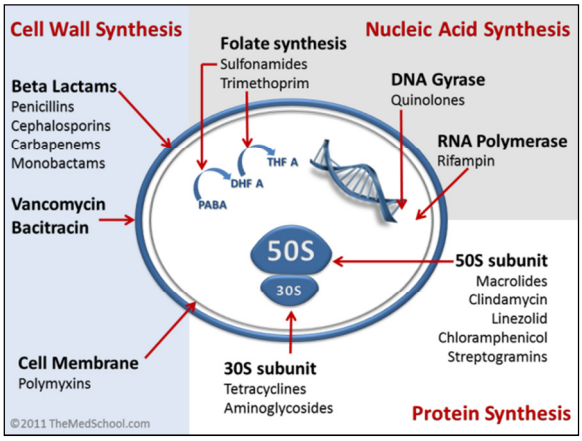

FIGURE 1| Points of action of antibiotics within a bacterial cell[2].

1.4 Antibiotic Resistance

Antibiotic resistance is a common, natural and ancient phenomenon [3, 4]. In the year 1952 Esther and Joshua Lederberg conducted first experiments showing that penicillin resistant strains existed before penicillin treatment and Joshua Lederberg in addition could show the occurrence of resistant strains against streptomycin. Genes transferring antibiotic resistance are collected in the so-called resistome[5]. But in general the occurrence of natural antibiotic-resistant strains is not the reason for the present-day's situation. It's the today's misuse and overuse of antibiotics in human and veterinary medicine and in agriculture that increased the evolutionary pressure on bacterial strains to form resistance phenotypes. Flu and colds, which are caused by viruses, are frequently treated with antibiotics, which do not have any biological influence on their life cycle. This practice seems to be so prevalent that the Food and Drug Administration (FDA) has to run dedicated information programs (Figure 2). The exposure time of a pathogen to a drug and the prescribed dose are as well of high importance. A low dose or a short exposure time for example does not kill all bacteria, but instead puts a selection pressure on the microorganism, allowing spontaneous drug target mutations. In addition, antibiotics were and still are deployed in certain countries in livestock breeding as growth promoters

for cattle, pigs and chickens[6]. The use of antibiotics as growth enhancer in fish farms is as well in common use. Development of antibiotic resistance simply follows the law of natural selection described by Charles Darwin, which means the adaptation to a changed, tightened environment with subsequent survival advantage. Figure 3 shows bacterial cells forming colonies plated on two agar plates containing paper discs soaked with antibiotics. The cells on the left plate are much more susceptible to the tested antibiotics than the cells grown on the right plate with the same antibiotics. This is because the cells on the right plate built up a resistance against the antibiotics.

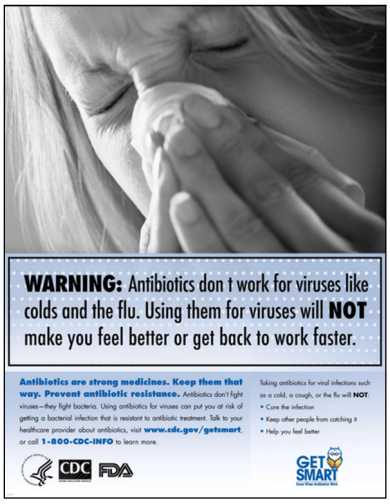

FIGURE 2| Food and Drug Administration (FDA) warning[7].

FIGURE 3| Antibiotic susceptibility, disc growth assays[8].

Resistance phenotypes can evolve by spontaneous or induced genetic mutations or by the acquisition of genes in a process called horizontal gene transfer[9]. This transfer is often facilitated by the fact that these resistance genes are encoded on plasmids, which allow a simplified transfer via conjugation, transformation or transduction. In the lower panel of Figure 4 the appearance of first phenotypes of resistance against a developed antibiotic are shown. It is frightening how fast such an adaptation to a certain antibiotic can proceed. Therefore, infectious diseases are today again a world leading cause of death and forgotten infection diseases experience a renaissance[10].

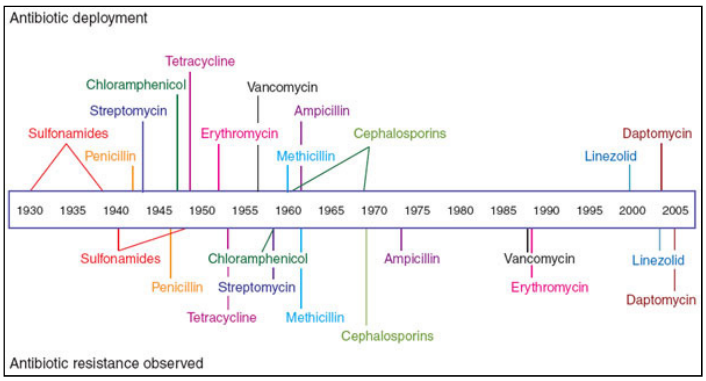

FIGURE 4| Development of antibiotics and appearance of first resistant bacterial strains[11].

1.5 Molecular Resistance Mechanisms

Horizontal gene transfer is in many cases the reason for the acquisition of antibiotic resistance. The presence of an antibiotic against pathogens puts them under selection pressure. Pathogens with a genetic alteration in an affected antibiotic-targeted protein then receive a survival or growth advantage. Four principal resistance mechanisms that are employed by microorganisms are distinguished (Figure 5). 1. Drug modification or inactivation. Drugs can be chemically modified and thereby become inactive. Penicillin resistant strains produce β-lactamases (e.g. penicillinase) that enzymatically hydrolyse the β-lactam ring[12]. To overcome this problem, penicillinase stable antibiotics like methicillin were developed. But this success did not last for long, because as seen in Figure 4 resistance against the penicillinase stable methicillin appeared very rapidly. 2. Target modification. The target of penicillins, the penicillin binding protein (PBP) can be modified by mutations lowering the affinity of the antibiotic to PBP[12]. Other examples are modifications of the gyrase or the methylation of the ribosome, for example in the ribosomal RNA[13], which inhibits the interaction with the antibiotic. 3. Changes in metabolic pathways. Sulfonamide resistant bacteria no longer require *p*-aminobenzoic acid (PABA), the precursor for the synthesis of folic and the subsequent nucleic acids. Folic acid synthesis is blocked by sulfonamides[14]. 4. Lowered drug accumulation. In many bacteria, membrane permeability for antibiotics or other antibacterial agents decreases. This is achieved by down-regulation of the expression of outer-membrane proteins called porins[15] or increased expression of polyspecific efflux pumps or multidrug transporters (MDR) with a wide range of specificity to extrude noxious substances from the cells.

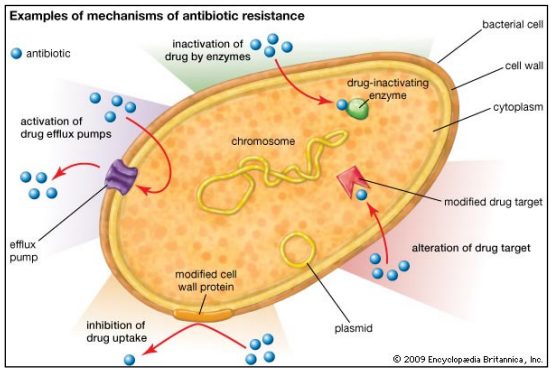

Figure 5| Resistance mechanisms[16]

1.6 Efflux Pumps and (MDR) Transporters

Multidrug transporters belong to five superfamilies[17], the ATP binding cassette (ABC) family, the major facilitator superfamily (MFS), the multidrug and toxic-compound extrusion (MATE) family, the small multidrug resistance (SMR) family and the resistance nodulation division (RND) family. Next to primary active ABC transporters, using the energy of ATP binding and hydrolysis, the MDR family contains another four secondary active transporters (MSF, MATE, SMR, and RND). They use the energy that is stored in the proton (H^+) or the sodium (Na^+) gradient across cellular membranes. Transporters of the MATE (e.g. NorM from *Erwinia amylovora*) and SMR (e.g. QacC from *Staphylococcus aureus*) family only exist in Gram-positive bacteria. ABC transporters are found in Gram-positive (e.g. LmrA from *L. lactis*) and in Gram-negative bacteria (e.g. MacB from *Escherichia coli*). MFS are as well found in both Gram species, e.g. QacA (*S. aureus*) and EmrB (*E. coli*). RNDs (e.g. AcrB from *E. coli*) are mainly present in Gram-negative bacteria. MDR transporters from Gram-negative bacteria (e.g. AcrB, MacB and EmrB, examples are given for *E. coli*) are part of tripartite efflux systems, containing an additional membrane fusion protein (AcrA, MacA and EmrA), which connects the transporter to the outer membrane protein TolC[18]. Figure 6 shows the described transporters in an overview.

Functional, biochemical and especially structural data for these MDR transporters help to understand the mechanism of drug transport mediated by these medically important proteins. Obtaining structural data for membrane proteins is a difficult task. Nevertheless, structures of all five classes described above could be solved by x-ray crystallography. The structure of the first member was solved in 2002 by Murakami *et al.*, namely the structure of the homotrimeric RND transporter AcrB crystallized in a symmetric form[19]. In 2006 and 2007, three further structures of AcrB were described, all crystallized in an asymmetric form[20-22]. Two additional RND structures were solved thereafter, the structure of MexB from *Pseudomonas aeruginosa* and the heavy-metal efflux transporter CusA[23, 24]. CusA was crystallized as well together with its membrane fusion protein CusB[25]. Finally, in 2011 and 2012 researchers were able to solve AcrB structures with the bound substrates rifampicin, erythromycin, minocycline and doxorubicin, giving the first insight into drug binding and possible sites for efflux pump inhibition[26, 27]. With the three structures of homodimeric Sav1866 (ABC), homodimeric MsbA (ABC) and monomeric EmrD (MFS) all published in 2006 two additional structures of members of the MDR family were made accessible[28-30]. EmrD was shown to be very similar to the MFS transporters LacY, a lactose permease and GlpT, a glycerol-3-phosphate transporter described before[31, 32]. In 2009 the structure of mouse P-glycoprotein (P-gp), a transporter shown to be involved in drug resistance in cancer cells, was solved and binding of two artificial, cyclic substances was described[33]. Another P-gp structure of *C. elegans* was published in 2012. In 2007, the structure of the homodimeric SMR transporter EmrE was added to the quintet[34]. And finally in 2010 the structure of monomeric NorM from *Vibrio cholerae* belonging to the MATE superfamily was solved, thereby completing the gallery of MDR transporters[35]. Recently, two further structures of NorM from *Neisseria gonorrheae* and of a MATE from *Pyrococcus furiosus* (PfMATE) were solved with bound drugs[36, 37]. Even though the number of transporter structures has increased in the past years, the amount of data is unfortunately still not sufficient to propose a substantiated mechanism for all the

different MDR transporters. Not for all transporter families structures with bound substrates are available. Moreover crystal structures describing the various states and conformations of the transport cycle are missing and efforts to combine structural and functional experiments are limited. Further studies are therefore needed to understand how multidrug transporters function to reach the long-term goal to specifically target or inhibit MDR efflux.

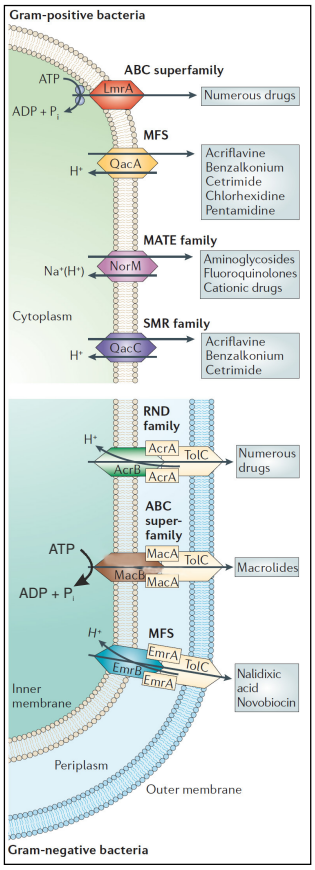

FIGURE 6| Multidrug-resistance efflux pumps, adapted from[38].

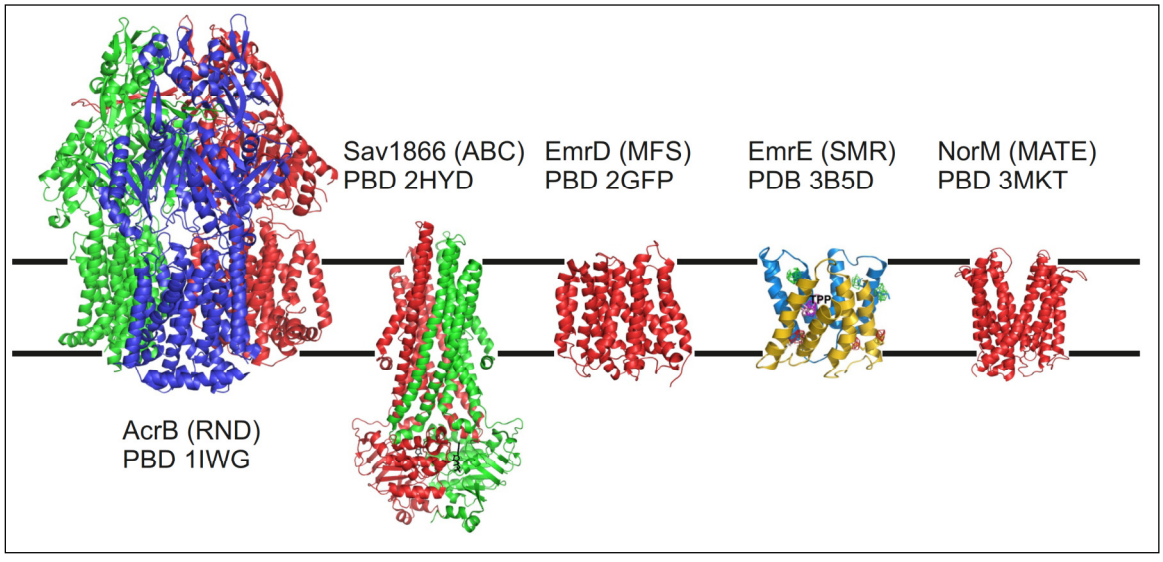

Figure 7| Side by side x-ray structure comparison of the five existing MDR transporter families

1.7 ABC Exporters

One major cause of antibiotic resistance is the increased pumping activity of microbial ABC exporters, which diminishes the effective drug concentration inside the microbial cell. The same holds true for eukaryotic ABC transporters, which were found to be connected to multidrug resistance (MDR) in cancer cells by extruding broad ranges of anticancer agents.

As for all transporters, it is generally accepted that ABC transporters work according to the alternating access mechanism[39]. In the inward-facing state, ABC exporters bind their cargo in a large cavity formed by the transmembrane domains (TMDs)[33]. After binding of ATP at the nucleotide binding domains (NBDs), leading to their dimerization in a head to tail manner, the transporter adopts an outward-facing conformation involving major conformational changes in the TMDs and the cargo can be released[28]. The conformational rearrangements in the NBDs are transmitted via the so-called coupling helices to the TMDs. The ATP-driven dimerization upon ATP binding at the NBDs has been proposed as the power stroke of ABC transporters[40]. After hydrolysis of ATP, ADP and inorganic phosphate is released, the NBDs separate and the transporter returns back into an inward-facing state. ABC exporters exist in homodimeric and heterodimeric forms, bearing either two or only one consensus ATPase site per transporter, respectively. Many medically important eukaryotic ABC transporters are heterodimers; examples are the transporter associated with antigen processing (Tap1/2)[41], the cystic fibrosis transmembrane regulator (CFTR)[42], the sulfonylurea receptor 1 (SUR1)[43] and the multidrug resistance-associated protein 1 (MRP1)[44]. Bacterial heterodimeric ABC transporters such as LmrCD and PatAB have been shown to be responsible for resistance against several antibacterial agents. Whereas the amino acid sequences of the TMDs of ABC transporters are variable, the NBDs contain highly conserved sequence motifs (Chapter 4, Figure 1).

The A-loop motif contains an aromatic amino acid (Tyr, Phe or Trp) and is involved in nucleotide binding by making π-stacking interactions with the adenine moiety of ATP. It is positioned about 25 residues upstream of the Walker A motif[45]. The Walker A (consensus: GxxGxGK) itself, contains a well conserved lysine residue and is involved in ATP binding. The lysine side chain orients the β- and the γ-phosphate of the ATP and is therefore as well involved in nucleotide hydrolysis[46]. Another common motif of many ATPases, the Walker B motif (consensus: ΦΦΦΦDE; Φ = aliphatic amino acid) is critical for ATP hydrolysis. The Walker B glutamate plays the role of the catalytic base, and is responsible for the orientation and polarisation of a water molecule, which is itself attacking and hydrolysing the γ-phosphate of the nucleotide[47]. The ABC signature motif (consensus: LSGGQ), which interacts in a head-to-tail manner with the Walker A motif of the other NBD is involved in ATP binding by sandwiching it in between[48]. The other motif involved in ATP hydrolysis is the H- (switch-) loop, which has a consensus histidine that functions as the general acid[48]. The Walker B glutamate and the H-loop histidine together build a catalytic dyad[47]. The Q-loop, a conserved glutamine is believed to be involved in nucleotide sensing and in addition in interdomain communication. Last but not least the D-loop (consensus: SALD) plays a role in inter-NBD communication as proposed based on isolated NBD structures[47].

In heterodimeric ABC transporters some of these conserved motifs deviate from the consensus sequence. In the prokaryotic heterodimeric ABC transporter LmrCD for example the Walker B

sequence is ΦΦΦΦDD in LmrC deviating from consensus ΦΦΦΦDE in LmrD. The sequence of the D-loop is changed from SALD to SNVD and the switch histidine is changed to a glutamine[49]. In addition, the sequence of the ABC signature motif is changed from FSGGQ to FSVGQ. Therefore these ATPase sites are called the degenerate ATPase sites.

In the last ten years progress has been made in solving crystal structures of full-length ABC transporters. For the exporter subtype there are four bacterial and three eukaryotic structures available (all heterodimeric, ABCB10 counted as one). In Sav1866, a protein from the bacteria *S. aureus* solved at a resolution of 3 Å, the NBDs are dimerized and show an outward-facing conformation with two nucleotides (either ADP or AMP-PNP) tightly bound at the NBDs[28]. MsbA from *E. coli, V. cholerae* and *S. typhimurium* were crystallized in three different conformations. In the 3.7 Å structure of the *S. typhimurium* protein, binding of two AMP-PNP or ADP·Vi can be observed and it shows an outward-facing conformation, very similar to that of Sav1866. In the 5.3 Å *E. coli* and the 5.5 Å *V. cholerae* structures no nucleotides are bound and the proteins show inward-facing conformations[30] with the nucleotide binding domains (NBDs) separated by 68.46 Å and 32.75 Å, respectively (Chapter 4, Figure 9). The first eukaryotic ABC transporter structure of mouse P-gp solved at 3.8 Å resolution depicts an inward-facing conformation, with no nucleotides bound[33]. The second eukaryotic structures of ABCB10 from human mitochondria solved at 3.3 Å, 2.9 Å and 2.85 Å again show inward-facing conformations, but binding of two AMP-PNP or two AMP-PCP molecules could be observed. Two more ABCB10 structures are available in nucleotide-free form[50]. The third, most recent eukaryotic structure is a structure of nucleotide-free *C. elegans* P-gp solved to a resolution of 3.4 Å[51]. A gallery of these ABC transporter structures is shown in Figure 9, Chapter 4. At the time when this PhD thesis was started in 2009, no structure was available for a heterodimeric transporter neither eukaryotic nor prokaryotic, despite the fact that they are of high medical relevance and include the proteins CFTR, MRP1 or Tap1/2[41, 42, 44].

1.8 Aim of Thesis

ABC exporters have been shown to be involved in multidrug resistance (MDR) in prokaryotes as well as in eukaryotes. Examples for eukaryotic multidrug ABC transporters are P-gp and MRP1, which both confer resistance against anticancer drugs in tumor cells. Furthermore, mutations in the heterodimeric ABC transporters CFTR and SUR1 are responsible for the hereditary diseases cystic fibrosis, congenital hyperinsulinism and for susceptibility to type 2 diabetes. Heterodimeric, prokaryotic ABC exporters like LmrCD or PatAB confer drug resistance against antibiotics in *L. lactis* and *Streptococcus pneumoniae*. At the onset of this project in 2009, structural data was unavailable for prokaryotic and eukaryotic members of the subclass of heterodimeric ABC exporters. Little was known about potential differences or similarities between the ATP binding and the hydrolysis mechanism of homodimeric or heterodimeric ABC exporters.

The aim of this thesis was to obtain deeper insights into the transport and hydrolysis mechanism of ABC exporters in general and more precisely into the subclass of heterodimeric ABC exporters. To this end, x-ray crystallography was combined with biochemical and microbiological analyses. In a first step, prokaryotic homologues of the heterodimeric ABC exporter LmrCD from *Lactococcus lactis* were

probed for their stability and crystallizability (Chapter 2). Subsequently, the structure of the first heterodimeric ABC exporter, TM287/288 from *Thermotoga maritima*, was solved with one bound AMP-PNP and its function was analyzed *in vitro* as well as *in vivo* (Chapter 3). TM287/288 was as well crystallized in the absence of nucleotides, which revealed novel insights into the molecular communication between the asymmetric catalytic sites of heterodimeric ABC exporters (Chapter 4). Finally, the isolated NBDs of TM287/288 were crystallized to understand the importance of interdomain contacts between the NBDs themselves and the coupling between the NBDs and the TMDs in the context of the full-length transporter (Chapter 5).

1.9 Bibliography

1. Madigan, M.T. and J.M. Martinko, *Brock Biology of Microorganisms*. Vol. Eleventh Edition. 2006: Pearson.
2. Wikimedia. http://commons.wikimedia.org/wiki/File:Antibiotics_Mechanisms_of_action.png
3. D'Costa, V.M., C.E. King, L. Kalan, M. Morar, W.W. Sung, C. Schwarz, D. Froese, G. Zazula, F. Calmels, R. Debruyne, G.B. Golding, H.N. Poinar, and G.D. Wright, *Antibiotic resistance is ancient.* Nature, 2011. 477(7365): p. 457-61.
4. Wright, G.D., *Antibiotic resistance in the environment: a link to the clinic?* Curr Opin Microbiol, 2010. 13(5): p. 589-94.
5. Wright, G.D., *The antibiotic resistome: the nexus of chemical and genetic diversity.* Nat Rev Microbiol, 2007. 5(3): p. 175-86.
6. Purvis, H.T., 2nd and J.C. Whittier, *Effects of ionophore feeding and anthelmintic administration on age and weight at puberty in spring-born beef heifers.* J Anim Sci, 1996. 74(4): p. 736-44.
7. FDA. https://www.boundless.com/microbiology/antimicrobial-drugs/drug-resistance
8. Wikipedia. http://en.wikipedia.org/wiki/File:Antibiotic_sensitvity_and_resistance.JPG
9. Dowson, C.G., A. Hutchison, J.A. Brannigan, R.C. George, D. Hansman, J. Linares, A. Tomasz, J.M. Smith, and B.G. Spratt, *Horizontal transfer of penicillin-binding protein genes in penicillin-resistant clinical isolates of Streptococcus pneumoniae.* Proc Natl Acad Sci U S A, 1989. 86(22): p. 8842-6.
10. Livermore, D.M., *Has the era of untreatable infections arrived?* J Antimicrob Chemother, 2009. 64 Suppl 1: p. i29-36.
11. Clatworthy, A.E., E. Pierson, and D.T. Hung, *Targeting virulence: a new paradigm for antimicrobial therapy.* Nat Chem Biol, 2007. 3(9): p. 541-8.
12. Pantosti, A., A. Sanchini, and M. Monaco, *Mechanisms of antibiotic resistance in Staphylococcus aureus.* Future Microbiol, 2007. 2(3): p. 323-34.

13. Cundliffe, E., *Ribosomal modification and resistance in antibiotic-producing organisms.* Biochem Soc Symp, 1987. 53: p. 1-8.

14. Platteeuw, J.J., *Resistance to sulphadrug-based antifolate therapy in malaria: are we looking in the right place?* Trop Med Int Health, 2006. 11(6): p. 804-8.

15. Jetter, M., V. Spaniol, R. Troller, and C. Aebi, *Down-regulation of porin M35 in Moraxella catarrhalis by aminopenicillins and environmental factors and its potential contribution to the mechanism of resistance to aminopenicillins.* J Antimicrob Chemother, 2010. 65(10): p. 2089-96.

16. Encyclopaedia Britannica, I. http://www.britannica.com/EBchecked/media/129670/There-are-multiple-mechanisms-by-which-bacteria-can-develop-resistance.

17. Chung, Y.J. and M.H. Saier, Jr., *SMR-type multidrug resistance pumps.* Curr Opin Drug Discov Devel, 2001. 4(2): p. 237-45.

18. Symmons, M.F., E. Bokma, E. Koronakis, C. Hughes, and V. Koronakis, *The assembled structure of a complete tripartite bacterial multidrug efflux pump.* Proc Natl Acad Sci U S A, 2009. 106(17): p. 7173-8.

19. Murakami, S., R. Nakashima, E. Yamashita, and A. Yamaguchi, *Crystal structure of bacterial multidrug efflux transporter AcrB.* Nature, 2002. 419(6907): p. 587-93.

20. Seeger, M.A., A. Schiefner, T. Eicher, F. Verrey, K. Diederichs, and K.M. Pos, *Structural asymmetry of AcrB trimer suggests a peristaltic pump mechanism.* Science, 2006. 313(5791): p. 1295-8.

21. Murakami, S., R. Nakashima, E. Yamashita, T. Matsumoto, and A. Yamaguchi, *Crystal structures of a multidrug transporter reveal a functionally rotating mechanism.* Nature, 2006. 443(7108): p. 173-9.

22. Sennhauser, G., P. Amstutz, C. Briand, O. Storchenegger, and M.G. Grütter, *Drug export pathway of multidrug exporter AcrB revealed by DARPin inhibitors.* PLoS Biol, 2007. 5(1): p. e7.

23. Sennhauser, G., M.A. Bukowska, C. Briand, and M.G. Grütter, *Crystal structure of the multidrug exporter MexB from Pseudomonas aeruginosa.* J Mol Biol, 2009. 389(1): p. 134-45.

24. Long, F., C.C. Su, M.T. Zimmermann, S.E. Boyken, K.R. Rajashankar, R.L. Jernigan, and E.W. Yu, *Crystal structures of the CusA efflux pump suggest methionine-mediated metal transport.* Nature, 2010. 467(7314): p. 484-8.

25. Su, C.C., F. Long, M.T. Zimmermann, K.R. Rajashankar, R.L. Jernigan, and E.W. Yu, *Crystal structure of the CusBA heavy-metal efflux complex of Escherichia coli.* Nature, 2011. 470(7335): p. 558-62.

26. Nakashima, R., K. Sakurai, S. Yamasaki, K. Nishino, and A. Yamaguchi, *Structures of the multidrug exporter AcrB reveal a proximal multisite drug-binding pocket.* Nature, 2011. 480(7378): p. 565-9.

27. Eicher, T., H.J. Cha, M.A. Seeger, L. Brandstatter, J. El-Delik, J.A. Bohnert, W.V. Kern, F. Verrey, M.G. Grütter, K. Diederichs, and K.M. Pos, *Transport of drugs by the multidrug transporter AcrB involves an access and a deep binding pocket that are separated by a switch-loop.* Proc Natl Acad Sci U S A, 2012. 109(15): p. 5687-92.

28. Dawson, R.J. and K.P. Locher, *Structure of a bacterial multidrug ABC transporter.* Nature, 2006. 443(7108): p. 180-5.

29. Yin, Y., X. He, P. Szewczyk, T. Nguyen, and G. Chang, *Structure of the multidrug transporter EmrD from Escherichia coli.* Science, 2006. 312(5774): p. 741-4.

30. Ward, A., C.L. Reyes, J. Yu, C.B. Roth, and G. Chang, *Flexibility in the ABC transporter MsbA: Alternating access with a twist.* Proc Natl Acad Sci U S A, 2007. 104(48): p. 19005-10.

31. Abramson, J., I. Smirnova, V. Kasho, G. Verner, H.R. Kaback, and S. Iwata, *Structure and mechanism of the lactose permease of Escherichia coli.* Science, 2003. 301(5633): p. 610-5.

32. Huang, Y., M.J. Lemieux, J. Song, M. Auer, and D.N. Wang, *Structure and mechanism of the glycerol-3-phosphate transporter from Escherichia coli.* Science, 2003. 301(5633): p. 616-20.

33. Aller, S.G., J. Yu, A. Ward, Y. Weng, S. Chittaboina, R. Zhuo, P.M. Harrell, Y.T. Trinh, Q. Zhang, I.L. Urbatsch, and G. Chang, *Structure of P-glycoprotein reveals a molecular basis for poly-specific drug binding.* Science, 2009. 323(5922): p. 1718-22.

34. Chen, Y.J., O. Pornillos, S. Lieu, C. Ma, A.P. Chen, and G. Chang, *X-ray structure of EmrE supports dual topology model.* Proc Natl Acad Sci U S A, 2007. 104(48): p. 18999-9004.

35. He, X., P. Szewczyk, A. Karyakin, M. Evin, W.X. Hong, Q. Zhang, and G. Chang, *Structure of a cation-bound multidrug and toxic compound extrusion transporter.* Nature, 2010. 467(7318): p. 991-4.

36. Lu, M., J. Symersky, M. Radchenko, A. Koide, Y. Guo, R. Nie, and S. Koide, *Structures of a Na+-coupled, substrate-bound MATE multidrug transporter.* Proc Natl Acad Sci U S A, 2013. 110(6): p. 2099-104.

37. Tanaka, Y., C.J. Hipolito, A.D. Maturana, K. Ito, T. Kuroda, T. Higuchi, T. Katoh, H.E. Kato, M. Hattori, K. Kumazaki, T. Tsukazaki, R. Ishitani, H. Suga, and O. Nureki, *Structural basis for the drug extrusion mechanism by a MATE multidrug transporter.* Nature, 2013. 496(7444): p. 247-51.

38. Piddock, L.J., *Multidrug-resistance efflux pumps - not just for resistance.* Nat Rev Microbiol, 2006. 4(8): p. 629-36.

39. Jardetzky, O., *Simple allosteric model for membrane pumps.* Nature, 1966. 211(5052): p. 969-70.

40. Doshi, R., A. Ali, W. Shi, E.V. Freeman, L.A. Fagg, and H.W. van Veen, *Molecular disruption of the power stroke in the ATP-binding cassette transport protein MsbA.* J Biol Chem, 2013. 288(10): p. 6801-13.

41. Koch, J., R. Guntrum, S. Heintke, C. Kyritsis, and R. Tampé, *Functional dissection of the transmembrane domains of the transporter associated with antigen processing (TAP).* J Biol Chem, 2004. 279(11): p. 10142-7.

42. Cui, G., C.S. Freeman, T. Knotts, C.Z. Prince, C. Kuang, and N.A. McCarty, *Two salt bridges differentially contribute to the maintenance of CFTR channel function.* J Biol Chem, 2013.

43. de Wet, H., M.G. Rees, K. Shimomura, J. Aittoniemi, A.M. Patch, S.E. Flanagan, S. Ellard, A.T. Hattersley, M.S. Sansom, and F.M. Ashcroft, *Increased ATPase activity produced by mutations at arginine-1380 in nucleotide-binding domain 2 of ABCC8 causes neonatal diabetes.* Proc Natl Acad Sci U S A, 2007. 104(48): p. 18988-92.

44. Kim, H.S., Y.D. Min, and C.H. Choi, *Double-edged sword of chemosensitizer: increase of multidrug resistance protein (MRP) in leukemic cells by an MRP inhibitor probenecid.* Biochem Biophys Res Commun, 2001. 283(1): p. 64-71.

45. Ambudkar, S.V., I.W. Kim, D. Xia, and Z.E. Sauna, *The A-loop, a novel conserved aromatic acid subdomain upstream of the Walker A motif in ABC transporters, is critical for ATP binding.* FEBS Lett, 2006. 580(4): p. 1049-55.

46. Haffke, M., A. Menzel, Y. Carius, D. Jahn, and D.W. Heinz, *Structures of the nucleotide-binding domain of the human ABCB6 transporter and its complexes with nucleotides.* Acta Crystallogr D Biol Crystallogr, 2010. 66(Pt 9): p. 979-87.

47. Zaitseva, J., S. Jenewein, T. Jumpertz, I.B. Holland, and L. Schmitt, *H662 is the linchpin of ATP hydrolysis in the nucleotide-binding domain of the ABC transporter HlyB.* Embo J, 2005. 24(11): p. 1901-10.

48. Buchaklian, A.H. and C.S. Klug, *Characterization of the LSGGQ and H motifs from the Escherichia coli lipid A transporter MsbA.* Biochemistry, 2006. 45(41): p. 12539-46.

49. Lubelski, J., R. van Merkerk, W.N. Konings, and A.J. Driessen, *Nucleotide-binding sites of the heterodimeric LmrCD ABC-multidrug transporter of Lactococcus lactis are asymmetric.* Biochemistry, 2006. 45(2): p. 648-56.

50. Shintre, C.A., A.C. Pike, Q. Li, J.I. Kim, A.J. Barr, S. Goubin, L. Shrestha, J. Yang, G. Berridge, J. Ross, P.J. Stansfeld, M.S. Sansom, A.M. Edwards, C. Bountra, B.D. Marsden, F. von Delft, A.N. Bullock, O. Gileadi, N.A. Burgess-Brown, and E.P. Carpenter, *Structures of ABCB10, a human ATP-binding cassette transporter in apo- and nucleotide-bound states.* Proc Natl Acad Sci U S A.

51. Jin, M.S., M.L. Oldham, Q. Zhang, and J. Chen, *Crystal structure of the multidrug transporter P-glycoprotein from Caenorhabditis elegans.* Nature, 2012. 490(7421): p. 566-9.

2 From many to few: A funnel approach to obtain the first crystal structure of a heterodimeric ABC exporter

From many to few: A funnel approach to obtain the first crystal structure of a heterodimeric ABC exporter

Michael Hohl, Markus G. Grütter and Markus A. Seeger

Manuscript in preparation

References for the following manuscript are numbered separately and are listed directly at the end of this section.

2.1 Introduction

Membrane proteins constitute a class of very important molecules. About 20-30 % of the genes in a genome encode for these lipophilic proteins(1). The importance is underlined by the fact that more than 50 % of the current medical drugs target membrane embedded proteins(2). Membrane proteins facilitate the exchange of signals and substances between the extracellular and the intracellular environment. Transport proteins have a wide spectrum of substrates that ranges from trace elements to vitamins to even entire proteins. The transport of a cargo has often directionality, meaning that it can either be imported into or exported out of a cell(3). In addition, the field discriminates between a direct (primary active, using ATP) and an indirect (secondary active, exploiting the electrochemical gradient) energy coupling. It has been shown that some membrane transporters are involved in multidrug resistance (MDR)(4). MDR describes the ability of microorganisms or cancer cells to extrude noxious substances, such as antibiotics or anticancer drugs, out of the cell by hijacking existing transport systems, which originally evolved to transport physiological substrates.

Despite the importance of membrane proteins and the progress that has been made in handling these labile, flexible and often poorly expressed molecules, less than 0.1 % of the deposited structures in the protein data bank (PDB) originate from membrane embedded proteins (http://blanco.biomol.uci.edu/mpstruc/listAll/list).

The superfamily of ATP binding cassette (ABC) transporters belongs to the class of primary active transport proteins. They are found in all kingdoms of life(5). ABC transporters exist as substrate binding protein (SBP) dependent importers in prokaryotes, and as exporters in all organisms. In eukaryotes, the ABC exporters P-glycoprotein, MRP1 and ABCG2 were connected to resistance against anticancer agents(6, 7). The two prokaryotic ABC exporters PatAB from *Streptococcus pneumoniae* and LmrCD from *Lactococcus lactis* have been shown to extrude a large variety of drugs out of the cell(8, 9). PatAB and LmrCD belong to the subclass of prokaryotic, heterodimeric ABC exporters(10). The structure of the recently solved TM287/288, a heterodimeric ABC transporter from the thermophilic bacterium *Thermotoga maritima*, sheds for the first time light on the structure of this subclass(11). TM287/288 serves as a structural model for LmrCD, PatAB and other medically relevant eukaryotic, heterodimeric ABC exporters such as CFTR, MRP1, SUR1 and Tap1/2 (7, 12-14).

The aim of this thesis was to crystallize a heterodimeric ABC exporter. In this chapter we present a funnel approach(15) to select for stable homologues of this subclass with favorable biophysical and biochemical properties for functional and structural studies. This attempt resulted in two different x-ray structures of the heterodimeric ABC transporter TM287/288 from *T. maritima*(11) (Chapter 3 and Chapter 4). In addition, we were able to express and additionally crystallize some of the other selected homologues. All crystals were tested for their diffraction quality and for some full data sets were collected.

2.2 Material and Methods

2.2.1 Blastp

The amino acid sequence of LmrC of the heterodimeric ABC transporter LmrCD from *Lactococcus lactis subsp. cremoris MG1363* (NC_009004.1 (311092..312831); Gene ID: 4798592) was used as the query sequence for a protein blast (blastp) analysis (http://blast.ncbi.nlm.nih.gov/Blast.cgi?PAGE=Proteins) applying default settings. Due to redundancies of transporters from the same organism or strain, the 100 closest homologues of LmrC were reduced to 45 sequences. The gene *lmrD* was found directly adjacent to *lmrC* in the same operon, building a bicistronic expression cassette. The same arrangement was observed for the other transporters. Some of the transporters were not only adjacent, but even overlapping. Two examples of such a grouping are shown in Figure 1a.

2.2.2 Regional order neural network (RONN) analysis

These 45 heterodimeric ABC transporters were all of prokaryotic origin and were further validated by a structural biology server from the University of Oxford (http://www.strubi.ox.ac.uk/RONN). Each chain was analyzed separately. The server detects natively disordered regions in proteins which may affect solubility and crystallizability(18). As an output, RONN predicts the probability for each amino acid (aa) to be disordered by providing a value between 0 and 1. We exploited this output by adding penalty points. Disorder probability values of ≥ 0.5 received one penalty point/aa; values of ≥ 0.6 were punished with three penalty points/aa and values of ≥ 0.7 were given ten penalty points/aa. The 25 best performing transporters in this analysis were chosen to search for the availability of genetic material. The penalty points were summed up and are shown for the final selection of transporters (Table 1).

2.2.3 Preparation of genomic DNA from cell pellets

Both the “Deutsche Sammlung von Mikroorganismen und Zellkulturen” (DSMZ) and the American Type Culture Collection (ATCC) were searched to obtain genetic material of these 25 transporters in the form of genomic DNA (gDNA) or as cell pellets. The gDNA from *Enterococcus faecalis V583* was ordered from ATCC (ATCC 700802D-5). The gDNA from *Thermotoga maritima MSB8* (ATCC 43589D-2) was used before in our lab (Dissertation Daniel Frey). Cell pellets from *Bacillus subtilis subsp. subtilis str. 168* (DSM4424)*, Dictyoglomus thermophilum H-1-12* (DSM3960)*, Dictyoglomus turgidum* (DSM6724)*, Lactobacillus gasseri ATCC33323* (DSM20243 [63 AM])*, Thermotoga petrophila RKU-1* (DSM13995)*, Thermotoga sp. RQ2* (DSM4138)*, Listeria welshimeri serovar 6b str. SLCC5334* (DSM20650) and *Thermotoga neapolitana* (DSM4359) were ordered from DSMZ. The gDNA from the cell pellets was extracted with the help of the GenElute^{TM} Bacterial Genomic DNA Kit (Sigma Aldrich, NA2100-1KT) according to the manufacturer’s protocol. Plasmids encoding the two transporters PatAB (*Streptococcus pneumoniae R6*) and LmrCD (*Lactococcus lactis subsp. cremoris MG1363*) were kind gifts of H. van Veen (Department of Pharmacology, University of Cambridge).

2.2.4 Gene amplification and cloning into pBXC3GH and pBXNH3

All the below specified transporter genes were amplified directly from the purchased or extracted gDNA by polymerase chain reaction (PCR). Exceptions are the two transporters PatAB and LmrCD, where the amplification was performed from the donated plasmids. All PCR products except the ones of PatAB (see below) were inserted in the FX-plasmids pBXC3GH and pBXNH3 for test expressions(20). Both, pBXC3GH and pBXNH3 are pBAD24 based expression vectors. In pBXC3GH the protein of interest (POI) is fused to a C-terminal green fluorescent protein (GFP) that is further connected to a deca-His-tag (3C PreScission protease cleavable) for purification purposes (Figure 1b, upper panel). In pBXNH3 the POI is fused to an N-terminal, cleavable deca-His-tag (Figure 1b, lower panel). The primers used for the amplification of the transporters for the FX-cloning are listed below. One forward and one reverse primer were used to amplify the heterodimeric transporters as bicistronic gene operon. In contrast to the genes listed, PatAB is encoded on distinct locations on the chromosomal DNA. The preparation of the special expression vector pBAD24_duet and the cloning and expression of PatAB are described in the following sections.

TM287/288 from *Thermotoga maritima*:

5'-ATATATGCTCTTCTAGTAAAACACTCGCCAGATATTTAAAGC-3'

5'-TATATAGCTCTTCATGCTTCTTTTTCTACAACGAGACCGTATTGG-3'

Tpet from *Thermotoga petrophila*:

5'-ATATATGCTCTTCTAGTAAAACACTCGCCAGATATTTAAAACCTTACTGGC-3'

5'-TATATAGCTCTTCATGCTCTTTCTACAACGAGACCG-3'

TRQ from *Thermotoga sp. RQ2*:

5'-ATATATGCTCTTCTAGTAAAACACTCGCCAGATATTTAAAGCCG-3'

5'-TATATAGCTCTTCATGCTCTTTCTACAACGAGACCGTATTGGC-3'

CTN from *Thermotoga neapolitana*:

5'-ATATATGCTCTTCTAGTAGAACGCTTGCAGGCTATCTTAAGCC-3'

5'-TATATAGCTCTTCATGCTCTTTCTACAACGAGACCG-3'

EF1 from *Enterococcus faecalis V583*:

5'-ATATATGCTCTTCTAGTAAAGTATACAAAAAATTATTTAGTTATGTCCC-3'

5'-TATATAGCTCTTCATGCTCGTGATTGAGCTTCTTTTTCATAGACG-3'

EF2 from *Enterococcus faecalis V583*:

5'-ATATATGCTCTTCTAGTGACCTTATTATTCAACACGCC-3'

5'-TATATAGCTCTTCATGCTTCAAAAACAAATTGATTTTTATAAAGTTCCGC-3'

Lwe from *Listeria welshimeri serovar 6b str. SLCC5334*:

5'-ATATATGCTCTTCTAGTAAAGTATTGTTTCACCATCTC-3'

5'-TATATAGCTCTTCATGCTTCAATAACGAATTGATTATGATATAGC-3'

BmrCD from *Bacillus subtilis subsp. subtilis str. 168*:

5'-ATATATGCTCTTCTAGTTTTTCAGTTTTGAAAAAGCTTGGC-3'

5'-TATATAGCTCTTCATGCTGCAATGGAATGTTTCTGTCCC-3'

Dtur from *Dictyoglomus turgidum*:

5'-ATATATGCTCTTCTAGTAGAAAACTTTTGAAGTTTTTAAAACC-3'

5'-TATATAGCTCTTCATGCTTTTATTTCTACTTCATCGGC-3'

DICT from *Dictyoglomus thermophilum H-1-12*:

5'-ATATATGCTCTTCTAGTAAAAAACTTTTGAAATTTTTAAAACC-3'

5'-TATATAGCTCTTCATGCTTTTATTTCCACTTCGTCGGC-3'

LGAS from *Lactobacillus gasseri ATCC33323*:

5'-ATATATGCTCTTCTAGTCAGATTTTGAAGCCACAC-3'

5'-TATATAGCTCTTCATGCTTCAAATGCCATTTGATTAGTATATAGTCCG-3'

LmrCD from *Lactococcus lactis subsp. cremoris MG1363*:

5'-ATATATGCTCTTCTAGTATTTTCAAATCAATCATGAAGCATAAATG-3'

5'-TATATAGCTCTTCATGCTTCAAAAACGAATTGATTATGATAAAG-3'

FX cloning, a simple one cup cloning method was performed as described by Geertsma *et al.*(20). Briefly, the gel purified PCR product was mixed with the selected FX vector (pBXNH3 or pBXC3GH) and incubated with the SapI restriction enzyme for one hour at 37 °C. After inactivation of the enzyme, ligase and ATP were added to the mixture and incubated for another hour at 25 °C. After a final inactivation step the mixture was directly used to transform *E. coli*. All the reactions were performed in a standard PCR machine.

2.2.5 Small scale expression and whole cell *in gel* analysis

The constructs pBXC3GH_TM287/288, pBXC3GH_Tpet, pBXC3GH_TRQ, pBXC3GH_CTN, pBXC3GH_EF1, pBXC3GH_EF2, pBXC3GH_Lwe, pBXC3GH_BmrCD, pBXC3GH_Dtur, pBXC3GH_DICT, pBXC3GH_LGAS and pBXC3GH_LmrCD were transformed into the *Escherichia coli* expression strain C43(DE3). A preculture was grown for each construct. The preculture was used 1:40 to inoculate 1 ml 2YT expression cultures in a 96-well plate. Cells were grown at 30 °C for three hours and then induced for another three hours at three different L-arabinose inducer concentrations of 10^{-1}, 10^{-3} and 10^{-5} % (w/v). After centrifugation, the cells were resuspended in 50 mM KPi pH 7.2, 1 mM $MgSO_4$, 10 % (v/v) glycerol, 1 mM PMSF and traces of DNase(21). Glass beads (300 mg, acid-washed, ≤ 106 µm, Sigma G4649) were added to each 1 ml culture and the cells were disrupted with a

Fast Prep device for two times 20 seconds at force 6 with five minutes cooling on ice in between. 40 µl of the supernatant were taken and sodium dodecyl sulfate-polyacrylamide gel electrophoresis (SDS-PAGE) loading dye was added. The samples were separated by SDS-PAGE and the gels were then analysed in a LAS-3000 imaging system (Fujifilm). The Precision Plus Protein^{TM} Dual Color Standards (Bio-Rad) was loaded as size marker. The two bands at 25 kD and 75 kD are colored and show a fluorescence signal (Figure 2).

2.2.6 Comparison of expression levels and purification yields of selected GFP-constructs

The five best expressing transporter-GFP fusion constructs were transformed in C43(DE3) and the proteins were expressed as described above, but this time in 1.2 litre expression cultures. pBXC3GH_Dtur, pBXC3GH_EF2, pBXC3GH_LmrCD, pBXC3GH_TM287/288, pBXC3GH_BmrCD were selected for this experiment. The cells were lysed by three passages through a French press in 20 mM Tris pH 8, 200 mM NaCl. The buffer was additionally supplemented with 2 mM $MgCl_2$ and DNase (Sigma). Undisrupted cells were removed by centrifugation at 8'000 rpm for 15 min in a SS34 rotor. Cell membranes were obtained by ultracentrifugation in a Beckman Ti70 rotor at 40'000 rpm for 40 min. This pellet was then resuspended in 50 mM Tris pH 7.4, 150 mM NaCl and 10 % (v/v) glycerol and solubilized by the addition of 1.5 % (w/v) n-dodecyl-β-D-maltopyranoside (β-DDM, Glycon) for 2 hours. Unsolubilized material was removed by ultracentrifugation for 30 min at 45'000 rpm. The soluble supernatant was loaded onto Ni^{2+}-NTA agarose gravity flow columns (Qiagen). The columns were then washed with 30 mM imidazole pH 7.5, 200 mM NaCl, 10 % (v/v) glycerol and 0.03 % (w/v) β-DDM. The transporters were eluted from the column with 200 mM imidazole pH 7.5, 200 mM NaCl, 10 % (v/v) glycerol and 0.03 % (w/v) β-DDM. Protein from the same amount of cells were separated by SDS-PAGE and analysed via *in gel* fluorescence in the LAS-3000 imaging system, as described above and Coomassie staining (Figure 3).

2.2.7 Expression vector pBAD24_duet for $PatAB_{His}$ and $PatA_{His}B$ expression

Two primers were designed to amplify the regulatory elements from pBAD24, which include the AraC binding sites, the promoter sequence and the Shine Dalgarno sequence. The forward primer inserts a SalI restriction site. The reverse primer was initially designed to be 133 base pairs (bp) long and was therefore divided into two smaller, overlapping primers. Reverse primer 1 inserts a 3C PreScission protease cleavage site and a deca-His-tag. The first PCR with the pBAD24_duet forward primer and the pBAD24_duet reverse primer 1 amplifies a product of 384 bp. This fragment was purified from an agarose gel and used for the second PCR with the primers pBAD24_duet forward and the pBAD24_duet reverse primer 2. The second reverse primer inserts a HindIII, a SbfI and a KpnI restriction enzyme site, plus a glycine-serine linker. The resulting fragment from the second PCR had a length of 439 bp. The second, purified PCR fragment plus the vector pBAD24 were SalI and HindIII digested and ligated to yield the pBAD24_duet vector. The two genes *patA* and *patB* were cloned in the two possible combinations $PatAB_{His}$ and $PatA_{His}B$ into this arabinose-based expression vector via the restriction sites NcoI/XmaI and KpnI/SbfI, respectively. First, the fragment with the flanking two restriction sites NcoI/XmaI was ligated. This removes a KpnI site, which is a prerequisite that the

second KpnI/SbfI fragment can be ligated. The primers for the amplification of the two genes *patA* and *patB* and the primers for the pBAD24_duet construction are listed below. A summary of the cloning procedure is given in Figure 4.

pBAD24_duet forward:

5'-ATATGTCGACAGAAACCAATTGTCCATATTGCATCAGACATTGCCG-3'

pBAD24_duet reverse primer 1:

5'-CCCTGGAACAGAACTTCTAGATGATGGTGATGGTGATGGTGATGGTGATGGCTCATGGTGAAT

TCCTCCTGCTAGCCC-3'

pBAD24_duet reverse primer 2:

5'-ATATAAGCTTCCTGCAGGGGTACCAGAACCGCCACCGCCGCCGGAACCACTCGGCCCCTGGA

ACAGAACTTCTAG-3'

$\underline{\text{PatAB}_{\text{His}}}$ from *Streptococcus pneumoniae R6*:

PatA: 5'-ATATCCATGGGCCTGATTCAGAAAATAAAAACC-3'

5'-ATATCCCGGGTCATTTCTGTGTTTCATAGATTTCACGG-3'

PatB: 5'-ATATGGTACCAAGACAGTTCAATTTTTTTGGC-3'

5'-ATATCCTGCAGGTTATTCGAAAACAAATTGATTGTG-3'

$\underline{\text{PatA}_{\text{His}}\text{B}}$ from *Streptococcus pneumoniae R6*:

PatA: 5'-ATATGGTACCCTGATTCAGAAAATAAAAACC-3'

5'-ATATCCTGCAGGTCATTTCTGTGTTTCATAGATTTCACGG-3'

PatB: 5'-ATATCCATGGGCAAGACAGTTCAATTTTTTTGGC-3'

5'-ATATCCCGGGTTATTCGAAAACAAATTGATTGTG-3'

2.2.8 Expression and purification of the pBXNH3 constructs

The pBXNH3 constructs were transformed into *E. coli* C43(DE3) cells and the proteins were expressed and purified as described above for the pBXC3GH constructs. After elution from the Ni^{2+}-NTA column the protein was concentrated to 2.5 ml using an Amicon Ultra-4 or Ultra-15 concentrator unit (Millipore) with a molecular weight cut-off of 50 kDa and then incubated over night with 3C PreScission protease (1:10 (w/w), GE healthcare) at 4 °C. After the digest, the transporter samples were desalted (PD-10, Amersham Biosciences) to remove imidazole. Afterwards the proteins were reloaded on a Ni^{2+}-NTA column to remove the cleaved deca-His affinity tag and the hexa-His affinity tagged 3C protease. To recapture the transporters quantitatively from the rebinding step, 30 mM imidazole had to be added to the elution buffer. The protein was then concentrated and separated by

size exclusion chromatography (Superdex 200 column (GE Healthcare)) in 20 mM Tris pH 7.5, 150 mM NaCl, 0.03 % β-DDM. Figure 5 shows the SEC profiles of the transporters expressed from the pBXNH3 constructs and Table 1 summarizes the molecular weights of the individual half-transporters.

2.2.9 Limited tryptic digest analysis

To further test the stability of the selected transporters a limited tryptic digest was performed. The purified transporters (2.2 µg) from SEC were mixed with trypsin in ratios 1:5'000, 1:500 or 1:25 (w/w), incubated for 30 minutes at 30 °C and then separated via SDS-PAGE. The gels were analysed by Coomassie Brilliant Blue R-250 staining.

2.2.10 Crystallization and diffraction analysis

After size exclusion chromatography (SEC) the fractions from the main peak of the transporters were combined and concentrated to 14-16 mg/ml using an Amicon Ultra-4 concentrator unit (Millipore) with a molecular weight cut-off of 50 kDa. The proteins were then mixed 1:1 (100 nl droplets) with the mother liquor in MRC 2 Well Crystallization Plates (Swissci) and incubated in a Crystal farm at 20 °C. All described manipulations were performed by the NCCR high throughput Crystallization Facility. Dtur was crystallized in 50 mM Na-acetate pH 5.5, 0.5 M NaCl and 11 % (w/v) poly ethylene glycol (PEG) 4'000. Prior to flash-freezing, the crystals were cryo-protected in mother liquor containing 30 % ethylene glycol (EG, v/v) and 0.03 % β-DDM (w/v). TRQ crystallized in 50 mM glycine pH 9.4, 200 mM $CaCl_2$ and 35 % (v/v) PEG 400. Due to high concentrations of PEG 400, the crystals could be frozen directly without further cryo-protection. Tpet crystallized in 50 mM 2-[(2-amino-2-oxoethyl)-(carboxymethyl)amino]acetic acid (ADA) pH 6.5, 50 mM zinc acetate and 25 % (v/v) PEG 400 and crystals were frozen without further cryo protection. The *Thermotoga* transporter TM287/288 formed crystals in 29 % (v/v) polyethylene glycol (PEG) 400, 50 mM Na-cacodylate pH 5.5 and 100 mM $CaCl_2$ (low $CaCl_2$ form) and by the addition of 3 mM $MgCl_2$ and 2.5 mM AMP-PNP. Another more lens-like crystal form was obtained for TM287/288, but instead of the 100 mM $CaCl_2$, higher concentrations of 300 – 600 mM $CaCl_2$ (high $CaCl_2$ form) and PEG 400 concentrations of 32 – 39 % (v/v) were used. No cryoprotectant was added to freeze the TM287/288 crystals. EF2 crystals were obtained in 100 mM NaCl pH 9.5, 50 mM glycine and 33 % (v/v) PEG 300. These crystals were as well frozen directly. Diffraction data were collected at the protein crystallography beamline X06SA at the Swiss Light Source (SLS) of the Paul Scherrer Institut (PSI) (Figure 9) and processed using the program XDS(27). For Dtur, molecular replacement with a homology model (SWISS-MODEL(24)) based on the structure of TM287/288 using Phaser(25) was successful. For TRQ, molecular replacement using the structure of TM287/288 with manually mutated side-chains (COOT) was performed successfully (Figure 10). The sequence of TRQ obtained from sequencing and the sequence deposited in the databank differ in some amino acid positions. Figure 11 shows the alignment of TM287/288, Tpet and TRQ (sequencing). Molecular replacement with the TM287/288 structure (low $CaCl_2$) was successful for TM287/288 (high $CaCl_2$ form). In addition, a round of refinement using the program PHENIX(26) was performed. The analysis of the crystallographic data is summarized in Table 2.

2.3 Results

2.3.1 Selection of potentially stable LmrCD homologues based on peptide disorder prediction

The expression and purification to homogeneity of the multidrug transporter LmrCD from *Lactococcus lactis* have been described previously (16). However, all our attempts to crystallize this transporter, when purified from *Lactococcus lactis* or *Escherichia coli* membrane vesicles did not result in crystals. To search for homologues more suitable to x-ray crystallography we performed a protein blast (blastp) using the primary sequence of LmrC as the query sequence (Material and Methods)(17). The *lmrD* gene directly follows *lmrC* on the chromosome and the two genes constitute an operon. The genes of some half-transporters even overlap. Figure 1a shows two examples of such a bicistronic arrangement. The output from the blast search, minimized to 45 non-redundant sequences from different organisms or strains, was further analysed by the online bioinformatics tool RONN that predicts natively disordered regions of proteins(18). Based on sequence analysis by RONN the number of possible constructs could be decreased to 25 (Materials and Methods). The last selection criterion was the availability of genomic DNA, which again restricted the number of homologues to a total of twelve. The finally chosen homologues for further biochemical analysis were TM287/288 from *Thermotoga maritima*, Tpet624/625 from *Thermotoga petrophila* (Tpet), TRQ2649/650 from *Thermotoga sp. RQ2* (TRQ), CTN396/397 from *Thermotoga neapolitana* (CTN), EF583/584 from *Enterococcus faecalis* (EF1), EF789/790 from *Enterococcus faecalis* (EF2), Lwe2699/2700 from *Listeria welshimeri* (Lwe), YheHI from *Bacillus subtilis* (BmrCD), Dtur641/642 from *Dictyoglomus turgidum* (Dtur), DICT477/478 from *Dictyoglomus thermophilum* (DICT), LGAS525/526 from *Lactobacillus gasseri* (LGAS) and PatAB from *Streptococcus pneumoniae*. The identities to LmrCD (%) of the above listed transporters are shown in Table 1 and a phylogenetic tree is shown in Figure 12.

2.3.2 GFP-fusion proteins and *in gel* fluorescence

Recombinant membrane protein production for functional and structural studies is often hampered by low expression levels(19). Therefore the proteins often have to be expressed in large fermented cultures or well expressing and stable homologues have to be found. The evaluation of expression levels of a broader ensemble of proteins of interest (POIs) is often performed at smaller scale. The standard technique for the detection of such small amounts of protein is typically Western blotting, which is however comparatively time consuming and relies on good antibodies. We decided to use a high-throughput *in gel* fluorescence detection method, which is based on the GFP-fusion expression vector pBXC3GH(20). The resulting translated protein is schematically shown in Figure 1b (upper panel). This construct combines the detection of properly folded protein monitored by GFP-fluorescence with the SapI restriction enzyme dependent one cup fragment exchange (FX) cloning technique(20, 21). pBXC3GH is a derivate of pBAD24 and is therefore L-arabinose inducible. Figure 2 shows the small scale expression tests using three different inducer concentrations. The evaluated transporters are TRQ, BmrCD, Tpet, CTN, EF2, LGAS, DICT, Dtur, TM287/288 and Lwe. An expression level variability is visible on the gels that seems to be dependent on the inducer

concentration. TM287/288 for example shows a significant difference of the expression level between the different inducer concentrations. At a concentration of 10^{-5} % L-arabinose the induction is too weak. At a concentration of 10^{-3} L-arabinose the yield is significantly higher. If one increases the inducer concentration again by a factor one hundred, the expression decreases again which is most probably the result of an overload of the folding machinery, resulting in major amounts of badly folded protein which does not insert into the membrane. Dtur and EF2 are other examples behaving in a similar way as TM287/288.

The best expressing homologues Dtur, EF2, TM287/288, BmrCD and LmrCD were subsequently expressed at larger scale (1.2 l culture), purified by Ni^{2+}-NTA and separated via SDS-PAGE. Protein purified from the same amount of cells was loaded on the polyacrylamide gel. Figure 3 shows purified transporters by *in gel* fluorescence and Coomassie staining. LmrCD and TM287/288 appear to be expressed at a lower level than the other three transporters. All five transporters were purified as stable heterodimers by virtue of a His-tagged GFP fused to the C-terminus of the second half-transporter (Figure 1b).

2.3.3 The construct pBAD24_duet for $PatAB_{His}$ and $PatA_{His}B$ expression

The two genes *patA* and *patB* are arranged differently than the genes of the other analysed transporters (Figure 1a), because they are separated by a transposable element on the genomic DNA (gDNA). Therefore the genes had to be amplified separately and not as a single bicistronic cassette. For the expression of $PatAB_{His}$ and $PatA_{His}B$ a special vector, named pBAD24_duet was designed (Materials and Methods). This vector allows for the coexpression of two genes from the same plasmid. Therefore a vector with two arabinose-inducible promoters (pBAD) both containing the regulatory AraC binding sites and the ribosome binding site (RBS) upstream of the promoter was constructed. Figure 4 summarizes the whole cloning procedure. The pBAD24_duet expression vector for $PatAB_{His}$ and $PatA_{His}B$ does not produce GFP-fusion proteins.

2.3.4 pBXNH3 expression vector

pBXNH3, a further FX-expression vector described in Geertsma *et al*. was additionally tested for LmrCD expression(20). The expression in this construct increased the expression levels of all tested proteins by a factor of at least two to three as compared to the pBXC3GH constructs (data not shown). In addition, 3C protease cleavage of an N-terminal His-tagged protein results in a shorter remaining overhang compared to a C-terminal His-tagged protein. Therefore the transporters CTN, Tpet, BmrCD, DICT, Dtur, TRQ, TM287/288, EF1 and EF2 were additionally cloned into pBXNH3. A schematic overview of a translated protein expressed from the pBXNH3 construct is shown in Figure 1b (lower panel). Lwe and LGAS were omitted for this analysis, because these two homologues did not show an appropriate expression level in the initial expression tests (Figure 2). All other nine transporters plus LmrCD were expressed and purified. In addition to the affinity column a size exclusion chromatography (SEC) step was added to the purification protocol. Furthermore the deca-His-tag was cleaved off by 3C PreScission protease. Figure 5 shows the gelfiltration runs for all the ten transporters that were considered for crystallization experiments. Most of these transporters elute as a monodisperse peak from the gelfiltration column corresponding to the molecular weight of a

heterodimer and fractions of the main peak were used for further proteolytic digest analysis or crystallization experiments.

2.3.5 Limited tryptic digest

Limited tryptic proteolysis is a simple method to test for stability and degradation of a protein(22). Preferably, highly accessible loops containing lysines or arginines are cleaved. Nine of the ten transporters were analysed by limited tryptic digestion. SEC-purified transporter samples were used for this experiment (upper gel, Figure 6). The dimers are highlighted by a red box. EF2 was not utilized in this analysis. The lower three gels in Figure 6 show the Coomassie stained SDS-PAGE gels from the tryptic digest analysis performed at increasing trypsin concentrations while the amount of each transporter was kept constant. There are two bands in all lanes running at a molecular weight higher than 70 kDa. These bands stem from two impurities purified along with all the transporters under investigation. The higher band presumably represents AcrB, a multidrug pump from *Escherichia coli*(23). The identity of the lower band is not known and was not investigated further. Most of the heterodimeric transporters show two bands on the SDS-PAGE gel (upper gel). CTN and EF1 are the two exceptions. In these cases, the monomers of the heterodimers either exhibit identical electrophoretic mobility, or the untagged chain B of the heterodimer was lost during purification. The SEC retention volume, corresponding to the molecular mass of a dimer rather supports the first assumption, namely an indistinguishable electrophoretic mobility (Figure 5). However, the purification of Chain A-homodimers cannot be excluded based on this analysis. For LmrCD only the upper band (LmrD) is clearly visible and the lower band (LmrC) is stoichiometrically underrepresented at 1:5000 trypsin to protein ratio. This is a known phenomenon and can be explained by the degradation of LmrC, visible in the additional bands in this lane (Seeger *et al.*, unpublished). At a trypsin to protein ratio of 1:500, CTN and EF1 are further degraded and LmrC has totally disappeared. All the other transporters show only minor degradation. At a trypsin to protein ratio of 1:25, Tpet, TRQ, TM287/288 still show the characteristic two bands and DICT and Dtur are only partially degraded. Interestingly, four of these five highly trypsin-resistant transporters could be crystallized and showed diffraction around 10 Å or better. This analysis is shown below.

2.3.6 Expression and SEC runs of the $PatAB_{His}$ and $PatA_{His}B$ constructs

As described above, we had to construct a special expression vector, named pBAD24_duet for the production of PatAB having the deca-his-tag attached either to PatA ($PatA_{His}B$) or PatB ($PatAB_{His}$) (Figure 4). Figures 7a-c show the Ni^{2+}-NTA, the SEC purification and the tag-cleavage of $PatA_{His}B$ and $PatAB_{His}$. When expressing $PatAB_{His}$ the two chains exhibit a different electrophoretic mobility on the SDS-PAGE (62250.7 kDa and 66445.8 kDa). In $PatA_{His}B$, where the tag, the cleavage site and the linker are connected with PatA, the two chains (65297.9 kDa and 65718.1 kDa) are inseparable with the method used (Figure 7a). Figure 7b shows the 3C PreScission protease cleavage experiments of $PatA_{His}B$ and $PatAB_{His}$. In this analysis it becomes apparent that $PatA_{His}B$ effectively consists of two chains (lane 2). Two additional bands with a calculated molecular weight of 49427.5 kDa and 17036.2 kDa for $PatAB_{His}$, 48699.9 kDa and 17036.2 kDa for $PatA_{His}B$, respectively, can be observed in both lanes were the protease (calculated molecular weight: 21674.8 kDa) was added. These bands result

from the unspecific cleavage of PatB by the 3C protease. Both, uncleaved $PatA_{His}B$ and $PatAB_{His}$ show a monodisperse peak in SEC (Figure 7c). Figure 7d shows the sequence of PatB from $PatAB_{His}$ and highlights, C-terminal to the deca-his-tag, the 3C protease recognition site (LEVLFQGP) in red. The cleavage site is indicated by a blue vertical line. A second, non-canonical 3C cleavage site (..VLF.G.) further downstream is highlighted in red and a possible cleavage site is indicated in blue. Partial cleavage of this non-canonical cleavage site results in the two additional cleavage products seen in Figure 7b.

2.3.7 Crystallization and diffraction analysis

Ni^{2+}-NTA purified, tag-cleaved and SEC-purified Tpet, TRQ, TM287/288, DICT, Dtur, BmrCD and EF2 were set-up for crystallization experiments using the in house NCCR crystallization facility. Dtur, TRQ, Tpet, TM287/288 and EF2 all formed diffracting protein crystals. Figure 8 shows the obtained crystals for all these homologues. The crystals were fished and flash-frozen in liquid nitrogen and measured at the Swiss Lightsource (SLS) of the Paul Scherrer Institut (PSI) (Materials and Methods). Figure 9 shows the diffraction patterns collected for Dtur, TRQ, Tpet, TM287/288 and EF2, respectively. For TM287/288 two different crystal forms were obtained, one at high and the other at low $CaCl_2$ concentration, belonging to different space groups. Dtur diffracted to 7.4 Å, TRQ to 3.6 Å, Tpet to about 8.5 Å, TM287/288 (low $CaCl_2$ form) to 2.9 Å, TM287/288 (high $CaCl_2$ form) to 4.6 Å and EF2 to about 14.5 Å. For Dtur, TRQ and TM287/288, complete datasets were collected that allowed for data processing and determination of the space group. For TM287/288 (low $CaCl_2$ form) the structure could be solved, which is described in Chapter 3(11). Table 2 summarizes the molecular replacement and refinement results. Figure 10 shows the arrangement of the heterodimers Dtur versus TRQ and versus TM287/288 (high $CaCl_2$ form).

2.4 Discussion

Membrane proteins and especially membrane transporters are a class of proteins that are difficult to produce and even more difficult to crystallize. This is because transporters are very flexible which is a prerequisite to full-fill their task in cycling from one conformation into another one to shuttle their substrate across the plasma membrane. A successful strategy to crystallize a certain membrane protein of interest is to clone and express many homologous proteins to search for those with favourable biophysical and biochemical properties. High-throughput cloning methods facilitate the construction of the large number of necessary genetic constructs. We were interested in obtaining structural and functional information for a special class of ABC exporters, namely the subclass of heterodimeric exporters. We selected the well-characterized prokaryotic heterodimeric ABC transporter LmrCD for *Lactococcus lactis* as our starting molecule. However all attempts to crystallize LmrCD purified from *Lactococcus lactis* or from *Escherichia coli* membrane vesicles did not result in any crystals. For this reason we searched for a more stable homologue with better biophysical properties. After searching for suitable homologues in the databank, performing a disorder prediction and a limited tryptic digest analysis we cloned several transporters using the high-throughput fragment exchange (FX) cloning technique. With this attempt we were able to express and purify 13 transporters and were able to crystallize almost half of them. However, the three *Thermotoga* transporters (TRQ,

Tpet and TM287/288) share a high sequence identity (Figure 11 and Figure 12) and TRQ was crystallized in the same space group with similar cell edges as TM287/288. Therefore, these *Thermotoga* transporters should be regarded as one hit only. We were able to solve the structure of the heterodimeric ABC exporter TM287/288 from *Thermotoga maritima* at a resolution of 2.9 Å. This was the first structure solved from the subclass of heterodimeric ABC transporters(11) and now serves as a model system to study ABC exporters of pathogenic bacteria (PatAB, EF1, EF2) and medically relevant eukaryotic transporters such as Tap1/2, MRP1, CFTR and SUR1.

2.5 Bibliography

1. Krogh, A., B. Larsson, G. von Heijne, and E.L. Sonnhammer, *Predicting transmembrane protein topology with a hidden Markov model: application to complete genomes.* J Mol Biol, 2001. 305(3): p. 567-80.
2. Overington, J.P., B. Al-Lazikani, and A.L. Hopkins, *How many drug targets are there?* Nat Rev Drug Discov, 2006. 5(12): p. 993-6.
3. Hellmich, U.A. and C. Glaubitz, *NMR and EPR studies of membrane transporters.* Biol Chem, 2009. 390(8): p. 815-34.
4. Piddock, L.J., *Multidrug-resistance efflux pumps - not just for resistance.* Nat Rev Microbiol, 2006. 4(8): p. 629-36.
5. Higgins, C.F., *ABC transporters: from microorganisms to man.* Annu Rev Cell Biol, 1992. 8: p. 67-113.
6. Gottesman, M.M. and V. Ling, *The molecular basis of multidrug resistance in cancer: the early years of P-glycoprotein research.* FEBS Lett, 2006. 580(4): p. 998-1009.
7. Ramaen, O., N. Leulliot, C. Sizun, N. Ulryck, O. Pamlard, J.Y. Lallemand, H. Tilbeurgh, and E. Jacquet, *Structure of the human multidrug resistance protein 1 nucleotide binding domain 1 bound to Mg2+/ATP reveals a non-productive catalytic site.* J Mol Biol, 2006. 359(4): p. 940-9.
8. Garvey, M.I., A.J. Baylay, R.L. Wong, and L.J. Piddock, *Overexpressionand patB, which encode ABC transporters, is associated with fluoroquinolone resistance in clinical isolates of Streptococcus pneumoniae of patA* Antimicrob Agents Chemother, 2011. 55(1): p. 190-6.
9. Lubelski, J., A. de Jong, R. van Merkerk, H. Agustiandari, O.P. Kuipers, J. Kok, and A.J. Driessen, *LmrCD is a major multidrug resistance transporter in Lactococcus lactis.* Mol Microbiol, 2006. 61(3): p. 771-81.
10. Locher, K.P., *Review. Structure and mechanism of ATP-binding cassette transporters.* Philos Trans R Soc Lond B Biol Sci, 2009. 364(1514): p. 239-45.
11. Hohl, M., C. Briand, M.G. Grütter, and M.A. Seeger, *Crystal structure of a heterodimeric ABC transporter in its inward-facing conformation.* Nat Struct Mol Biol, 2012. 19(4): p. 395-402.

12. Hunt, J.F., C. Wang, and R.C. Ford, *Cystic fibrosis transmembrane conductance regulator (ABCC7) structure.* Cold Spring Harb Perspect Med, 2013. 3(2): p. a009514.

13. Aittoniemi, J., C. Fotinou, T.J. Craig, H. de Wet, P. Proks, and F.M. Ashcroft, *Review. SUR1: a unique ATP-binding cassette protein that functions as an ion channel regulator.* Philos Trans R Soc Lond B Biol Sci, 2009. 364(1514): p. 257-67.

14. Hinz, A. and R. Tampé, *ABC transporters and immunity: mechanism of self-defense.* Biochemistry, 2012. 51(25): p. 4981-9.

15. Lewinson, O., A.T. Lee, and D.C. Rees, *The funnel approach to the precrystallization production of membrane proteins.* J Mol Biol, 2008. 377(1): p. 62-73.

16. Yang, Z.R., R. Thomson, P. McNeil, and R.M. Esnouf, *RONN: the bio-basis function neural network technique applied to the detection of natively disordered regions in proteins.* Bioinformatics, 2005. 21(16): p. 3369-76.

17. Geertsma, E.R. and R. Dutzler, *A versatile and efficient high-throughput cloning tool for structural biology.* Biochemistry, 2011. 50(15): p. 3272-8.

18. Geertsma, E.R., M. Groeneveld, D.J. Slotboom, and B. Poolman, *Quality control of overexpressed membrane proteins.* Proc Natl Acad Sci U S A, 2008. 105(15): p. 5722-7.

19. Kabsch, W., *Xds.* Acta Crystallogr D Biol Crystallogr, 2010. 66(Pt 2): p. 125-32.

20. Arnold, K., L. Bordoli, J. Kopp, and T. Schwede, *The SWISS-MODEL workspace: a web-based environment for protein structure homology modelling.* Bioinformatics, 2006. 22(2): p. 195-201.

21. McCoy, A.J., R.W. Grosse-Kunstleve, P.D. Adams, M.D. Winn, L.C. Storoni, and R.J. Read, *Phaser crystallographic software.* J Appl Crystallogr, 2007. 40(Pt 4): p. 658-674.

22. Adams, P.D., P.V. Afonine, G. Bunkoczi, V.B. Chen, I.W. Davis, N. Echols, J.J. Headd, L.W. Hung, G.J. Kapral, R.W. Grosse-Kunstleve, A.J. McCoy, N.W. Moriarty, R. Oeffner, R.J. Read, D.C. Richardson, J.S. Richardson, T.C. Terwilliger, and P.H. Zwart, *PHENIX: a comprehensive Python-based system for macromolecular structure solution.* Acta Crystallogr D Biol Crystallogr, 2010. 66(Pt 2): p. 213-21.

23. Seeger, M.A., A. Mittal, S. Velamakanni, M. Hohl, S. Schauer, I. Salaa, M.G. Grütter, and H.W. van Veen, *Tuning the drug efflux activity of an ABC transporter in vivo by in vitro selected DARPin binders.* PLoS One, 2012. 7(6): p. e37845.

24. Lubelski, J., P. Mazurkiewicz, R. van Merkerk, W.N. Konings, and A.J. Driessen, *ydaG and ydbA of Lactococcus lactis encode a heterodimeric ATP-binding cassette-type multidrug transporter.* J Biol Chem, 2004. 279(33): p. 34449-55.

25. Carpenter, E.P., K. Beis, A.D. Cameron, and S. Iwata, *Overcoming the challenges of membrane protein crystallography.* Curr Opin Struct Biol, 2008. 18(5): p. 581-6.

26. Pingoud, V., W. Grindl, W. Wende, H. Thole, and A. Pingoud, *Structural and functional analysis of the homing endonuclease PI-sceI by limited proteolytic cleavage and molecular cloning of partial digestion products.* Biochemistry, 1998. 37(22): p. 8233-43.

27. Psakis, G., J. Polaczek, and L.O. Essen, *AcrB et al.: Obstinate contaminants in a picogram scale. One more bottleneck in the membrane protein structure pipeline.* J Struct Biol, 2009. 166(1): p. 107-11.

Figure 1

a

...CACTGCAAACCCTATCGAGAGATATATGAATCCCAG
TTTGGAAACGGGGTGATGAACGATGCCTGAGATCAG
AAGAAGGCCACACGGACCAATTTTAGAAAAACCCG...

…AGACAGCAGCTGTTCACTGCGGAAGAAGGGGGAG
CAGGGGCATGAAAATAGGAAAAACGTTATGGAGATAC
GCACTTCTTTATCGAAAATTGCTGATCACAGCCGTC…

b

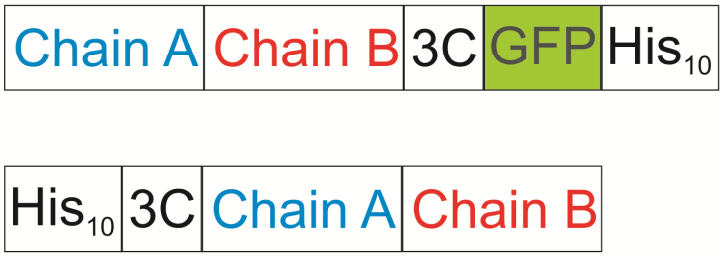

Figure 1:
Operon arrangement and schematic expression construct overview. (a) The operon arrangement of TM287/288 and BmrCD are shown. The nucleotide sequences of Chain A of both transporters are colored in blue. Chains B are highlighted in red. Both chains A end with the Stop codon sequence TGA. Chains B both start with the trinucleotide ATG, which is underlined in the sequence of the preceding Chain A. (b) The composition of the translated proteins resulting from the expression constructs pBXC3GH (upper) and pBXNH3 (lower), used in this work, are schematically shown. Figure 1a and 1b use the same color for Chain A and Chain B.

Figure 2

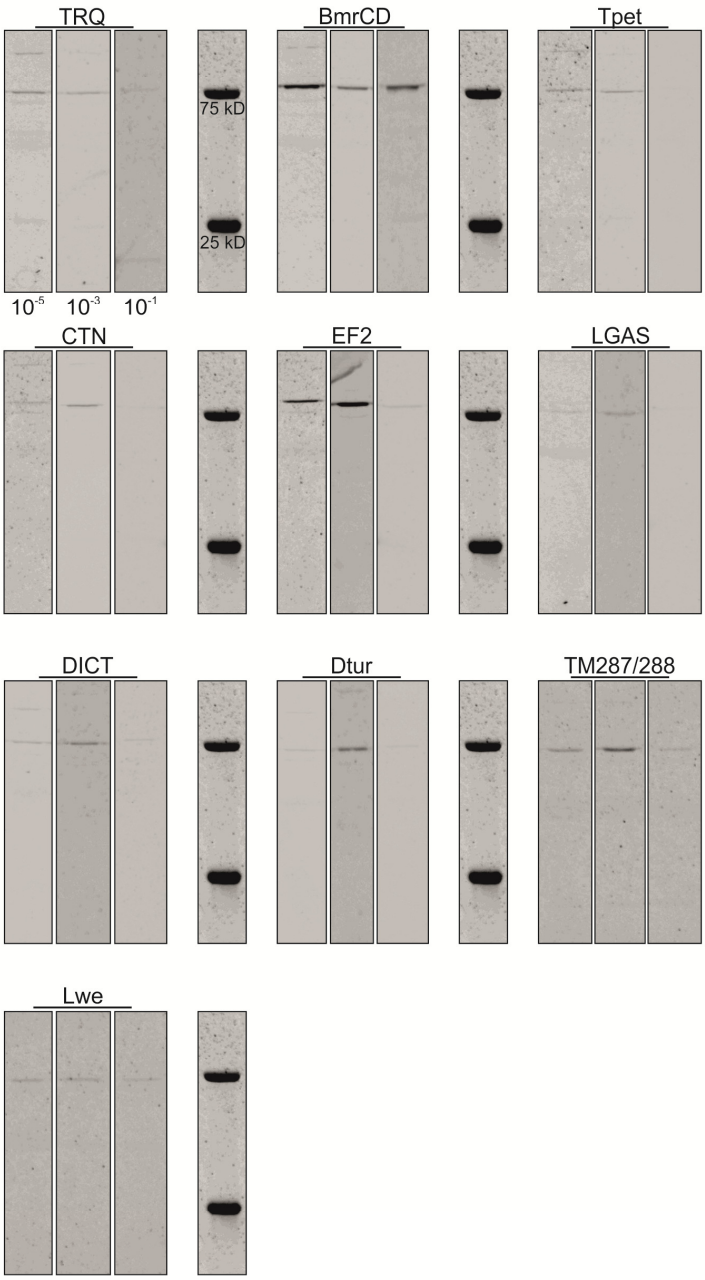

Figure 2:
In gel fluorescence of total proteins obtained from 1 ml cultures expressing heterodimeric ABC transporters fused with a C-terminal GFP. Three different L-arabinose inducer concentrations (10^{-5}, 10^{-3} and 10^{-1} % (w/v)) were tested for all constructs (increasing from left to right). Two bands of the Precision Plus Protein™ Dual Color Standards are fluorescent and indicate a molecular weight of 25 and 75 kDa, respectively.

Figure 3

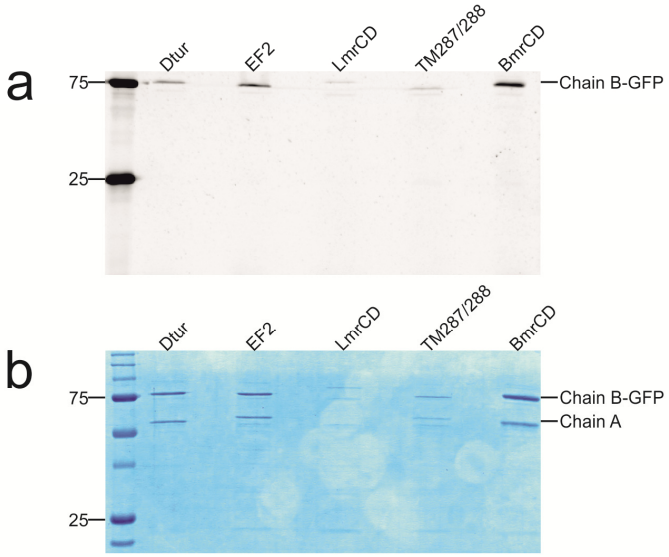

Figure 3:
Purification of five well-expressed heterodimeric ABC transporters expressed using pBXC3GH. (a) *In gel* fluorescence analysis of Dtur, EF2, LmrCD, TM287/288 and BmrCD after separation of purified transporters by SDS-PAGE. (b) Coomassie staining of the purified transporter homologues as in (a). The Precision Plus Protein™ Dual Color Standards was used as size marker.

Figure 4

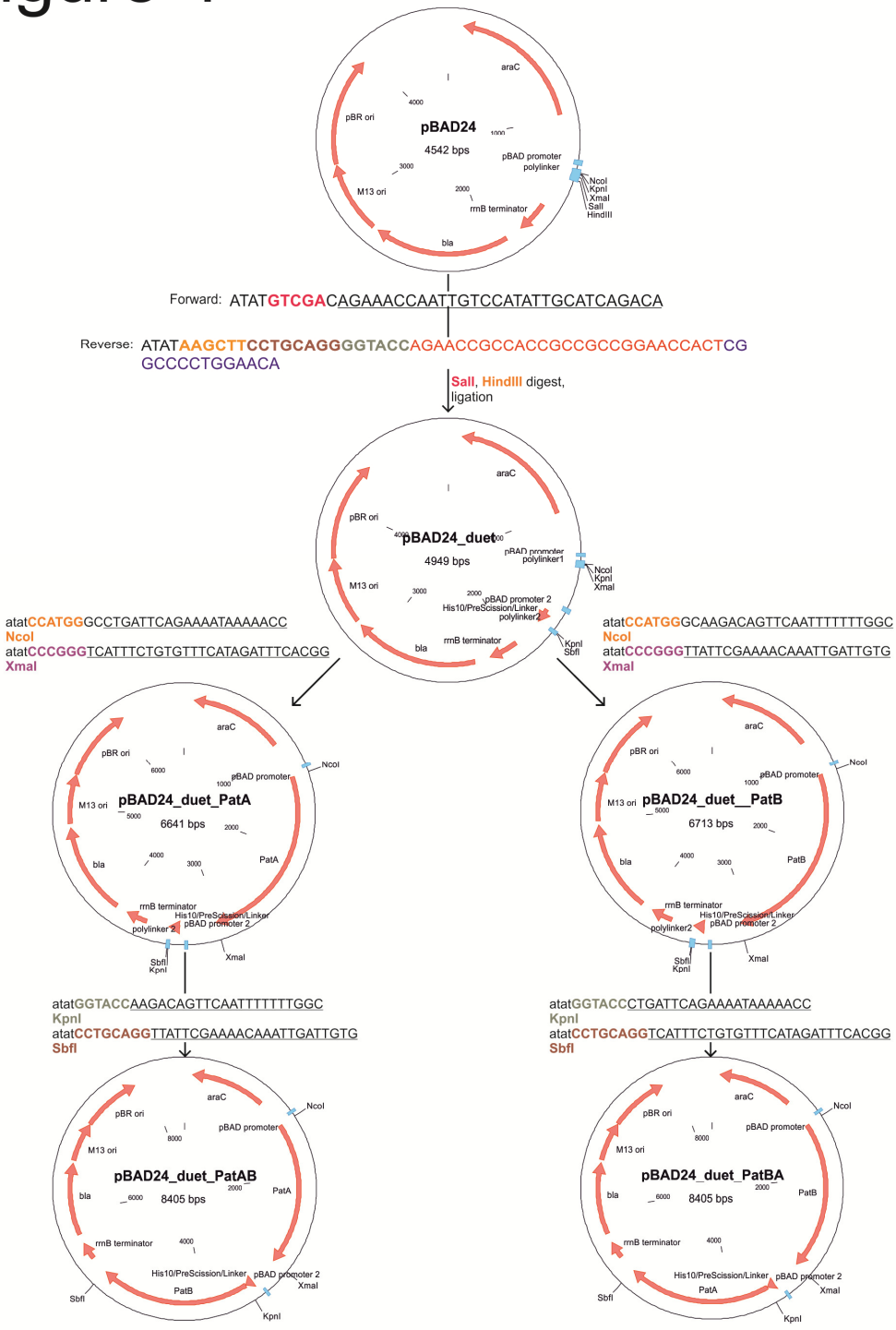

Figure 4:
Vector design for the expression of $PatA_{His}B$ and $PatBA_{His}$. The flow chart shows in a first step the cloning of the L-arabinose inducible expression construct pBAD24_duet. In a second step the cloning of the constructs pBAD24_duet_PatA and pBAD24_duet_PatB is illustrated, leading to the final constructs pBAD24_duet_PatAB and pBAD24_duet_PatBA. The upper primer always represents the forward primer, the lower primer the reverse one. Restriction sites are colored and bold. The underlined bases are the stretches that anneal.

Figure 5

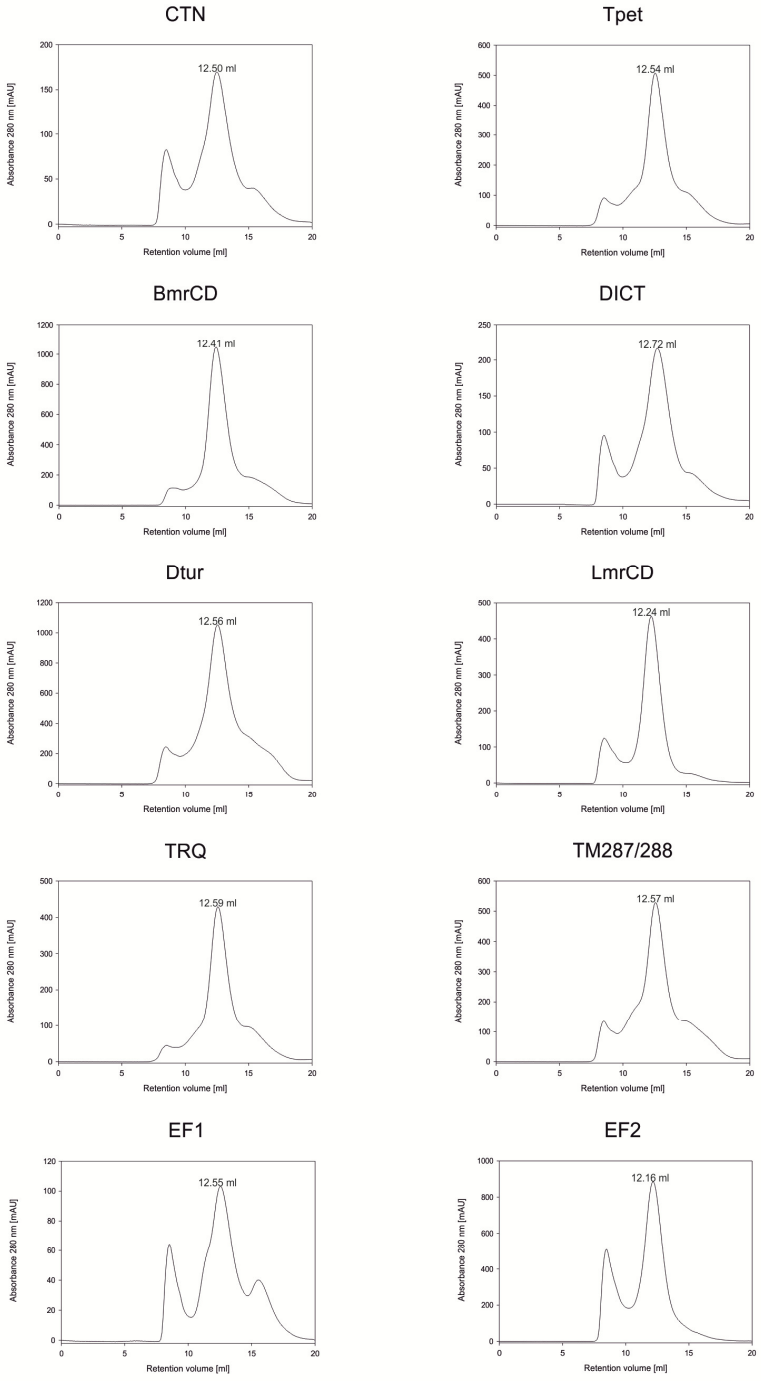

Figure 5:
Size exclusion chromatograms of heterodimeric ABC exporters expressed from the pBXNH3 constructs. Shown are chromatography profiles of CTN, Tpet, BmrCD, DICT, Dtur, LmrCD, TRQ, TM287/288, EF1 and EF2. The retention volume is plotted against the absorbance at 280 nm in milliarbitrary units [mAU]. The retention volume of the main peak maximum, corresponding to the molecular weight of the heterodimer is indicated in millilitre [ml] above the corresponding peak.

Figure 6

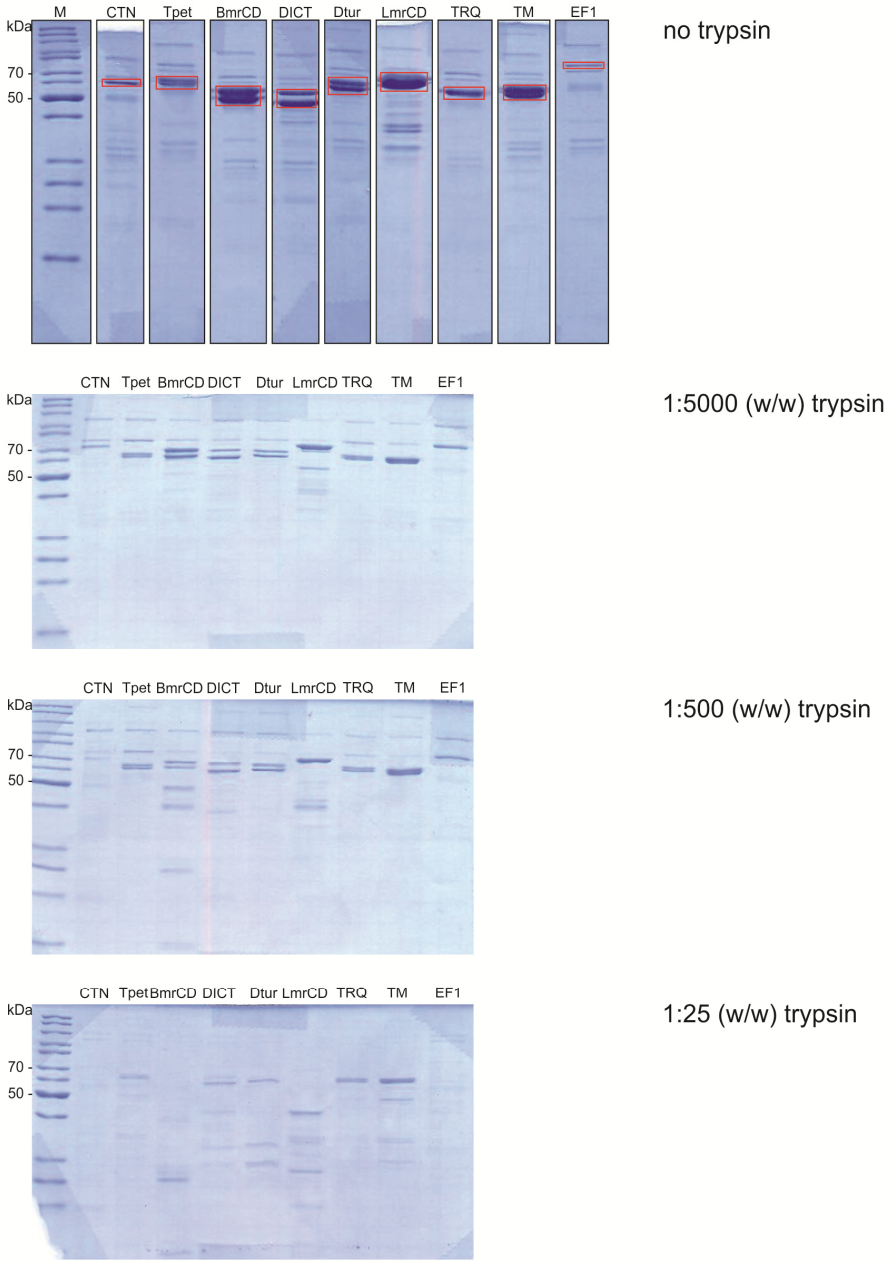

Figure 6:
Limited tryptic digest of ABC exporters under study. The nine purified transporters CTN, Tpet, BmrCD, DICT, Dtur, LmrCD, TRQ, TM287/288 and EF 1 as eluted from SEC were subjected to a limited tryptic digest analysis. The topmost gel shows the proteins before the addition of trypsin. The proteins were mixed in ratios 1:5000, 1:500 and 1:25 (w/w) with trypsin and subsequently analysed by SDS-PAGE (lower three gels). Two bands (50 and 70 kDa) of the PageBlue™ Protein Staining Solution marker are indicated. TM287/288 is abbreviated with TM in this figure. The red boxes highlight the transporter bands.

Figure 7

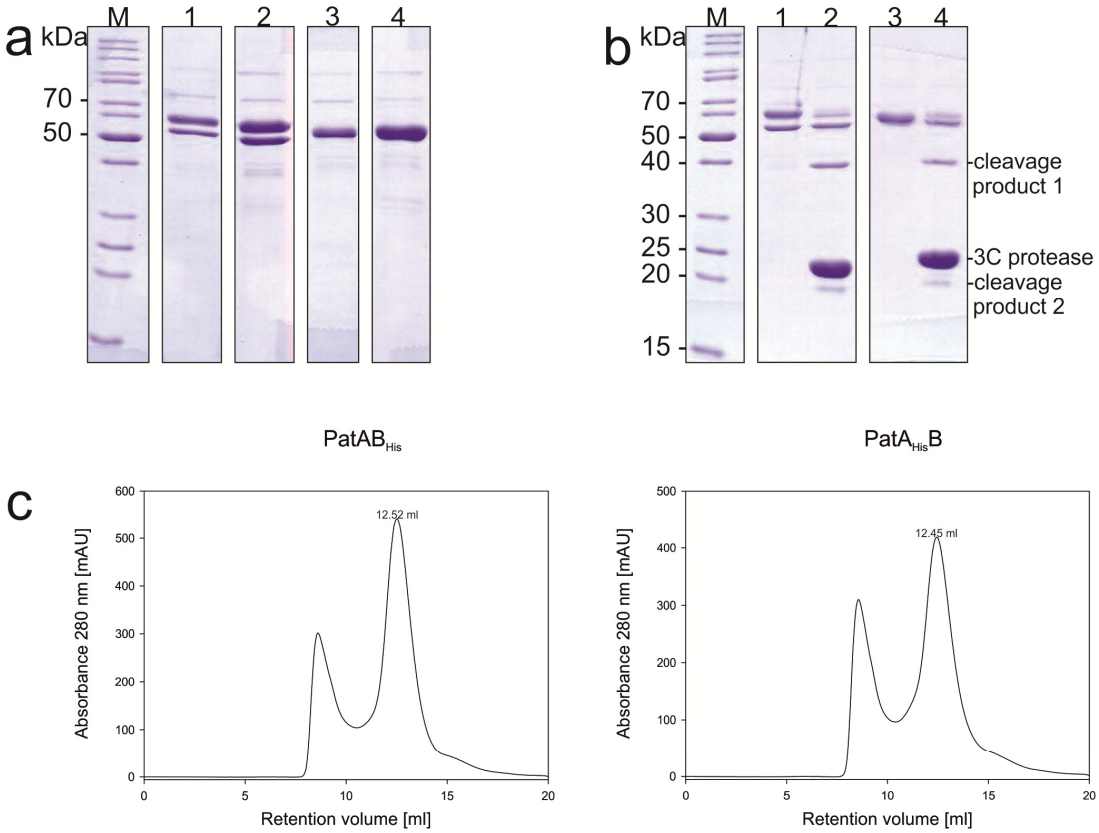

d

MSHHHHHHHHHHLEVLFQ|GPSGSGGGGGSGTKTVQFFWHYFKVYKFSFVVVILMIVLATFAQSLFPV
FSGQAVTQLANLVQAYQNGNPELVWQSLSGIMVNLGLLVLVLFISSVIYMCLMTRVIAESTNEMRKGLF
GKLAQLTVSFFDRRQDGDILSHFTSDLDNILQAFNESLIQVMSNIVLYIGLILVMFSRNVTLALITIASTPLA
FLMLIFIVKMARKYTNLQQKEVGKLNAYMDESISGQKAVIVQGIQEDMMAGFLEQNERVRKATFKGRMF
SGILFPVMNGMSLINTAIVIFAGSAVLLNDKSIETSTALGLIVMFAQFSQQYYQPIIQVAASWGSLQLAFTG
AERIQEMFDAEEEIRPEKAPTFTKLQESVEISHIDFSYLPDKPILKDVSISAPKGQMTAVVGPTGSGKTTI
MNLINRFYDVDAGGIYFDGKDIRGYDLDSLRSKVGIVLQDSVLFS|GTIRDNIRFGVPDASQEMVEVAAK
ATHIHDYIESLPDKYDTLIDDDQSIFSAGQKQLISIARTLMTDPEVLILDEATSNVDTVTESKIQHAMEVVV
AGRTSFVIAHRLKTILNADQIIVLKDGEVIERGNHHELLKLGGFYSELYHNQFVFE

Figure 7:
Expression and purification of PatAB$_{His}$ and PatA$_{His}$B. (a) Different steps of the PatAB$_{His}$ (1-2) and PatA$_{His}$B (3-4) purification are visualized on a SDS-PAGE gel. Lanes 1 and 3 show the elutions from the Ni^{2+}-NTA column of PatAB$_{His}$ and PatA$_{His}$B, respectively. Lanes 2 and 4 are fractions of the main peak from the SEC analysis shown in (c). (b) The SDS-PAGE gel shows the 3C PreScission protease cleavage analysis of PatAB$_{His}$ (1 and 2) and PatA$_{His}$B (3 and 4). Prior to 3C cleavage the two chains of PatAB$_{His}$ are not separated (lane1, see also lanes 3-4 in (a)). After the addition of the 3C protease (lane 2) the two chains can be separated from each other. The 3C protease runs at about 25 kDa. Lane 2 and 4 show additional unspecific cleavage products of PatB, running at a molecular weight of about 40 kDa and 20 kDa, respectively. The PageBlue™ Protein Staining Solution marker is shown. (c) SEC analysis of the purified PatAB$_{His}$ and PatA$_{His}$B. The absorbance at 280 nm in milliarbitrary units [mAU] is plotted against the retention volume [ml]. The peak maximum is indicated. (d) Sequence of PatB from PatAB$_{His}$. In red the two recognition sequences (original (LEVLFQGP) and non-consensus (..VLF.G.)) of the 3C protease are highlighted and the blue vertical line indicates the cleavage site.

Figure 8

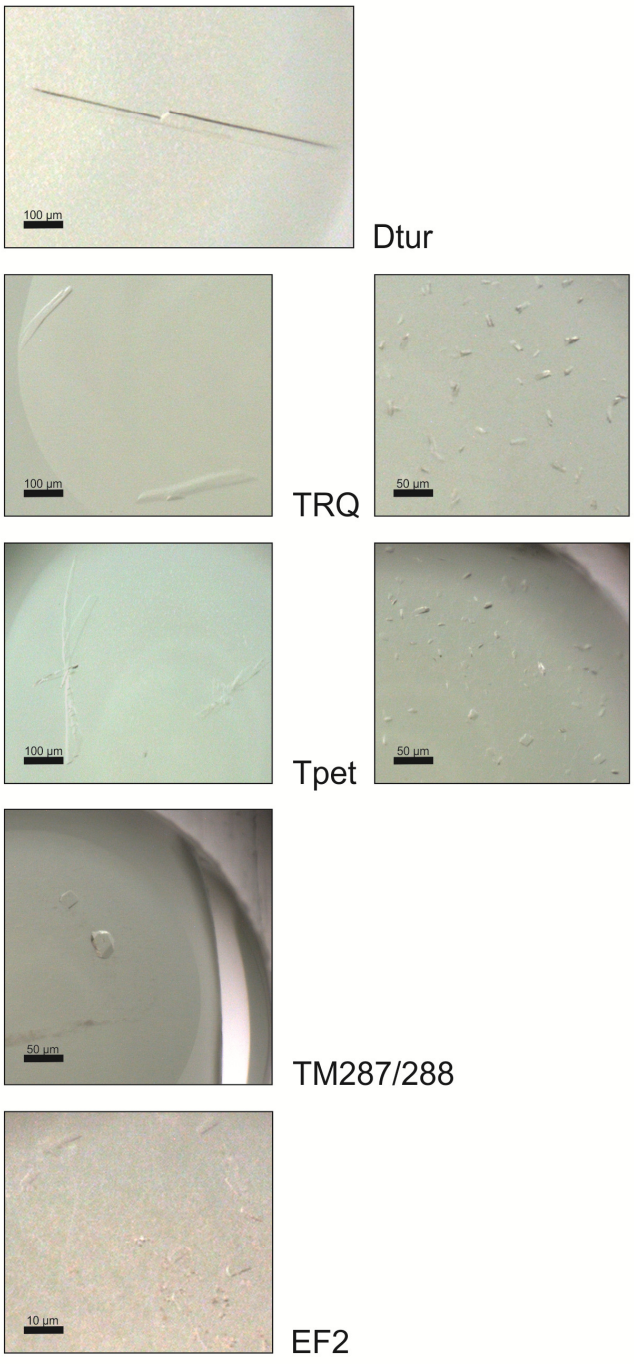

Figure 8:
Crystallization hits of heterodimeric ABC exporters. The initial crystallization hits from the crystallization trials of Dtur, TRQ, Tpet, TM287/288 and EF 2 (from top to bottom) are shown. The approximate sizes of the crystals are indicated by a black bar in the lower left corner of the crystal picture.

Figure 9

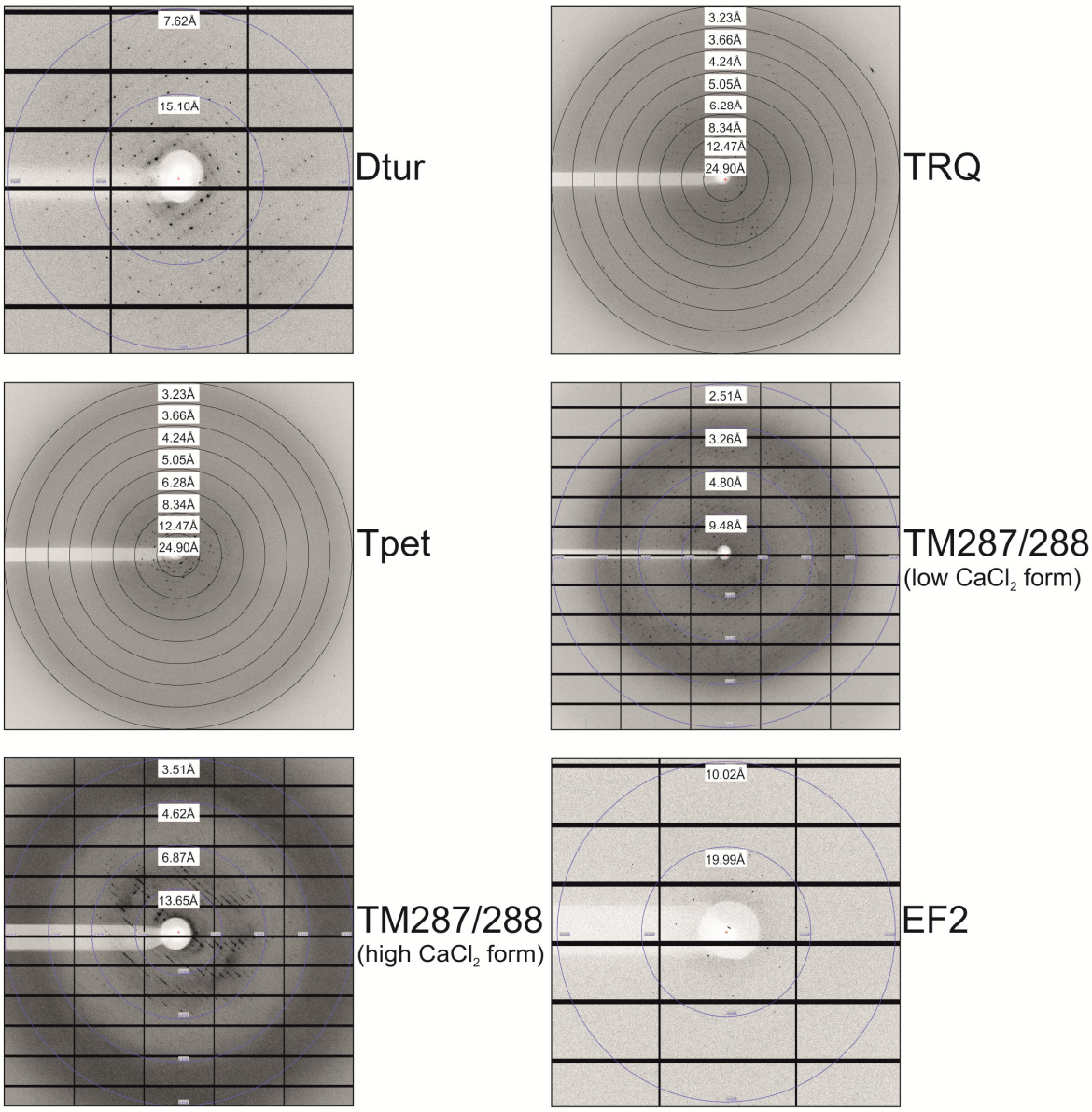

Figure 9:
X-ray diffraction patterns of Dtur, TRQ, Tpet, TM287/288 and EF 2 (top to bottom). Resolution rings are indicated.

Figure 10

Dtur ($P2_1$)

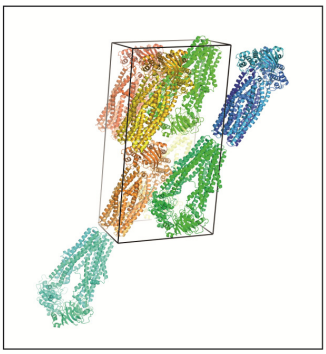

TRQ + TM287/288, low $CaCl_2$, (C2)

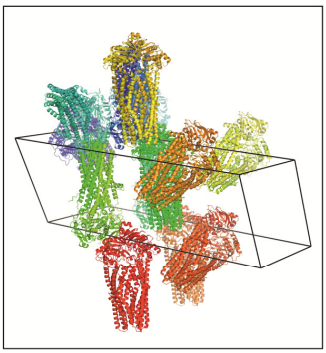

TM287/288, high $CaCl_2$ ($P3_121$)

Figure 10:
Crystal packing analysis. The arrangement of the heterodimeric ABC exporters Dtur, TRQ, TM287/288 (low $CaCl_2$) and TM287/288 (high $CaCl_2$) in the crystals is shown. The unit cell is indicated in black.

Figure 11

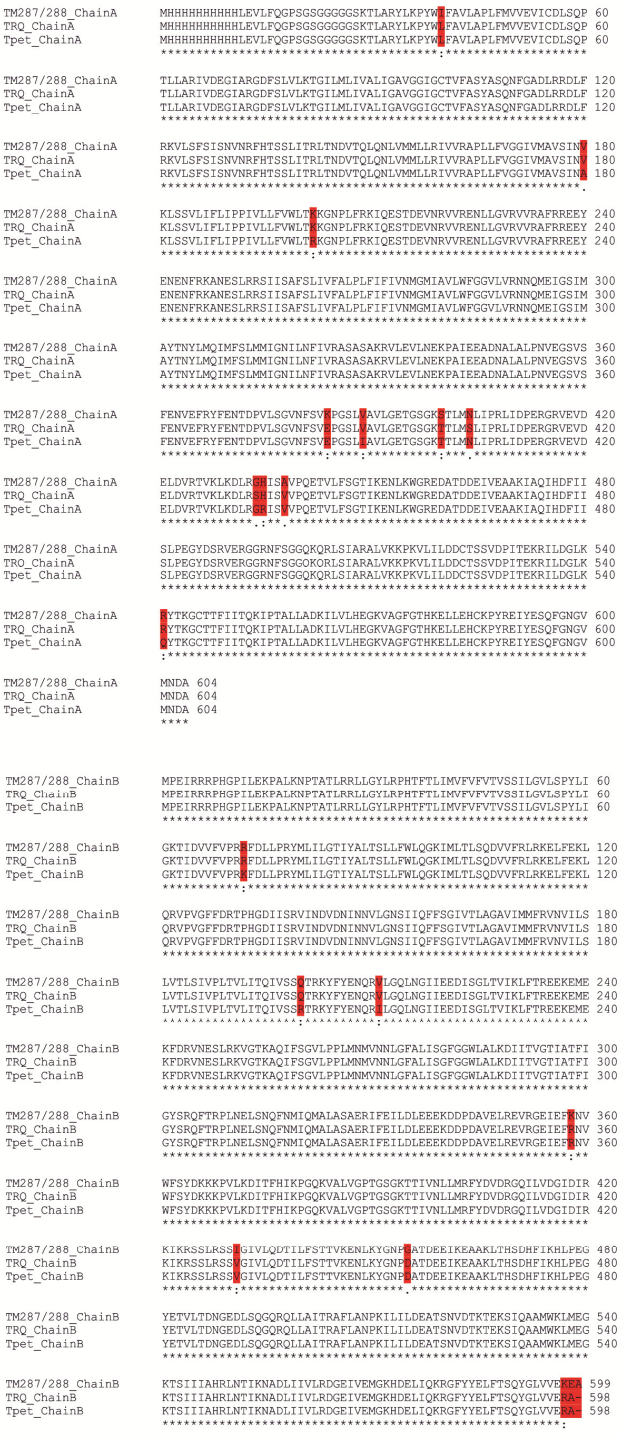

Figure 11:
Alignment of the amino acid sequences of the three closely related *Thermotoga* transporters TM287/288, TRQ and Tpet. In the upper panel, Chains A are aligned. The lower panel shows the alignment of Chains B. The alignment was performed using the program ClustalW. Differences between the sequences of the transporters are highlighted in red.

Figure 12

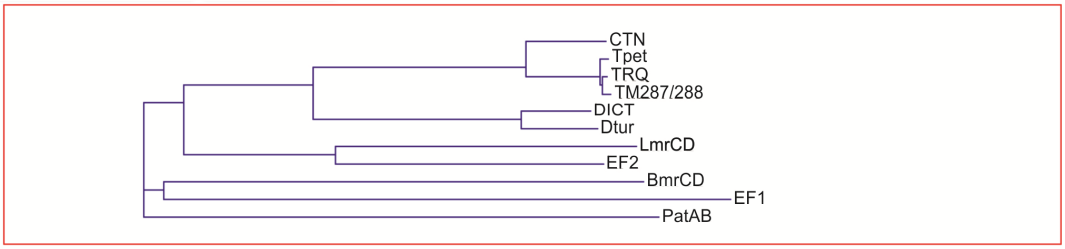

Figure 12:
Phylogram of the alignment of the amino acid sequences of all transporters analysed in this work. The amino acid sequences of the uncleaved pBXNH3 constructs were used. For PatAB the translated amino acid sequence of the pBAD24_duet_PatAB$_{His}$ construct was aligned. The program ClustalW was used.

TABLE 1 | PROTEIN PARAMETERS

Transporter	Identities to LmrCD (%)	RONN (penalty points)	M_w (g/mol) * Chain A (# amino acids)	M_w (g/mol) * Chain B (# amino acids)	Crystallizability
CTN	37.8%	224	67186.4 (604)	67959.3 (598)	-
Tpet	37.8 %	207	67267.4 (604)	67764.2 (598)	+
BmrCD	29.3 %	295	67970.5 (612)	76376.1 (674)	-
DICT	37.8 %	134	67866.1 (604)	70482.1 (621)	-
Dtur	37.3 %	108	67993.1 (604)	70182.8 (621)	+
LmrCD	100 %	329	66733.1 (606)	73997.7 (664)	-
TRQ	37.7 %	208	67297.5 (604)	67750.1 (598)	++
TM287/288	37.7 %	216	67219.4 (604)	67779.2 (599)	++
EF1	25.1 %	115	69097.5 (611)	65700.0 (581)	-
EF2	55.2 %	179	65698.5 (598)	66223.1 (590)	+
$PatAB_{His}$	56.6 %	90	62250.7 (565)	68765.3 (618)	-
$PatA_{His}B$			65297.9 (594)	65718.1 (589)	

*The molecular weights (M_W) are calculated with uncleaved Deca-His-tag.

TABLE 2 | DATA COLLECTION

	Dtur	TRQ	TM287/288 (low $CaCl_2$ form)	TM287/288 (high $CaCl_2$ form)
Data Collection				
Space group	$P2_1$	C2	C2	$P3_121$
Cell dimensions				
a, b, c (Å)	161.91	213.01	216.33	118.15
	93.37	83.81	84.31	118.15
	172.35	111.05	115.78	272.46
α, β, γ (º)	90.000	90.000	90.000	90.000
	99.156	95.315	91.200	90.000
	90.000	90.000	90.000	120.000
Resolution[a)] (Å)	7.4	3.6	2.9	4.7
	(7.59-7.40)	(3.69-3.60)	(2.98-2.90)	(4.82-4.70)
R_{merge} (%)	8.0 (98.2)	10.0 (77.4)	4.8 (71.7)	6.1 (91.9)
I/σ_I	13.76 (2.27)	8.02 (1.77)	24.14 (3.54)	25.07 (4.24)
Completeness (%)	96.8 (99.8)	92.0 (94.2)	99.5 (99.6)	99.8 (100)
Redundancy	6.7 (6.8)	2.7 (2.6)	6.8 (6.8)	19.1 (18.8)
Molecular Replacement				
LLG (log-likelihood gain)	353	4561	n.d.	1182
TFZ (the translation function Z-score)	11.9	18.2	n.d.	24.7
Water content (%)	48.03	66.92	n.d.	70.27
Molecules/ASU (asymmetric unit)	2	1	1	1
Refinement				
R_{work}/ R_{free}	n.d.	24.82/28.98	21.70 / 26.32	31.97/46.36

[a)] Highest resolution shell is shown in parenthesis. Not determined (n.d.)

3 Crystal structure of a heterodimeric ABC transporter in its inward-facing conformation

Crystal structure of a heterodimeric ABC transporter in its inward-facing conformation

Michael Hohl, Christophe Briand, Markus G. Grütter* and Markus A. Seeger*

Nat. Struct. Mol. Biol. 2012 March 25; 19(4):395-402.

*corresponding authors

ARTICLES

nature structural & molecular biology

Crystal structure of a heterodimeric ABC transporter in its inward-facing conformation

Michael Hohl, Christophe Briand, Markus G Grütter & Markus A Seeger

ATP-binding cassette (ABC) transporters shuttle a wide variety of molecules across cell membranes by alternating between inward- and outward-facing conformations, harnessing the energy of ATP binding and hydrolysis at their nucleotide binding domains (NBDs). Here we present the 2.9-Å crystal structure of the heterodimeric ABC transporter TM287–TM288 (TM287/288) from *Thermotoga maritima* in its inward-facing state. In contrast to previous studies, we found that the NBDs only partially separate, remaining in contact through an interface involving conserved motifs that connect the two ATP hydrolysis sites. We observed AMP-PNP binding to the degenerate catalytic site, which deviates from the consensus sequence in the same positions as the eukaryotic homologs CFTR and TAP1–TAP2 (TAP1/2). The TM287/288 structure provides unprecedented insights into the mechanism of heterodimeric ABC exporters and will enable future studies on this large transporter superfamily.

ABC transporters are found in all kingdoms of life. They couple the binding and hydrolysis of ATP to the energy-dependent shuttling of a wide variety of compounds across lipid bilayers[1,2]. In contrast to ABC importers, which are unique to bacteria, ABC exporters exist in both eukaryotes and prokaryotes and transport lipids, chemotherapeutics and even polypeptides out of the cell. They have been associated with multidrug resistance in cancer cells (P-glycoprotein and MRP1), antibiotic resistance in bacteria (PatAB and LmrCD) and common hereditary diseases, such as cystic fibrosis (CFTR) and neonatal diabetes (SUR1)[3–8]. ABC transporters consist of four domains: two transmembrane domains (TMDs), which determine substrate specificity, and two nucleotide-binding domains (NBDs), which dimerize upon binding of two molecules of ATP and disengage as a consequence of ATP hydrolysis[9]. The motional energy gained from the ATP-dependent association and dissociation at the NBDs is transmitted to the TMDs through coupling helices, resulting in conformational changes that orient a substrate binding cavity either to the inside or the outside of the cell membrane[10].

To fulfill their function as motor domains, NBDs feature highly conserved structural motifs. Upon ATP binding, which involves π-stacking of the adenosine moiety with a conserved tyrosine of the A-loop, NBDs tightly dimerize in a head-to-tail arrangement, and both subunits contribute conserved motifs and residues to form two composite ATP binding sites at the dimer interface[11,12] (**Supplementary Fig. 1**). In such a 'closed' NBD dimer, the γ-phosphate moiety of ATP is sandwiched between the Walker A motif of one NBD and the ABC signature motif of the other one and vice versa[13,14]. A highly conserved glutamate of the Walker B motif and a histidine of the switch motif constitute a catalytic dyad for ATP hydrolysis in which the glutamate acts as a general base to activate a water molecule attacking the γ-phosphate of ATP[15–17]. In addition, a conserved glutamine of the Q-loop interacts with the γ-phosphate of ATP and connects the site of catalysis with the coupling helices of the TMDs, whereas the D-loop has been proposed to functionally link the two catalytic sites[10,13,16]. ATP hydrolysis breaks the interaction between the ABC signature motif and the γ-phosphate moiety of ATP and leads to dimer disengagement resulting in an 'open' NBD dimer[18].

Whereas many bacterial ABC exporters, such as LmrA, MsbA, Sav1866 and BmrA, are homodimers, most of the eukaryotic ABC exporters are heterodimers[15,19–22]. About half of the human heterodimeric ABC exporters feature one composite nucleotide binding site in which the catalytically important Walker B glutamate and the switch histidine, as well as the ABC signature motif, deviate from the consensus sequence and is thus referred to as the degenerate site[22]. The second nucleotide-binding site agrees with the consensus sequence of ABC-type NBDs and is therefore denoted as the consensus site.

There are a number of clinically relevant examples of eukaryotic heterodimeric ABC exporters with nonequal nucleotide-binding sites, including CFTR, an ATP-gated chloride channel whose failure is responsible for the common hereditary disease cystic fibrosis[5]; TAP1/2, which transports peptides across the ER-membrane and has a central role in the cellular immune system[23]; and SUR1, which serves as the regulatory subunit of Kir6.2 and has been linked to congenital hyperinsulinism and neonatal diabetes[8]. MRP1 has been associated with chemotherapy failure because it extrudes a wide range of anticancer drugs when expressed in tumor cells[4]. The heterodimeric bacterial ABC exporters LmrCD, PatAB, BmrCD and TmrAB are also capable of drug extrusion[6,7,24,25].

Current molecular understanding of ABC exporters is based on a small number of X-ray structures of varying diffraction data quality.

Department of Biochemistry, University of Zürich, Zürich, Switzerland. Correspondence should be addressed to M.A.S. (m.seeger@bioc.uzh.ch) or M.G.G. (gruetter@bioc.uzh.ch).

Received 5 December 2011; accepted 17 February 2012; published online 25 March 2012; doi:10.1038/nsmb.2267

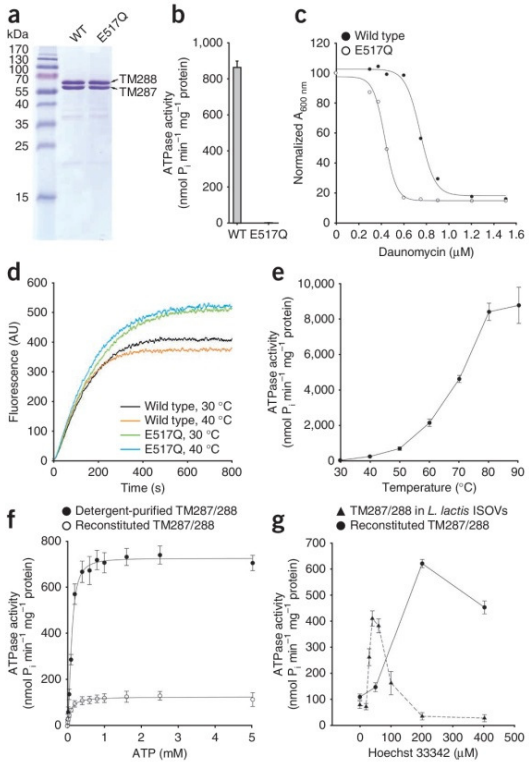

Figure 1 Functional analysis of TM287/288. (**a**) Expression of TM287/288 wild type and mutant (E517Q) is similar in *L. lactis* NZ9000 Δ*lmrA* Δ*lmrCD*, as shown by SDS-PAGE of purified protein from identical amount of cells. (**b**) TM287/288 (E517Q) shows negligible ATPase activity and was used for background subtraction in the following ATPase assays. (**c**) Daunomycin resistance of *L. lactis* NZ9000 Δ*lmrA* Δ*lmrCD* expressing wild-type and mutant (E517Q) TM287/288 ($n = 3$). (**d**) BCECF-AM transport in intact, energized *L. lactis* NZ9000 Δ*lmrA* Δ*lmrCD* expressing wild type and mutant (E517Q) TM287/288 at 30 °C and 40 °C ($n = 3$). Less fluorescence indicates active transport of BCECF-AM. (**e**) Temperature-dependent ATPase activity of detergent-purified TM287/288 determined at temperatures ranging from 30 °C to 90 °C. (**f**) Determination of the apparent nucleotide affinity ($K_{m,app}$) by measuring the ATPase activity of detergent-purified and reconstituted TM287/288 over a range of ATP concentrations. (**g**) Hoechst 33342 stimulates the ATPase activity of membrane-embedded TM287/288 in inside-out membrane vesicles (ISOV) derived from *L. lactis* and reconstituted in *E. coli* polar lipids–egg phosphatidylcholine. Error bars, s.d. AU, arbitrary units; WT, wild type.

The structures of Sav1866 and *Salmonella typhimurium* MsbA solved at resolutions of 3.0 Å and 3.7 Å, respectively, depict outward-facing conformations. In these structures, a large cavity is accessible from the outside of the cell, whereas the NBDs form dimers with two nucleotides bound[10,26,27]. By contrast, the structure of mouse P-glycoprotein (determined at 3.8-Å resolution) and two MsbA structures from *Vibrio cholerae* and *Escherichia coli* (solved at resolutions >5 Å) have been determined in the absence of nucleotides[27,28]. They show an inward-facing cavity accessible from the cytoplasm. The NBDs are spatially completely separated or, in the case of the *V. cholerae* MsbA structure, interact through a yet to be determined protein interface. Here we present the high resolution crystal structure of a heterodimeric ABC exporter bearing nonequal nucleotide binding sites crystallized in its inward-facing state.

RESULTS

Functional analysis and crystallization of TM287/288

In a screen of heterodimeric ABC exporter homologs, we found TM287/288 from the thermophilic bacterium *T. maritima* to be suitable for structure determination. TM287/288 shares 36% sequence identity to LmrCD, a well-characterized heterodimeric ABC exporter from *Lactococcus lactis*. Because LmrCD has been shown to transport Hoechst 33342 and the anticancer drug daunomycin[29], we tested whether TM287/288 was capable of transporting these compounds as well.

In our functional analysis, TM287/288 carrying a single mutation in the Walker B glutamate of the consensus site (E517Q) served as control. With respect to wild-type TM287/288, the mutant was expressed equally well (**Fig. 1a**) but showed only 0.2% of the ATPase activity (**Fig. 1b**). Expression of wild-type TM287/288 in *L. lactis* NZ9000 Δ*lmrA* Δ*lmrCD* increased the cell's resistance toward daunomycin ($IC_{50,dau}$) by a factor of 1.6 ± 0.1 (mean ± s.d.), compared with cells expressing the inactive mutant ($n = 3$) (**Fig. 1c**; see **Supplementary Methods** and ref. 30). The fluorescence increase of 2,7-bis(carboxyethyl)-5(6)-carboxyfluorescein (BCECF, the product of nonfluorescent 2,7-bis(carboxyethyl)-5(6)-carboxyfluorescein-acetoxymethylester (BCECF-AM) hydrolysis by intracellular esterases) in *L. lactis* NZ9000 Δ*lmrA* Δ*lmrCD* cells expressing wild-type TM287/288 was slower than in cells expressing the inactive mutant. This indicated active efflux of BCECF-AM (**Fig. 1d**).

The ATPase activity of detergent-purified TM287/288 was determined at various temperatures, and mutant TM287/288 (E517Q) was used to subtract the background ATP hydrolysis. The ATPase activity increased over the measured range of temperatures showing its maximal value of 8,819 ± 1,013 nmol P_i min^{-1} mg^{-1} protein at 90 °C (**Fig. 1e**). The apparent affinity for ATP was determined by measuring the ATPase activity of TM287/288 at various ATP concentrations at 50 °C, resulting in an apparent affinity ($K_{m,app}$) of 114 ± 6 μM and a maximal activity (V_{max}) of 725 ± 10 nmol P_i min^{-1} mg^{-1} protein (**Fig. 1f**). The same values were also determined for reconstituted TM287/288 for which a slightly higher affinity ($K_{m,app}$ = 80 ± 8 μM) and an 80% lower maximal activity (V_{max} = 126 ± 3 nmol P_i min^{-1} mg^{-1} protein) were observed (**Fig. 1f**). Hoechst 33342, a dye that has been shown to be transported by P-glycoprotein and many other multidrug ABC transporters[31], was found to stimulate the ATPase activity of TM287/288 embedded in inside-out membrane vesicles derived from *L. lactis* (increase of up to 520%) as well as in proteoliposomes (increase of up to 560%) (**Fig. 1g**). The Hoechst 33342–induced ATPase stimulations seen in TM287/288 were of the same order of magnitude as drug-stimulated ATPase activities observed for the well-characterized multidrug transporters P-glycoprotein and MsbA[32,33].

Well-diffracting crystals of wild-type TM287/288 were obtained in the presence of the ATP analog AMP-PNP and belonged to the space group *C*2, containing one TM287/288 heterodimer per asymmetric unit. The structure was solved at 2.9-Å resolution by single-wavelength anomalous dispersion phasing and showed good refinement statistics (R_{work} and R_{free} values of 21.7% and 26.3%, respectively) (**Table 1** and **Supplementary Fig. 2**). With the exception of eight C-terminal residues of TM287 (570–577) and nine N-terminal

Table 1 Data collection and refinement statistics

	Native	SeMet
Data Collection		
Space group	*C*2	*C*2
Cell dimensions		
a, *b*, *c* (Å)	216.33, 84.31, 115.78	215.51, 84.22, 114.93
α, *β*, *γ* (°)	90, 91.2, 90	90, 92.4, 90
Resolution (Å)	2.9 (2.98–2.90)	3.5 (3.59–3.50)
R_{merge} (%)	4.8 (71.7)	8.7 (62.0)
$I / \sigma I$	24.14 (3.54)	17.76 (4.61)
Completeness (%)	99.5 (99.6)	99.8 (99.8)
Redundancy	6.8 (6.8)	10.4 (10.8)
Refinement		
Resolution (Å)	25–2.9	
No. reflections (work / test)	43,939 / 2,313	
R_{work} / R_{free}	21.70 / 26.32	
No. atoms		
Protein	9,166	
AMP-PNP	31	
Mg^{2+}	1	
Water	4	
B-factors		
Protein	118	
Ligand	107	
Ion	66	
Water	46	
R.m.s. deviations		
Bond lengths (Å)	0.003	
Bond angles (°)	0.728	

Values for the highest resolution shell are shown in parentheses.

residues of TM288 (1–9), the complete polypeptide chain of TM287/288 was fitted into the electron density map.

Overall architecture of TM287/288

The TMDs of TM287/288 encompass a total of 12 transmembrane helices that constitute four intracellular loops (ICL1 and ICL2 in TM287 and ICL3 and ICL4 in TM288) and confine a large cavity that is accessible from the cytoplasm (**Fig. 2a**). All four ICLs contain coupling helices roughly parallel to the membrane plane that interact with the NBDs. As first described for Sav1866 (ref. 10), the coupling helices of ICL2 and ICL4 reach across and exclusively interact with the NBD of the opposite subunit, thereby providing the bulk of noncovalent interactions between the TMDs and the NBDs (**Fig. 2a**). TM287 and TM288 share an interface with a buried surface area of ~6,500 Å^2 per subunit (**Fig. 2b**). The majority of this interface is contributed by interactions between the ~75-Å long helices of the TMDs (61%) and interactions of the coupling helices of ICL2 and ICL4 with the NBDs (26%). The NBDs of TM287/288 are only partially disengaged and interact with each other over an interface of 832 Å^2 (13% of the total interface). Although the two polypeptide chains of heterodimeric TM287/288 share a moderate sequence identity of 33%, their conformations are quite similar (r.m.s. deviation of Cα-positions of 2.29 Å over 528 residues). Superimposing the TMDs of the two chains (r.m.s. deviation of 1.91 Å over 287 residues) shows a tilt between the NBDs of ~7° along an axis roughly parallel to the membrane plane (**Fig. 2c**).

Nucleotide binding to the degenerate site

A hallmark of TM287/288 and of many heterodimeric homologs are asymmetric NBDs containing one degenerate and one consensus nucleotide binding site[22]. The NBDs of TM287/288 are named NBD1 (TM287) and NBD2 (TM288). The degenerate site comprises noncanonical residues in the Walker B (aspartate instead of glutamate) and switch (glutamine instead of histidine) motifs of NBD1 and the ABC signature motif of NBD2 (LSQGQ instead of the consensus LSGGQ) (**Supplementary Fig. 3**). Notably, the sequences of many eukaryotic ABC exporters including CFTR, TAP1/2, MRP1 and SUR1 deviate from consensus in one nucleotide-binding site at the same amino acid positions as in TM287/288 (refs. 5,8,23,34). In the TM287/288 structure, AMP-PNP is bound to the degenerate ATPase site. No electron density for a second nucleotide is observed at the consensus site. The adenosine moiety of AMP-PNP π-stacks with the A-loop tyrosine (Tyr341) of NBD1, and the Walker A motif wraps around the β- and the γ-phosphate moiety of the bound nucleotide (**Fig. 3a**). In contrast to closed NBD dimers, the ABC signature motif of NBD2 is ~9 Å distant from the bound nucleotide (**Supplementary Fig. 1**). With respect to the bound AMP-PNP, crucial residues of the Walker A, the Walker B and the switch motifs of NBD1 are positioned as in the nucleotide-containing Sav1866 structure, representing a closed NBD dimer. Because NBD1 and the Sav1866 NBD superimpose with an r.m.s. deviation of 1.46 Å over 237 residues, only modest conformational changes are expected to occur at NBD1 during NBD closure of TM287/288 (**Supplementary Fig. 4a** and ref. 10).

Mutagenesis studies on CFTR, TAP1/2 and LmrCD suggest that ATP hydrolysis is impaired or even abrogated at the degenerate site[7,35,36]. In the degenerate site of TM287/288, the carboxyl moiety of noncanonical Asp495 of the Walker B motif is positioned farther away from the γ-phosphate of AMP-PNP with respect to the corresponding consensus glutamate residues in isolated NBD dimers of HlyB and MJ0796 or in Sav1866 (refs. 10,16,18). This affects Asp495's ability to act as a general base during ATP hydrolysis. Therefore, our structural observations suggest that one ATP is likely to remain bound to the degenerate site during the entire transport cycle without the necessity of becoming hydrolyzed (**Supplementary Video 1** and refs. 5,22). Recent studies on CFTR support this notion; the residence time of a bound ATP at the degenerate site is ~50 times longer than a gating cycle of the channel[37].

Strong intersubunit interactions through the D-loop of NBD2

When superimposing the two NBDs of TM287/288, their D-loop and switch motif positions differ by 6.4 Å and 4.7 Å, respectively (**Supplementary Fig. 4b**). A comparison with all deposited ABC-type NBD structures showed that these deviations represent structural changes in NBD2. The D-loop of NBD2, whose sequence deviates from the consensus sequence (SNVD instead of the consensus SALD) interacts with NBD1 through a hydrogen bonding network (**Fig. 3b**). In this network, the noncanonical Gln526 of the switch loop of NBD1 interacts with the backbone carbonyl of Ser520 and Asn521 of the D-loop of NBD2. The residue corresponding to Gln526 in HlyB (His662) has been dubbed the linchpin-histidine owing to its dual role in ATP hydrolysis and the inter-NBD interaction[16]. Asn521 of NBD2 is within hydrogen-bonding distance to the γ-phosphate moiety of AMP-PNP and thereby might have a role in the communication between the two nucleotide binding sites (**Fig. 3b**). As this hydrogen bond is the only interaction between AMP-PNP and NBD2, nucleotide binding at the degenerate site does not strongly contribute to the stability of the partially disengaged NBD dimer of TM287/288. This asparagine residue is highly conserved among heterodimeric bacterial homologs of TM287/288 and has been found to be substituted in a number of eukaryotic homologs including CFTR and SUR1 by polar residues instead of the consensus

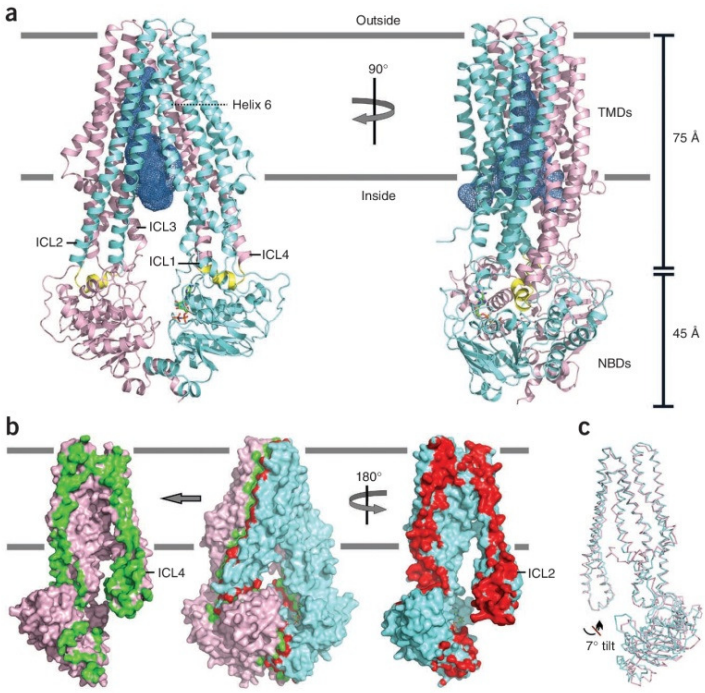

Figure 2 TM287/288 viewed along the membrane plane. The chains of TM287 and TM288 are colored cyan and pink, respectively. The expected membrane boundary is indicated by gray lines, and bound AMP-PNP is shown in ball-and-stick. (**a**) The TMDs feature four intracellular loops (ICL1 – 4) containing coupling helices (those of ICL2 and ICL4 are colored in yellow) that interact with the NBDs. The inward-facing cavity is shown as a blue mesh. (**b**) Open book surface representation of TM287/288. The surfaces of the heterodimeric interface are highlighted in red (TM287) and green (TM288), respectively. (**c**) Superimposition of the TMDs of TM287 and TM288 reveals structural similarity between the two polypeptide chains of heterodimeric TM287/288. The NBDs are tilted by an angle of ~7° along an axis roughly parallel to the membrane plane.

alanine (**Supplementary Fig. 3**). Mutating the residue corresponding to Gln521 in SUR1 to cysteine (S1511C) results in increased ADP-stimulated potassium-sensitive (K_{ATP})-channel activities, supporting the necessity of this residue in a mammalian homolog[38]. The carboxyl moiety of the highly conserved Asp523 of NBD2 does not interact with NBD1 (**Fig. 3b**). By contrast, the interaction of the second D-loop of TM287/288 is exclusively mediated by two hydrogen bonds between the carboxyl moiety of Asp501 (NBD1) and the amide backbone as well as the hydroxyl group of Thr390 (NBD2) of the Walker A motif (**Fig. 3c**). Overall, the interaction of the D-loop of NBD1 with NBD2 is much weaker than the corresponding interactions at the degenerate site, which is the reason for the tilt between the NBDs when TM287 and TM288 are superimposed (**Fig. 2c**).

Distorted catalytic dyad at the consensus site

The Walker B motif and the D-loop are separated by only two amino acid residues (**Fig. 3b**). As a consequence of the strong interaction of the D-loop of NBD2 with NBD1, the catalytically necessary Walker B glutamate (Glu517) of NBD2 is pointing away from the γ-phosphate position of a potentially bound ATP at NBD2 (**Fig. 3a**,**b**). In all heterodimeric ABC exporters studied thus far, the Walker B glutamate residue of the consensus site has an indispensable role for ATP hydrolysis. In addition, the Walker B aspartate (Asp516) and the Q-loop glutamine (Gln414) of NBD2 are shifted away from the expected nucleotide binding position (**Fig. 3a**,**d**). The switch histidine (His548), which in closed NBD dimers is in contact with the catalytic glutamate, is within hydrogen bonding distance from the Walker B aspartate (Asp516) (**Fig. 3b**,**d**). These combined conformational changes represent a distortion of the consensus site leading to a decrease of nucleotide affinity with respect to the degenerate site. Because the majority of crystal contacts reside on the surface of TM287, it is unlikely that crystal packing causes these distortions (**Supplementary Fig. 5**). The formation of the closed NBD dimer requires the binding of a second ATP molecule. Therefore, the consensus site might be formed during NBD closure, leading to an increase of its nucleotide affinity. The comparatively high $K_{m,app}$ for ATP (114 ± 6 μM and 80 ± 8 for detergent-purified and reconstituted TM287/288, respectively), which is composed of the consecutive events of ATP binding, NBD closure and ATP hydrolysis mainly at the consensus site, supports this notion.

Biochemical characterization of nucleotide binding

To further support our structural findings, purified TM287/288 was photolabeled with 8-N_3-[α-^{32}P]ATP (**Fig. 4a**,**b**). Nucleotide labeling occurred in a magnesium-dependent manner and the photolabeling was fully competed in the presence of an excess of cold ATP (**Fig. 4a**). At low 8-azido-[α-^{32}P]ATP concentration (0.75 μM), photolabeling of TM287 and TM288 differed by a factor of two, whereas at a concentration of 48 μM, both NBDs were labeled almost equally (**Fig. 4b**). This suggests that the ATPase sites show similar binding capacities but differ in their binding affinity for ATP. Preferential nucleotide binding to the degenerate site of TM287/288 agrees with previous studies on CFTR, MRP1 and LmrCD supporting the notion that heterodimeric ABC exporters from eukaryotes and prokaryotes share common biochemical properties[7,34,35].

Equilibrium binding of [^{3}H]ATP to TM287/288 was measured in a scintillation proximity assay (SPA)[39]. The data were fit to a one-site saturation and a two-site saturation model (**Fig. 4c**). An F-test analysis in which the one-site saturation fit represented the null hypothesis and the two-site saturation model was the alternative hypothesis resulted in a P value of 0.0009 and an F value of 19.17, therefore clearly favoring the two-site saturation model. Moreover, fitting to a one-site saturation model resulted in systematic deviations of the measured data in the residual plot (**Fig. 4c**, inset). The affinities of the first and the second binding site (K_{d1} and K_{d2}) were 26 ± 9 μM and 646 ± 367 μM, respectively. The binding capacities (B_{max1} and B_{max2}) were 2,493 ± 501 c.p.m. and 2,859 ± 348 c.p.m., respectively. We interpreted K_{d1} as representing the ATP binding affinity of the degenerate site. Competition binding experiments showed that AMP-PNP binds more weakly to TM287/288 than ATP (**Fig. 4d**). This could explain why just one nucleotide is found in the TM287/288 structure in the presence of 2.5 mM AMP-PNP, which was added before crystallization.

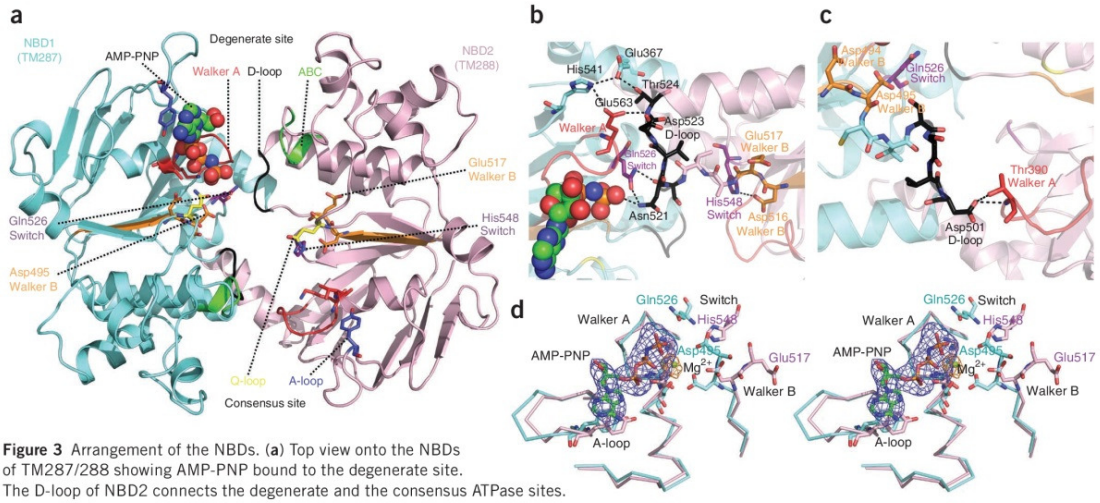

Figure 3 Arrangement of the NBDs. (**a**) Top view onto the NBDs of TM287/288 showing AMP-PNP bound to the degenerate site. The D-loop of NBD2 connects the degenerate and the consensus ATPase sites. Crucial residues are shown as sticks, and conserved motifs are highlighted by different colors. (**b**) The D-loop of NBD2 interacts with the Walker A motif and the switch Gln526 of NBD1 through a hydrogen bonding network. Residues involved in the NBD1-NBD2 interactions and crucial residues of the consensus catalytic site are shown as sticks. Hydrogen bonds (≤3.3 Å) between the two subunits are depicted as black dashed lines. Asn521 is the only residue of NBD2 interacting with the γ-phosphate moiety of AMP-PNP. The Walker B motif closely precedes the D-loop. Crucial residues Asp516, Glu517 and His548 of NBD2 adopt a distorted conformation involving a hydrogen bond between His548 and Asp516. (**c**) Asp501 of the D-loop of NBD1 forms two hydrogen bonds with Walker A Thr390 of NBD2. (**d**) Stereoview of structural differences between the degenerate and the consensus ATPase site. AMP-PNP and magnesium bound to NBD1 are shown as sticks and green sphere. Densities for AMP-PNP and magnesium are shown as blue and orange meshes contoured at 3 σ and 6 σ, respectively. Residues of the catalytic dyad, which point toward the bound AMP-PNP in NBD1 (Asp495 and Gln526), are rearranged in NBD2 (Glu517 and His548).

The transmembrane domains

Residues from all transmembrane helices contribute to the surface of a cavity through which substrates are likely to be transported. It opens to the cytoplasm but seems to be inaccessible from the inner leaflet of the lipid bilayer. However, because of the inherent protein flexibility of transporters, transient access of membrane-embedded substrates to the cavity cannot be excluded (**Fig. 2b**). The shape of the cavity is asymmetric because of clustering of bulky side chains in transmembrane helix 6 of TM287 (**Fig. 2a**). Three xenon binding sites line the cavity surface close to the cytoplasmic entry and indicate hydrophobic patches mainly at the cavity surface of TM287 (**Supplementary Fig. 6**). In P-glycoprotein and MsbA, transported substrates have been shown to bind to the surface of the corresponding cavity[3,28,40,41].

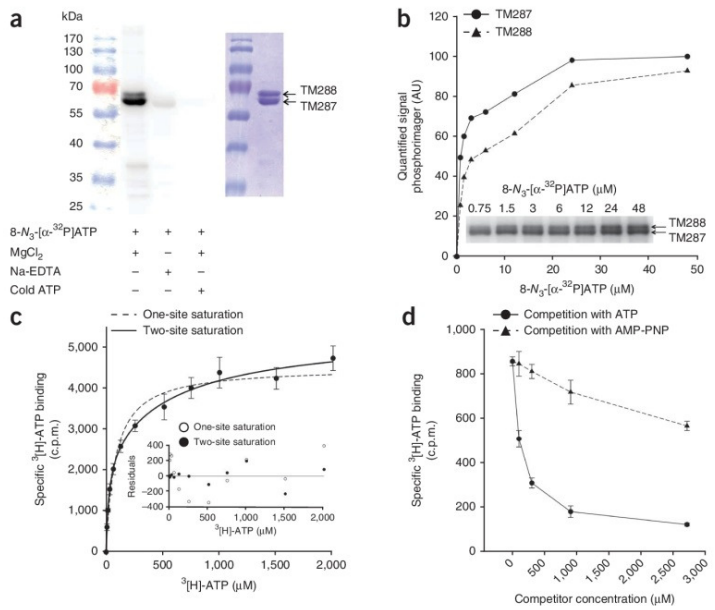

Figure 4 Preferential nucleotide binding to the degenerate site of TM287/288. (**a**) Cross-linking of 8-N_3-[α-^{32}P]ATP to detergent-purified TM287/288 in the presence of $MgCl_2$ or Na-EDTA and ATP analyzed by SDS-PAGE and autoradiography shows that nucleotide binding occurs preferentially at the degenerate site (TM287) and is magnesium dependent. Coomassie-stained TM287/288 used for the assay is shown in the right panel. (**b**) Concentration-dependent photolabeling of 8-azido-[α-^{32}P]ATP to TM287/288. The bands of labeled TM287 and TM288 (inset) were quantified and plotted. (**c**) Equilibrium binding of [^{3}H]ATP to purified TM287/288 determined by scintillation proximity assay. The data were fit to a one-site and a two-site saturation model. The fits were analyzed by a residual plot (inset). Error bars, s.d. (**d**) Binding of [^{3}H]ATP (100 μM) to TM287/288 measured as in **c** is competed more effectively by the addition of cold ATP than by cold AMP-PNP.

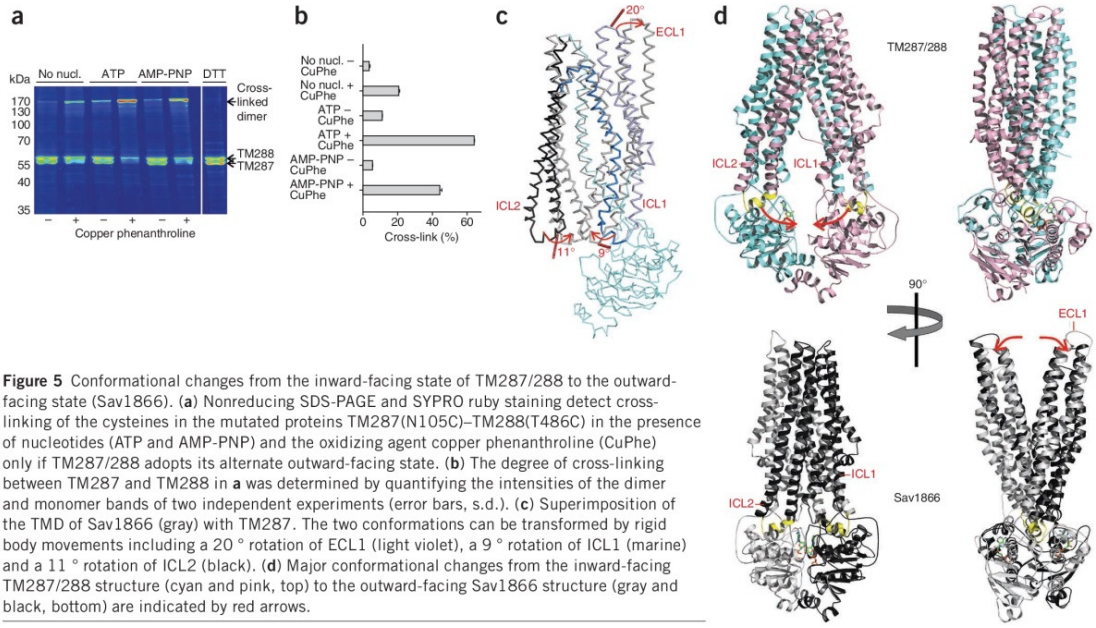

Figure 5 Conformational changes from the inward-facing state of TM287/288 to the outward-facing state (Sav1866). (**a**) Nonreducing SDS-PAGE and SYPRO ruby staining detect cross-linking of the cysteines in the mutated proteins TM287(N105C)–TM288(T486C) in the presence of nucleotides (ATP and AMP-PNP) and the oxidizing agent copper phenanthroline (CuPhe) only if TM287/288 adopts its alternate outward-facing state. (**b**) The degree of cross-linking between TM287 and TM288 in **a** was determined by quantifying the intensities of the dimer and monomer bands of two independent experiments (error bars, s.d.). (**c**) Superimposition of the TMD of Sav1866 (gray) with TM287. The two conformations can be transformed by rigid body movements including a 20 ° rotation of ECL1 (light violet), a 9 ° rotation of ICL1 (marine) and a 11 ° rotation of ICL2 (black). (**d**) Major conformational changes from the inward-facing TM287/288 structure (cyan and pink, top) to the outward-facing Sav1866 structure (gray and black, bottom) are indicated by red arrows.

The N terminus of TM288 is 25 residues longer than the one of TM287 and is partially defined in the crystal structure starting from residue 10 (**Supplementary Fig. 7**). It folds into an extended N-terminal elbow helix and interacts as a coiled structure with ICL4 of the membrane domain of TM288. This interaction appears to restrict the movement of ICL4 (and of NBD1 connected to it) with respect to the other transmembrane helices of TM288 and might therefore further strengthen the interaction between the NBDs.

Nucleotides drive NBD closure in TM287/288

A homology model of TM287/288 was created on the basis of the outward-facing Sav1866 structure and validated by introducing a cysteine pair at positions TM287(N105C) and TM288(T486C). These substitutions are expected to form disulfide bonds once TM287/288 adopts its outward-facing state. The distance between the thiol groups is 21 Å in the crystal structure and is anticipated to approach 4 Å during NBD closure. The purified double cysteine mutant was subjected to cysteine cross-linking with copper phenanthroline (1 mM) as an oxidizing agent in the presence of 2.5 mM ATP or AMP-PNP, as well as in the absence of nucleotides (**Fig. 5a**,**b**). The addition of ATP and to a lesser extent of AMP-PNP resulted in a strong cross-linking of the two chains both in the absence and particularly in the presence of copper phenanthroline. All cross-links were formed between TM287 and TM288, as the corresponding single mutants did not result in homodimerized species (data not shown). The cross-linking data support the existence of the outward-facing state modeled here and the notion that binding of hydrolyzable and nonhydrolyzable nucleotides drives NBD closure. This has been reported previously for a number of ABC exporters, such as P-glycoprotein and MsbA[9,42,43].

DISCUSSION

Molecular description of a heterodimeric NBD pair

Crystal structures of the isolated first NBD (corresponding to NBD1 in TM287/288) from a number of heterodimeric ABC exporters including CFTR, TAP1/2 and MRP1 have been solved as isolated domains or homodimers[44–46]. However, structural information on the NBD2 of these transporters in isolation or heterodimerized with NBD1 is lacking. Here, we provide new structural insight into heterodimeric NBDs, which probably needed to be crystallized in the context of a full-length ABC transporter to be analyzed. Our structural information indicates that the NBD heterodimer of TM287/288 is held together by virtue of a hydrogen-bond network mediated by the D-loop of NBD2. The D-loop sequence of NBD2 is noncanonical (SNVD instead of SALD), completing the picture of the degenerate site. The noncanonical Asn521 is of particular note, as it is within hydrogen-bonding distance of the γ-phosphate moiety of AMP-PNP bound to the opposite NBD; thereby, it might be able to communicate the presence of a nucleotide bound at the degenerate site to the consensus site. The consensus site is distorted as a consequence of the strong D-loop interaction with the opposite NBD, which is manifested by a flip of the catalytically essential Walker B glutamate pointing away from the site of nucleotide binding.

An inward-facing ABC exporter with contacting NBDs

In contrast to previously determined crystal structures of ABC exporters in their inward-facing states showing a complete separation of the NBDs, the NBDs of TM287/288 remain in contact. Our analysis demonstrates that a separation of the coupling helices of ICL2 and ICL4 by 15 Å is sufficient to open the substrate-binding cavity from the outside to the inside of the cell, without the need of complete NBD dimer disengagement. Future structural and functional studies will have to demonstrate whether this partial disengagement of the NBDs is unique to heterodimeric ABC exporters featuring asymmetric NBDs or if such an intermediate state is also found in other ABC exporters[27,28].

Proposed model of transport

The presumed outward-facing state of TM287/288 was modeled on the basis of the structure of Sav1866 and validated by cysteine cross-linking.

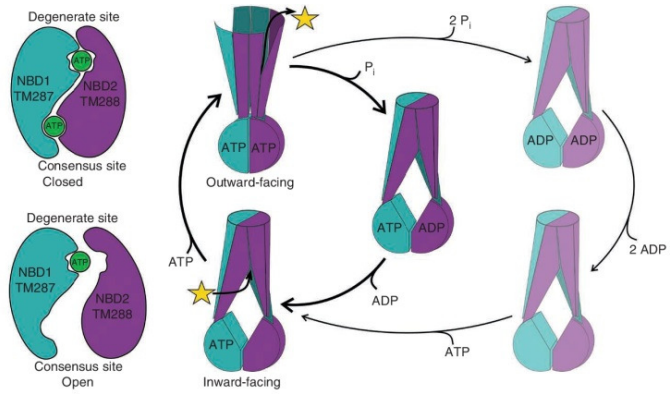

Figure 6 Proposed mechanism of transport in heterodimeric ABC transporters. Left, NBDs. Right, full transporter. TM287 and TM288 are colored in cyan and purple, respectively. The transport cycle starts (lower left) with TM287/288 in its inward-facing conformation with one ATP bound to the degenerate catalytic site of NBD1 at the open NBD dimer. Upon binding of a substrate (yellow star) and a second molecule of ATP, the NBDs close, and as a consequence, the transmembrane helices rearrange to adopt the outward-facing conformation. The substrate is released and ATP bound to the consensus catalytic site is hydrolyzed, which resets the transporter to its inward-facing state (thick arrows). Hydrolysis of ATP at the degenerate site occurs much less frequently than at the consensus site (thin arrows).

The transition from the inward- to the outward-facing conformation requires a tweezers-like closing of the NBDs and a rearrangement of the consensus site, which allows binding of the second ATP[10,27]. This results in the sandwiching of two ATPs between the Walker A and the ABC signature motifs[9,14] (**Supplementary Fig. 1**). The four coupling helices move along with the NBDs, thereby constricting the access to the substrate binding cavity from the cytoplasm. In the TMD of TM287, the extracellular loop between transmembrane helices 1 and 2 (ECL1), as well as ICL1 and ICL2, move as three individual rigid bodies, including a rotation by 20°, 9° and 11°, respectively (**Fig. 5c**). Movements in the TMD of TM288 occur accordingly. In the context of the full transporter, these conformational changes result in the separation of two bundles of transmembrane helices (referred to as wings in Sav1866 (ref. 10)) at the extracellular side along an axis roughly perpendicular to the one of the NBD closure (**Fig. 5d** and **Supplementary Video 2**). One bundle is composed of helices 1 and 2 of the first protomer and helices 3–6 of the second protomer and vice versa for the other bundle. The cavity is reoriented and reshaped, and a previously bound substrate can dissociate and be released to the extracellular space (**Fig. 6**). ATP hydrolysis at the consensus site (and occasionally also at the degenerate site) leads to the destabilization of the NBD dimer and initiates the resetting of the transporter to its inward-facing state[7]. With this two-state model, which fully supports current models for transporter cycling of CFTR and TAP1/2, substrate transport by ABC exporters can be explained by a simple alternating-access transport mechanism[5,22,47].

Conclusion

Our structure for TM287/288 describes the first heterodimeric ABC exporter with nonequal ATP binding sites at a molecular level. It provides a solid framework for future studies on bacterial and eukaryotic homologs, such as LmrCD, PatAB, CFTR, TAP1/2 and MRP1; therefore, our findings might contribute to the development of new therapies to combat multidrug resistance in tumor cells and pathogenic bacteria and to treat cystic fibrosis.

METHODS

Methods and any associated references are available in the online version of the paper at http://www.nature.com/nsmb/.

Accession codes. Protein Data Bank: The coordinates of the structure for TM287/288 in its inward-facing conformation have been deposited under accession code 3QF4.

Note: Supplementary information is available on the Nature Structural & Molecular Biology website.

ACKNOWLEDGMENTS

We thank A. Mittal, C. Madhurantakam and E. Geertsma for helpful discussions and R. Dutzler for critical reading of the manuscript. We acknowledge B. Blattmann and C. Stutz-Ducommun from the NCCR crystallization facility for crystal screening and the staff of the X06SA beamline at the Swiss Light Source of the Paul Scherrer Institute for support during data collection. We thank H. van Veen (Department of Pharmacology, University of Cambridge) for the *L. lactis* NZ9000 Δ*lmrA* Δ*lmrCD* strain. This work was funded by the Swiss NCCR Structural Biology program, an Ambizione grant of the Swiss National Science Foundation (to M.A.S.) and a Forschungskredit of the University of Zürich (to M.A.S.). M.H. is affiliated with the PhD program in Biomolecular Structure and Mechanism of the Life Science Zürich Graduate School.

AUTHOR CONTRIBUTIONS

M.H., M.G.G. and M.A.S. conceived the project. M.H. and M.A.S. cloned, purified and crystallized TM287/288 and carried out the functional assays. M.H., C.B. and M.A.S. collected and processed the crystallographic data. C.B., M.G.G. and M.A.S. solved the structure and built the model. All authors interpreted the structure and wrote the manuscript.

COMPETING FINANCIAL INTERESTS

The authors declare no competing financial interests.

Published online at http://www.nature.com/nsmb/.
Reprints and permissions information is available online at http://www.nature.com/reprints/index.html.

1. Davidson, A.L., Dassa, E., Orelle, C. & Chen, J. Structure, function, and evolution of bacterial ATP-binding cassette systems. *Microbiol. Mol. Biol. Rev.* **72**, 317–364 (2008).
2. Seeger, M.A. & van Veen, H.W. Molecular basis of multidrug transport by ABC transporters. *Biochim. Biophys. Acta* **1794**, 725–737 (2009).
3. Gottesman, M.M. & Ling, V. The molecular basis of multidrug resistance in cancer: the early years of P-glycoprotein research. *FEBS Lett.* **580**, 998–1009 (2006).
4. Pajic, M. *et al.* Moderate increase in Mdr1a/1b expression causes *in vivo* resistance to doxorubicin in a mouse model for hereditary breast cancer. *Cancer Res.* **69**, 6396–6404 (2009).
5. Gadsby, D.C., Vergani, P. & Csanady, L. The ABC protein turned chloride channel whose failure causes cystic fibrosis. *Nature* **440**, 477–483 (2006).
6. Garvey, M.I., Baylay, A.J., Wong, R.L. & Piddock, L.J. Overexpression of *patA* and *patB*, which encode ABC transporters, is associated with fluoroquinolone resistance in clinical isolates of *Streptococcus pneumoniae*. *Antimicrob. Agents Chemother.* **55**, 190–196 (2011).
7. Lubelski, J., van Merkerk, R., Konings, W.N. & Driessen, A.J. Nucleotide-binding sites of the heterodimeric LmrCD ABC-multidrug transporter of *Lactococcus lactis* are asymmetric. *Biochemistry* **45**, 648–656 (2006).
8. Aittoniemi, J. *et al.* SUR1: a unique ATP-binding cassette protein that functions as an ion channel regulator. *Phil. Trans. R. Soc. Lond. B* **364**, 257–267 (2009).
9. Higgins, C.F. & Linton, K.J. The ATP switch model for ABC transporters. *Nat. Struct. Mol. Biol.* **11**, 918–926 (2004).

10. Dawson, R.J. & Locher, K.P. Structure of a bacterial multidrug ABC transporter. *Nature* **443**, 180–185 (2006).
11. Schneider, E. & Hunke, S. ATP-binding-cassette (ABC) transport systems: functional and structural aspects of the ATP-hydrolyzing subunits/domains. *FEMS Microbiol. Rev.* **22**, 1–20 (1998).
12. Jones, P.M. & George, A.M. Subunit interactions in ABC transporters: towards a functional architecture. *FEMS Microbiol. Lett.* **179**, 187–202 (1999).
13. Hopfner, K.P. *et al.* Structural biology of Rad50 ATPase: ATP-driven conformational control in DNA double-strand break repair and the ABC-ATPase superfamily. *Cell* **101**, 789–800 (2000).
14. Chen, J., Lu, G., Lin, J., Davidson, A.L. & Quiocho, F.A. A tweezers-like motion of the ATP-binding cassette dimer in an ABC transport cycle. *Mol. Cell* **12**, 651–661 (2003).
15. Orelle, C., Dalmas, O., Gros, P., Di Pietro, A. & Jault, J.M. The conserved glutamate residue adjacent to the Walker-B motif is the catalytic base for ATP hydrolysis in the ATP-binding cassette transporter BmrA. *J. Biol. Chem.* **278**, 47002–47008 (2003).
16. Zaitseva, J., Jenewein, S., Jumpertz, T., Holland, I.B. & Schmitt, L. H662 is the linchpin of ATP hydrolysis in the nucleotide-binding domain of the ABC transporter HlyB. *EMBO J.* **24**, 1901–1910 (2005).
17. Oldham, M.L. & Chen, J. Snapshots of the maltose transporter during ATP hydrolysis. *Proc. Natl. Acad. Sci. USA* **108**, 15152–15156 (2011).
18. Smith, P.C. *et al.* ATP binding to the motor domain from an ABC transporter drives formation of a nucleotide sandwich dimer. *Mol. Cell* **10**, 139–149 (2002).
19. Venter, H., Shilling, R.A., Velamakanni, S., Balakrishnan, L. & Van Veen, H.W. An ABC transporter with a secondary-active multidrug translocator domain. *Nature* **426**, 866–870 (2003).
20. Doerrler, W.T., Reedy, M.C. & Raetz, C.R. An *Escherichia coli* mutant defective in lipid export. *J. Biol. Chem.* **276**, 11461–11464 (2001).
21. Velamakanni, S., Yao, Y., Gutmann, D.A. & van Veen, H.W. Multidrug Transport by the ABC Transporter Sav1866 from *Staphylococcus aureus*. *Biochemistry* **47**, 9300–9308 (2008).
22. Procko, E., O'Mara, M.L., Bennett, W.F., Tieleman, D.P. & Gaudet, R. The mechanism of ABC transporters: general lessons from structural and functional studies of an antigenic peptide transporter. *FASEB J.* **23**, 1287–1302 (2009).
23. Parcej, D. & Tampe, R. ABC proteins in antigen translocation and viral inhibition. *Nat. Chem. Biol.* **6**, 572–580 (2010).
24. Torres, C., Galian, C., Freiberg, C., Fantino, J.R. & Jault, J.M. The YheI/YheH heterodimer from *Bacillus subtilis* is a multidrug ABC transporter. *Biochim. Biophys. Acta* **1788**, 615–622 (2009).
25. Zutz, A. *et al.* Asymmetric ATP hydrolysis cycle of the heterodimeric multidrug ABC transport complex TmrAB from *Thermus thermophilus*. *J. Biol. Chem.* **286**, 7104–7115 (2011).
26. Dawson, R.J. & Locher, K.P. Structure of the multidrug ABC transporter Sav1866 from *Staphylococcus aureus* in complex with AMP-PNP. *FEBS Lett.* **581**, 935–938 (2007).
27. Ward, A., Reyes, C.L., Yu, J., Roth, C.B. & Chang, G. Flexibility in the ABC transporter MsbA: Alternating access with a twist. *Proc. Natl. Acad. Sci. USA* **104**, 19005–19010 (2007).
28. Aller, S.G. *et al.* Structure of P-glycoprotein reveals a molecular basis for poly-specific drug binding. *Science* **323**, 1718–1722 (2009).
29. Lubelski, J. *et al.* LmrCD is a major multidrug resistance transporter in *Lactococcus lactis*. *Mol. Microbiol.* **61**, 771–781 (2006).
30. Venter, H., Velamakanni, S., Balakrishnan, L. & van Veen, H.W. On the energy-dependence of Hoechst 33342 transport by the ABC transporter LmrA. *Biochem. Pharmacol.* **75**, 866–874 (2008).
31. Shapiro, A.B. & Ling, V. Extraction of Hoechst 33342 from the cytoplasmic leaflet of the plasma membrane by P-glycoprotein. *Eur. J. Biochem.* **250**, 122–129 (1997).
32. Ambudkar, S.V. *et al.* Partial purification and reconstitution of the human multidrug-resistance pump: characterization of the drug-stimulatable ATP hydrolysis. *Proc. Natl. Acad. Sci. USA* **89**, 8472–8476 (1992).
33. Eckford, P.D. & Sharom, F.J. Functional characterization of *Escherichia coli* MsbA: interaction with nucleotides and substrates. *J. Biol. Chem.* **283**, 12840–12850 (2008).
34. Yang, R., Cui, L., Hou, Y.X., Riordan, J.R. & Chang, X.B. ATP binding to the first nucleotide binding domain of multidrug resistance-associated protein plays a regulatory role at low nucleotide concentration, whereas ATP hydrolysis at the second plays a dominant role in ATP-dependent leukotriene C4 transport. *J. Biol. Chem.* **278**, 30764–30771 (2003).
35. Basso, C., Vergani, P., Nairn, A.C. & Gadsby, D.C. Prolonged nonhydrolytic interaction of nucleotide with CFTR's NH2-terminal nucleotide binding domain and its role in channel gating. *J. Gen. Physiol.* **122**, 333–348 (2003).
36. Perria, C.L., Rajamanickam, V., Lapinski, P.E. & Raghavan, M. Catalytic site modifications of TAP1 and TAP2 and their functional consequences. *J. Biol. Chem.* **281**, 39839–39851 (2006).
37. Tsai, M.F., Li, M. & Hwang, T.C. Stable ATP binding mediated by a partial NBD dimer of the CFTR chloride channel. *J. Gen. Physiol.* **135**, 399–414 (2010).
38. Masia, R. & Nichols, C.G. Functional clustering of mutations in the dimer interface of the nucleotide binding folds of the sulfonylurea receptor. *J. Biol. Chem.* **283**, 30322–30329 (2008).
39. Quick, M. & Javitch, J.A. Monitoring the function of membrane transport proteins in detergent-solubilized form. *Proc. Natl. Acad. Sci. USA* **104**, 3603–3608 (2007).
40. Smriti, Z.P. & McHaourab, H.S. Mapping daunorubicin-binding Sites in the ATP-binding cassette transporter MsbA using site-specific quenching by spin labels. *J. Biol. Chem.* **284**, 13904–13913 (2009).
41. Pleban, K. *et al.* P-glycoprotein substrate binding domains are located at the transmembrane domain/transmembrane domain interfaces: a combined photoaffinity labeling-protein homology modeling approach. *Mol. Pharmacol.* **67**, 365–374 (2005).
42. Borbat, P.P. *et al.* Conformational motion of the ABC transporter MsbA induced by ATP hydrolysis. *PLoS Biol.* **5**, e271 (2007).
43. Doshi, R., Woebking, B. & van Veen, H.W. Dissection of the conformational cycle of the multidrug/lipid A ABC exporter MsbA. *Proteins* **78**, 2867–2872 (2010).
44. Lewis, H.A. *et al.* Structure of nucleotide-binding domain 1 of the cystic fibrosis transmembrane conductance regulator. *EMBO J.* **23**, 282–293 (2004).
45. Ramaen, O. *et al.* Structure of the human multidrug resistance protein 1 nucleotide binding domain 1 bound to Mg^{2+}/ATP reveals a non-productive catalytic site. *J. Mol. Biol.* **359**, 940–949 (2006).
46. Procko, E., Ferrin-O'Connell, I., Ng, S.L. & Gaudet, R. Distinct structural and functional properties of the ATPase sites in an asymmetric ABC transporter. *Mol. Cell* **24**, 51–62 (2006).
47. Jardetzky, O. Simple allosteric model for membrane pumps. *Nature* **211**, 969–970 (1966).

ONLINE METHODS

Expression and purification of *T. maritima* TM287/288 heterodimer. The genes *TM0287* and *TM0288* that encode the heterodimeric ABC transporter TM287/288 were amplified from *T. maritima* MSB8 (DSM 3109)[48] and cloned into a modified pBAD24 expression vector with FX cloning[49], adding a deca-histidine affinity tag, a human rhinovirus 3C protease (GE healthcare) cleavage site and an $(SG)_2(G)_4S$ linker, to the N terminus of TM287. Cellular membranes of TM287/288 were prepared following standard methods[50], resuspended in 50 mM Tris pH 7.4, 150 mM NaCl and 10% (v/v) glycerol and solubilized by addition of 1.5% (w/v) n-dodecyl-β-D-maltopyranoside (β-DDM) for 2 h. TM287/288 was purified by nickel-nitrilotriacetic acid (Ni^{2+}-NTA) affinity purification, subjected to overnight cleavage using PreScission protease (1:10 (w/w)), desalted and reloaded on a Ni^{2+}-NTA column. Cleaved TM287/288 was polished by size-exclusion chromatography using a Superdex 200 column (GE Healthcare) in 20 mM Tris pH 7.5, 150 mM NaCl, 0.03% (w/v) β-DDM and concentrated to 16 mg ml^{-1}, with an Amicon Ultra-4 concentrator unit with an MWCO of 50 kDa, before crystallization.

Crystallization and structure determination. Protein crystals were obtained in sitting drops at 20 °C against a reservoir containing 29% (w/v) polyethylene glycol 400, 50 mM Na-cacodylate pH 5.5 and 100 mM $CaCl_2$. Prior to crystallization, AMP-PNP (2.5 mM) and $MgCl_2$ (3 mM) were added. Data at 2.9 Å were collected at the X06SA beamline of the Swiss Light Source of the Paul Scherrer Institute on a Pilatus detector (Dectris). The crystals were of space group *C*2, containing one TM287/288 heterodimer per asymmetric unit. The phases were solved by single-wavelength anomalous dispersion using SeMet-labeled TM287/288. The model encompassing residues 1–569 of TM287 and 10–597 of TM288 was refined to 2.9 Å with good refinement statistics and with no outliers in disallowed and generously allowed regions of the Ramachandran plot. Figures were prepared using PyMOL (http://www.pymol.org).

Daunomycin transport assay. Wild-type and mutant (E517Q) TM287/288 were cloned into the *L. lactis* expression vector pNZ8048 using the vector-backbone exchange (VBEx) cloning[51]. Resistance toward daunomycin was determined by growing *L. lactis* NZ9000 Δ*lmrA* Δ*lmrCD*–expressing wild-type and mutant TM287/288 in M17 growth medium supplemented with glucose (0.5% w/v), chloramphenicol (5 μg ml^{-1}), nisin A (2 ng ml^{-1}) and a dilution series of daunomycin for 15–18 h at 37 °C. Final A_{600nm} were measured and normalized by setting the final A_{600nm} reached in the absence of drug to 100. The data were fit with a 4-parameter sigmoidal equation (SigmaPlot 10)

$$y = \frac{a}{1 + e^{-\left(\frac{x - x_0}{b}\right)}} \quad (1)$$

The IC_{50} of daunomycin resistance corresponds to the inflection point (x_0) of the fitted curve.

BCECF-AM transport. *L. lactis* NZ9000 Δ*lmrA* Δ*lmrCD*–expressing wild-type and mutant (E517Q) TM287/288 were grown at 30 °C and the protein production was induced for 2 h with 2 ng ml^{-1} nisin at an optical density (A_{600nm}) of 0.4–0.6. Cells were washed twice with 50 mM KP_i (pH 7.5), 5 mM $MgSO_4$. For the fluorescence measurement at 30 °C or 40 °C the A_{600nm} was adjusted to 0.5 and cells were pre-energized by the addition of 0.5% glucose. 2′,7′-bis-(carboxyethyl)-5(6)-carboxyfluorescein-acetoxymethylester (BCECF-AM, 0.2 μM final concentration) was added and the fluorescence was measured at excitation and emission wavelengths of 502 nm and 525 nm, respectively.

ATPase activity assay. If not stated otherwise, steady-state ATPase activity of detergent-purified TM287/288 was measured at 50 °C in the presence of 1 mM ATP in 40 mM K-HEPES pH 7.4, 8 mM $MgSO_4$ containing 0.03% (w/v) β-DDM where required. The apparent affinity for ATP hydrolysis ($K_{m,app}$) was determined by measuring the ATPase activity of detergent-purified and reconstituted TM287/288 at various ATP concentrations and fitting the data to the Hill equation

$$y = \frac{ax^b}{c^b + x^b} \quad (2)$$

The TM287/288 (E517Q) mutant was used for background subtraction. In order to measure ATPase activities in proteoliposomes, detergent-purified wild- type and E517Q mutant TM287/288 was reconstituted into *E. coli* polar lipids–egg L-α-phosphatidylcholine mixed at a ratio of 3:1 (w/w) following a standard protocol[52]. Inside-out membrane vesicles (ISOVs) of *L. lactis* containing overexpressed wild-type and E517Q mutant TM287/288 were prepared[53].

8-N_3-[α-^{32}P]ATP photolabeling. Nucleotide binding assays and cysteine cross-linking experiments were done in 20 mM Tris pH 7.5, 150 mM NaCl, 0.03% β-DDM (Buffer A). For the single point measurements shown in **Figure 4a**, 8-N_3-[α-^{32}P]ATP (Affinity Photoprobes), 1 μM, 9.2 Ci $mmol^{-1}$ was added to purified TM287/288 (0.2 mg ml^{-1}, 10 μl) in Buffer A containing either 3 mM Na-EDTA or 3 mM $MgCl_2$ and 2.5 mM cold ATP. For the concentration dependent 8-N_3-[α-^{32}P]ATP photolabeling a two dilution series of 8-N_3-[α-^{32}P]ATP from 48 μM to 0.75 μM (4.6 Ci $mmol^{-1}$) was added (**Fig. 4b**). The reaction mixtures were incubated at 25 °C for 5 min and then UV irradiated on ice. Labeled TM287/288 was analyzed by SDS-PAGE, and photolabeling was visualized using a Phosphorimager.

Scintillation proximity assay (SPA). Purified TM287/288 (200 nM) was immobilized on PVT Copper His-Tag SPA beads (PerkinElmer, 2 mg ml^{-1}) in Buffer A containing 3 mM $MgCl_2$. [2,5,8-^{3}H] adenosine-5′-triphosphate ([^{3}H]ATP, 51 Ci $mmol^{-1}$, PerkinElmer), diluted with the appropriate amount of cold ATP, was added to the preloaded beads (140 μl per well). Empty scintillation beads served as the background subtraction control. The mixture was incubated on a microplate shaker at 6 °C overnight and then counted in a MicroBeta counter (Wallac) (SPA c.p.m. mode). The data points were fit to a one-site saturation and a two-site saturation model (**Fig. 4c**).
Equation of one-site saturation

$$y = \frac{B_{max}x}{K_d + x} \quad (3)$$

Equation of two-site saturation

$$y = \frac{B_{max1}x}{K_{d1} + x} + \frac{B_{max2}x}{K_{d2} + x} \quad (4)$$

The two different fits were compared with an *F*-test (GraphPad Prism 5), according to instructions in the program manual.

Introduction of engineered disulfide bonds. A cysteine-less TM287/288 clone (see **Supplementary Methods**) served as template for the introduction of the single mutants TM287(S105C) and TM288(T486C) and the corresponding double mutant. Mutant TM287/288 was purified and incubated with copper phenanthroline (1 mM) and nucleotides (2.5 mM) as indicated in Buffer A containing 3 mM $MgCl_2$ at room temperature for 20 min. The cross-linked protein was separated by nonreducing SDS-PAGE and quantified by SYPRO ruby staining (Invitrogen).

48. Huber, R. *et al. Thermotoga maritima* sp. nov. represents a new genus of unique extremely thermophilic eubacteria growing up to 90°C. *Arch. Microbiol.* **144**, 324–333 (1986).
49. Geertsma, E.R. & Dutzler, R. A versatile and efficient high-throughput cloning tool for structural biology. *Biochemistry* **50**, 3272–3278 (2011).
50. Seeger, M.A. *et al.* Engineered disulfide bonds support the functional rotation mechanism of multidrug efflux pump AcrB. *Nat. Struct. Mol. Biol.* **15**, 199–205 (2008).
51. Geertsma, E.R. & Poolman, B. High-throughput cloning and expression in recalcitrant bacteria. *Nat. Methods* **4**, 705–707 (2007).
52. Geertsma, E.R., Nik Mahmood, N.A., Schuurman-Wolters, G.K. & Poolman, B. Membrane reconstitution of ABC transporters and assays of translocator function. *Nat. Protoc.* **3**, 256–266 (2008).
53. Woebking, B. *et al.* Functional role of transmembrane helix 6 in drug binding and transport by the ABC transporter MsbA. *Biochemistry* **47**, 10904–10914 (2008).

Fig. S1

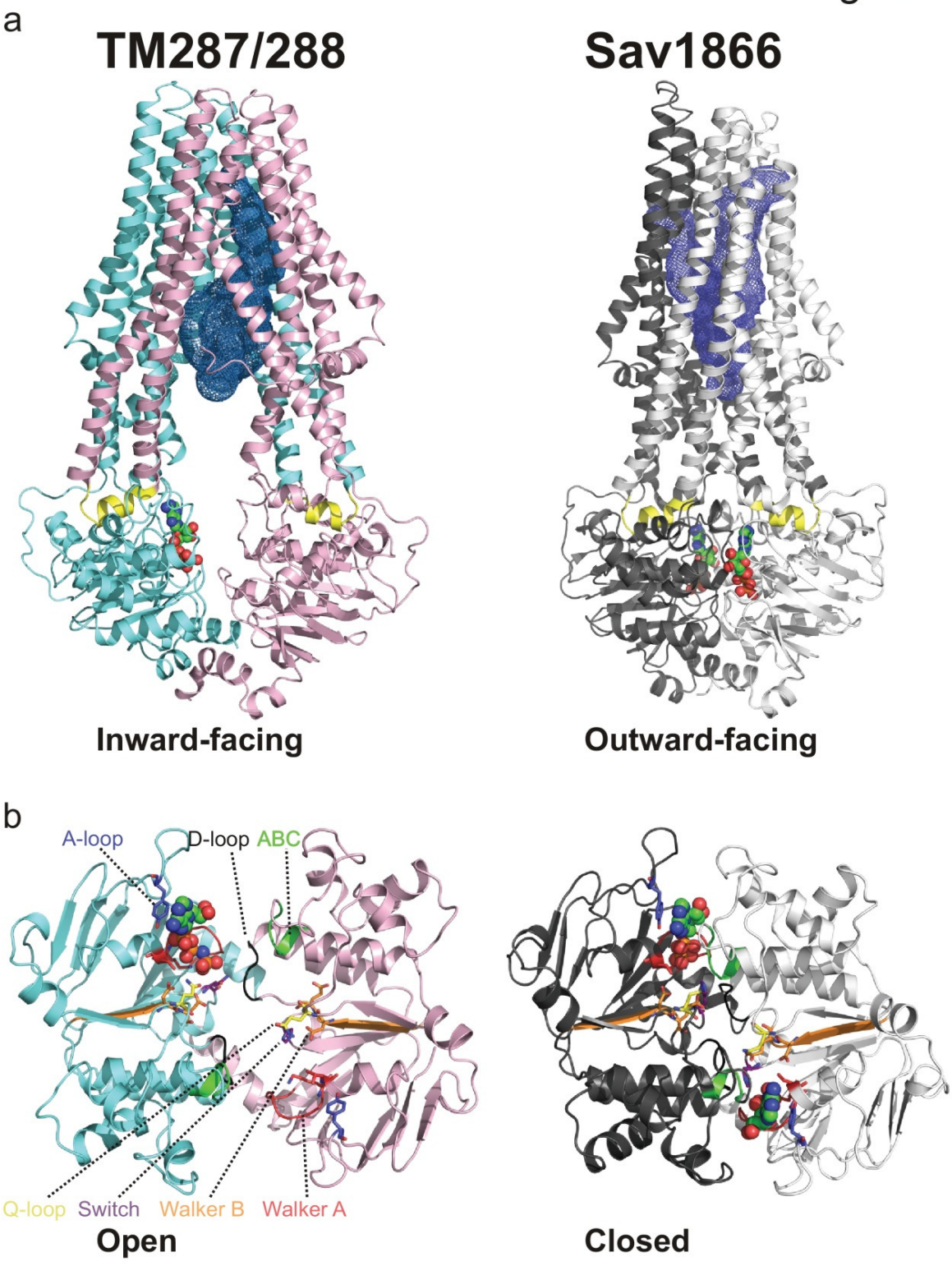

Nature Structural & Molecular Biology: doi:10.1038/nsmb.2267

Supplementary Figure 1

Side by side comparison of TM287/288 and Sav1866. TM287/288 (cyan/pink) and Sav1866 (black/grey; pdb code: 2HYD) are depicted as cartoons shown along the membrane plane (**a**) and at the level of the NBDs from the top (**b**). Nucleotides are shown as spheres (1 AMP-PNP in TM287/288 and 2 ADPs in Sav1866). Coupling helices reaching across to the opposite NBDs are highlighted in yellow. Key residues are shown as sticks and conserved motifs are emphasized by different colors.

Nature Structural & Molecular Biology: doi:10.1038/nsmb.2267

Fig. S2

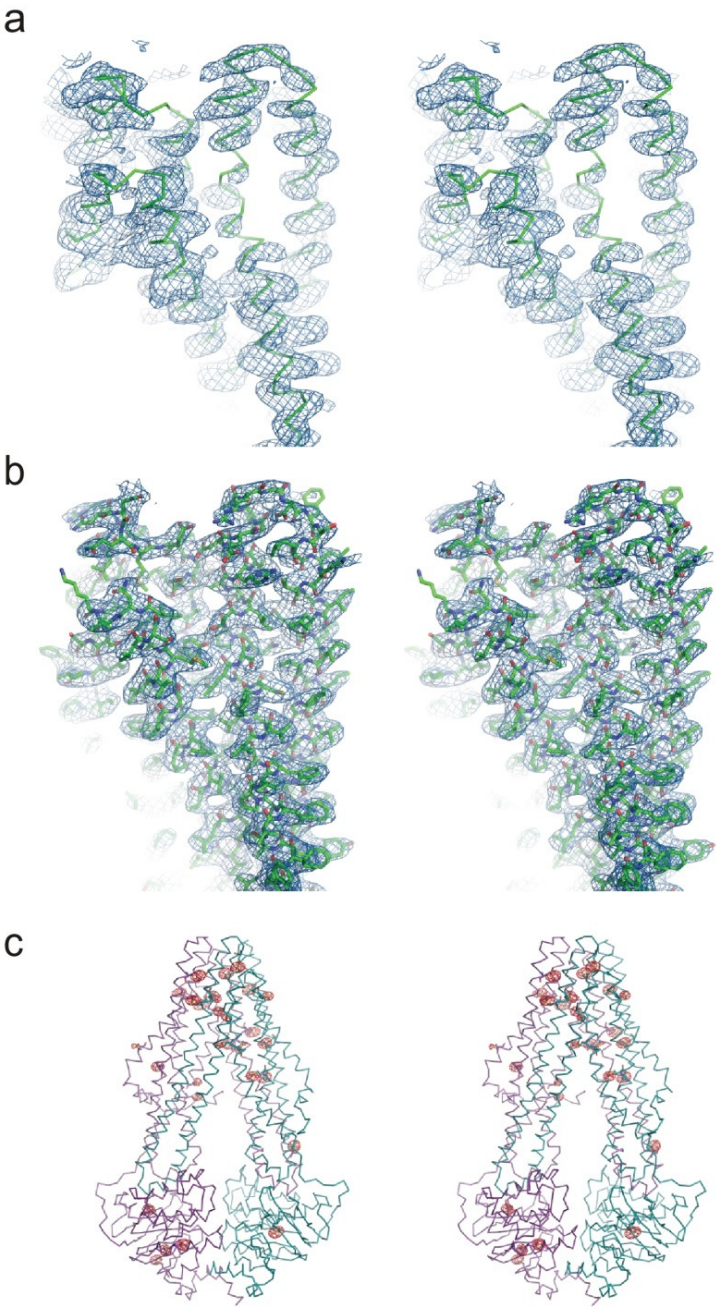

Supplementary Figure 2

Stereo-view of electron density maps of the TM287/288 model. (**a** and **b**) Electron density maps are shown as blue mesh contoured at 1 σ obtained after experimental SAD phasing using a selenomethionine derivative (**a**) and after structure refinement (**b**). The model of TM287/288 is shown as ribbon (**a**) or as sticks (**b**). (**c**) An anomalous difference Fourier electron density map depicting selenium atoms of selenomethionine TM287/288 is shown as red mesh contoured at 5 σ. The backbone of TM287/288 is shown as ribbon and the methionine residues are depicted as sticks.

Nature Structural & Molecular Biology: doi:10.1038/nsmb.2267

Fig. S3

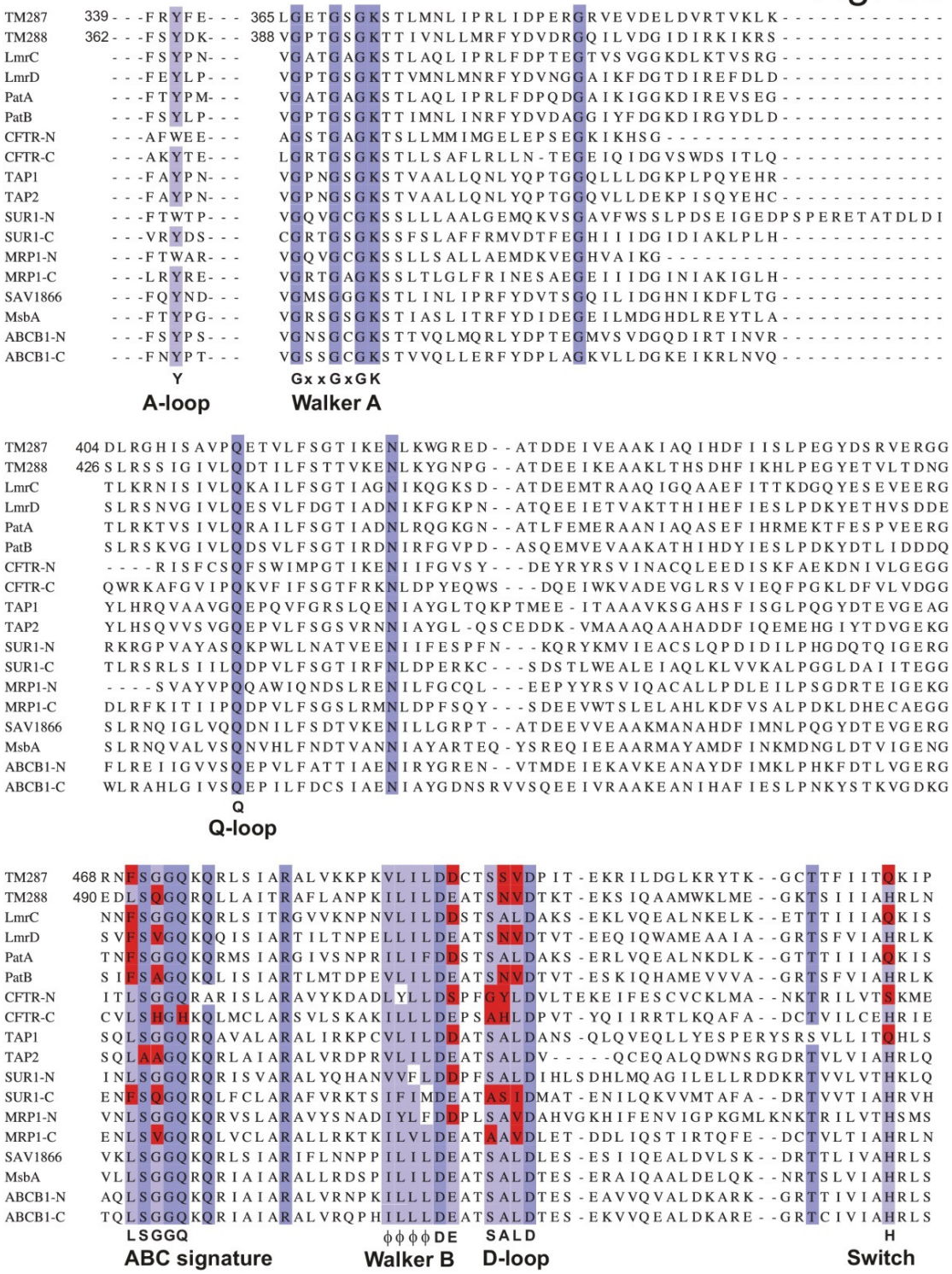

Supplementary Figure 3

Sequence alignment of ABC exporter NBDs. The consensus sequence of described structural motifs is given at the bottom of the alignment (Φ stands for an aliphatic amino acid). Positions in which the sequences deviate from consensus are highlighted in red.

Nature Structural & Molecular Biology: doi:10.1038/nsmb.2267

Fig. S4

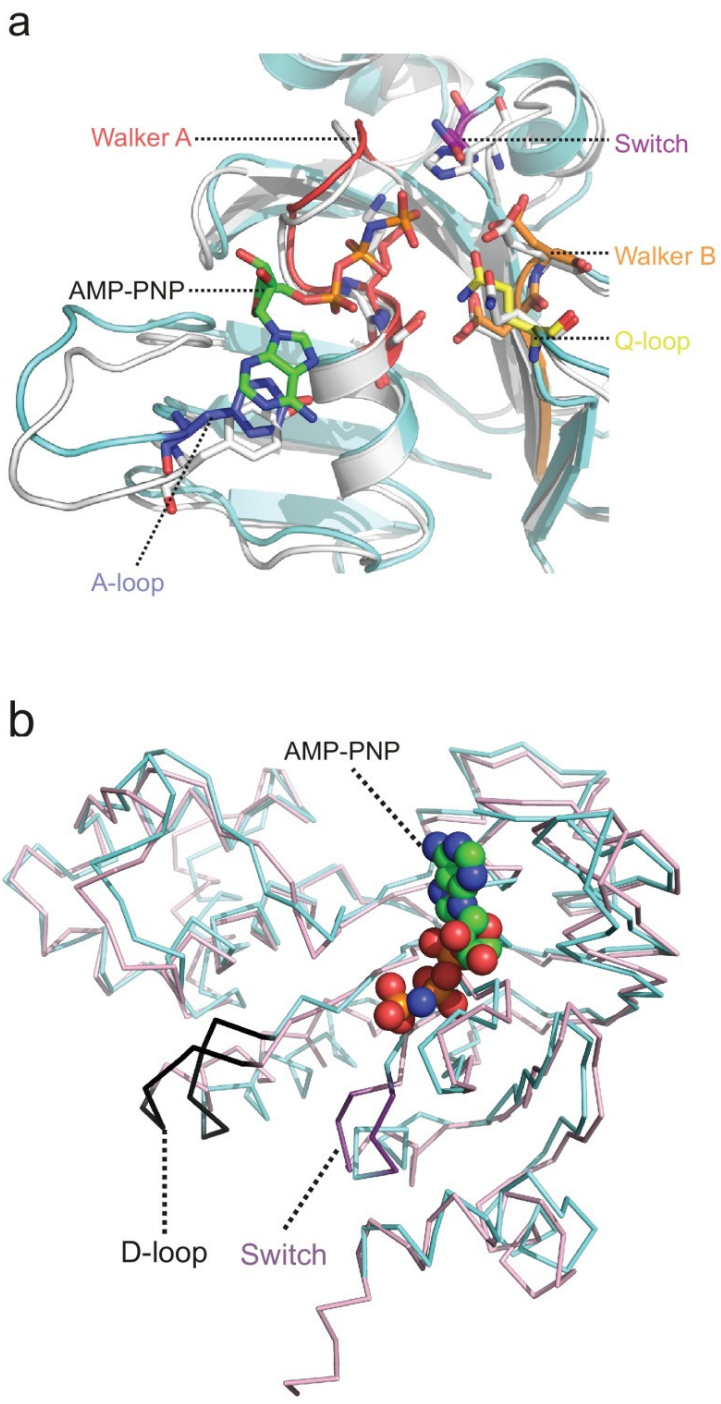

Supplementary Figure 4

Superimposition of NBD1 (TM287) and the NBD of Sav1866 and NBD2 (TM288). (**a**) Superimposition of NBD1 (TM287) and the NBD of Sav1866. The positions of key residues of NBD1 (cyan) depicted as colored sticks are almost identical to the respective residues in Sav1866 (white). AMP-PNP is shown as sticks. For clarity, ADP bound to Sav1866 is omitted. (**b**) Overlaid NBD1 (TM287) and NBD2 (TM288) mainly deviate at residues of the D-loop (black) and the switch motif (purple). AMP-PNP bound to NBD1 is shown as spheres.

Nature Structural & Molecular Biology: doi:10.1038/nsmb.2267

Fig. S5

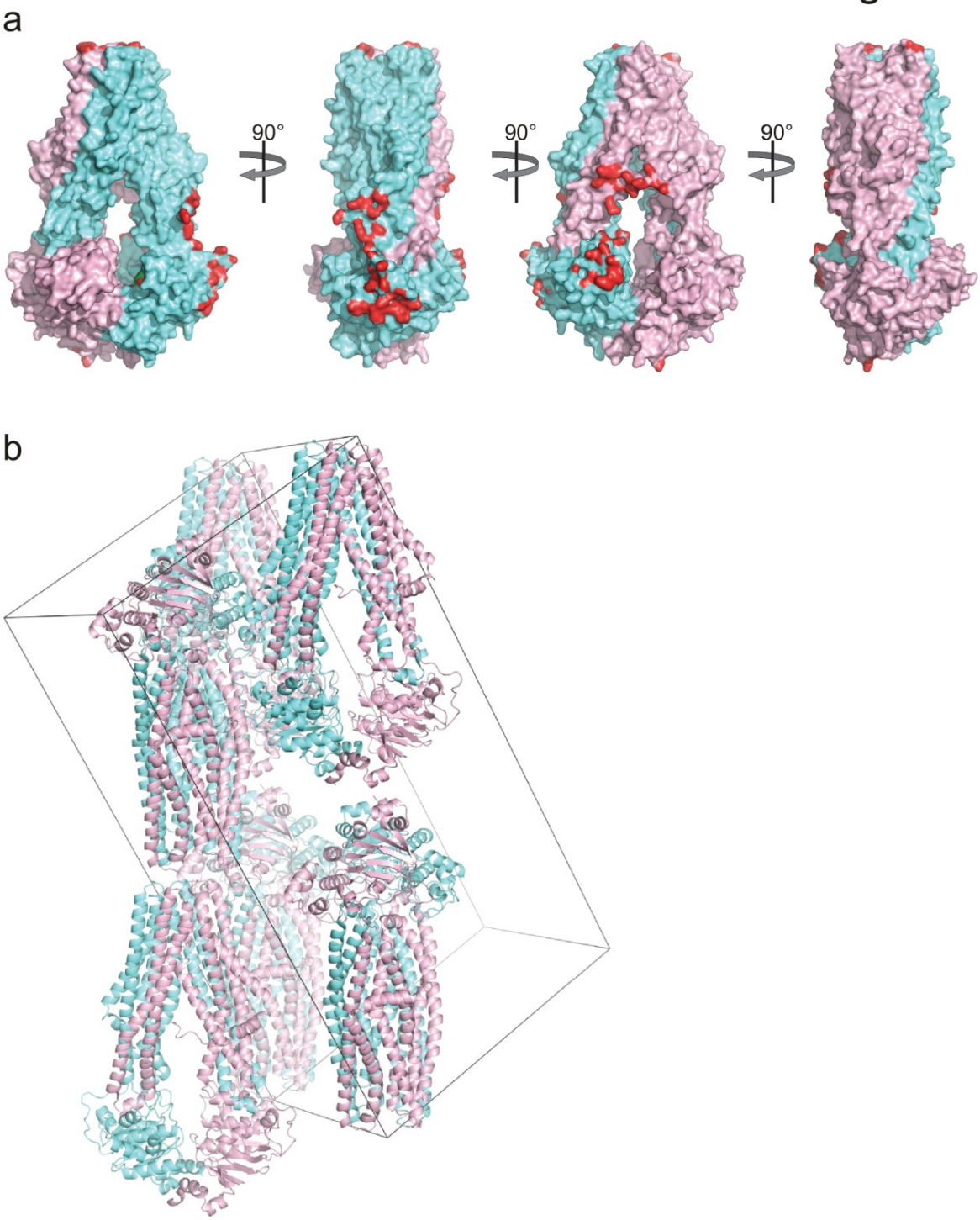

Supplementary Figure 5

Crystal packing. (**a**) Residues of TM287/288 involved in crystal contacts. TM287/288 (cyan/pink) is shown as surface representation and residues involved in crystals contacts are highlighted in red. Most of the crystal contacts reside on TM287. (**b**) Representation of the crystal packing within the unit cell indicated by black lines.

Nature Structural & Molecular Biology: doi:10.1038/nsmb.2267

Fig. S6

a

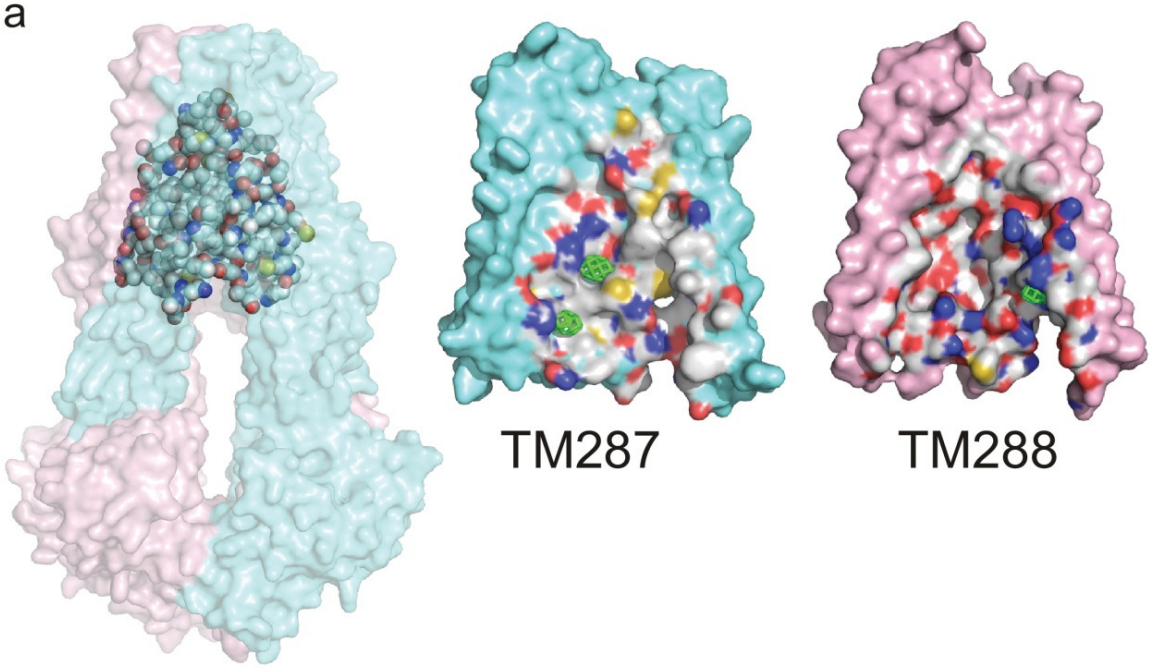

b

	Xenon
Data Collection	
Space group	C2
Cell dimensions	
a, *b*, *c* (Å)	214.66
	84.54
	113.96
α, *β*, *γ* (°)	90.000
	92.771
	90.000
Resolution (Å)	4.0
	(4.1-4.0)
R_{merge} (%)	7.4 (53.9)
I/σ_I	12.31 (3.98)
Completeness (%)	99.5 (99.7)
Redundancy	4.6 (4.7)

[a] Highest resolution shell is shown in parenthesis

Supplementary Figure 6

Cavity surface properties of the TMDs. (**a**) TM287 and TM288 are colored cyan and pink, respectively. Residues lining the cavity are represented as balls (left panel) or surfaces (middle and right panel) and are colored according to the atom type (grey (carbon), red (oxygen), blue (nitrogen) and yellow (sulfur)). The anomalous signal of three xenon atoms is shown as green mesh (difference map contoured at 8 σ and 6 σ for TM287 and TM288, respectively). (**b**) Crystallographic table of the xenon dataset used to calculate difference maps shown in (**a**).

Nature Structural & Molecular Biology: doi:10.1038/nsmb.2267

Fig. S7

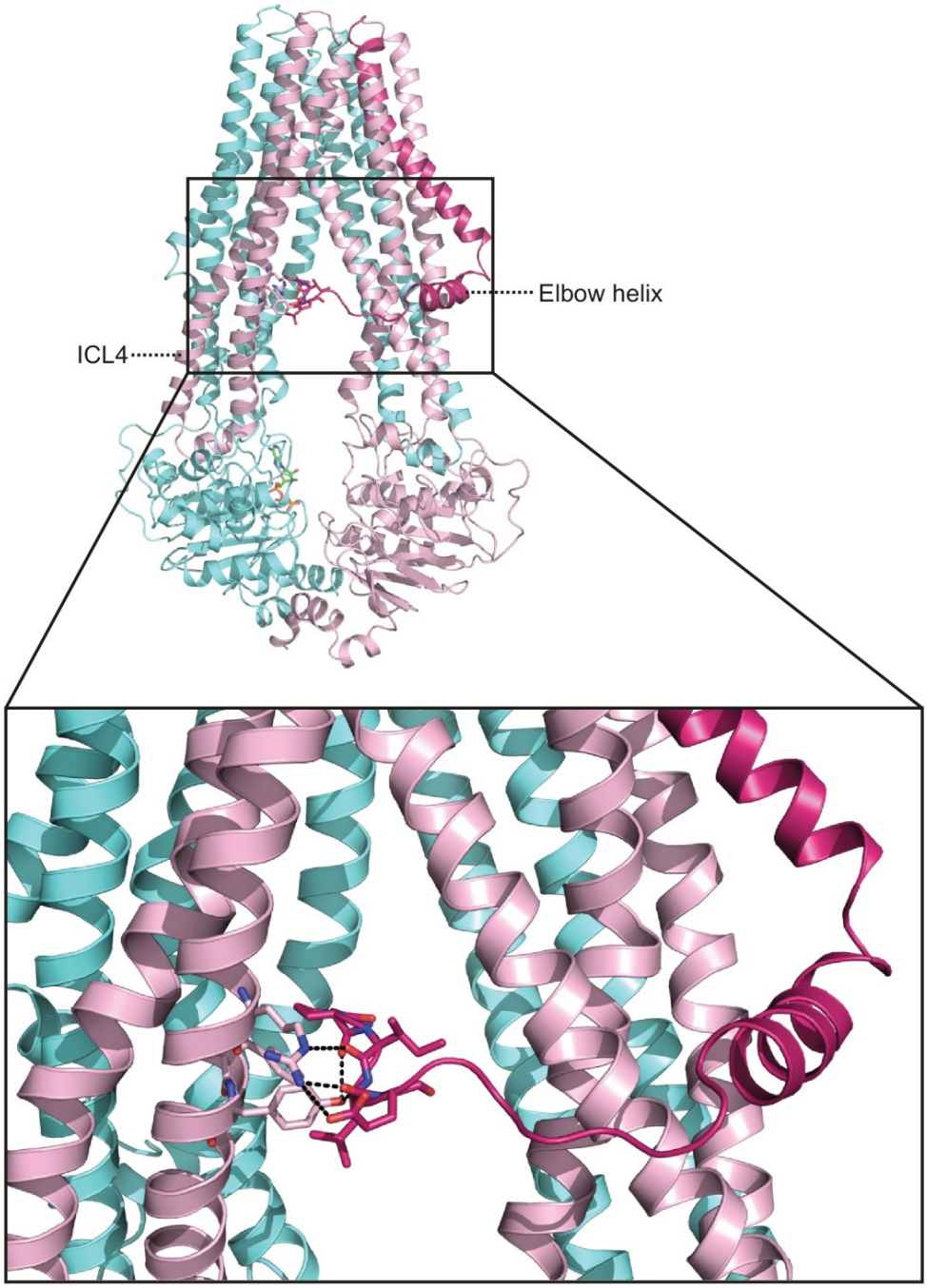

Supplementary Figure 7

Interaction of the N-terminal extension of TM288 with ICL4. TM287/288 (cyan/pink) depicted as cartoon with the N-terminal elbow-helix of TM288 colored in dark pink (top panel). Hydrogen bonding interactions between the N-terminus of TM288 and ICL4 are shown as dashed lines (close-up view; bottom panel).

Nature Structural & Molecular Biology: doi:10.1038/nsmb.2267

4 Interdomain communication between nucleotide binding sites of ABC transporters is promoted via the D-loops

Interdomain communication between nucleotide binding sites of ABC transporters is promoted via the D-loops

Michael Hohl, Markus G. Grütter and Markus A. Seeger

Manuscript in preparation

References for the following manuscript are numbered separately and are listed directly at the end of this section.

4.1 Introduction

ATP binding cassette (ABC) transporters are primary active transporters that use the energy of ATP binding and hydrolysis to shuttle a plethora of substrates across cellular membranes. They exist as importers and exporters. Whereas ABC importers are found in prokaryotes, ABC exporters exist both in prokaryotes and in eukaryotes(1). Importers are important for nutrient uptake, e.g. sugars, or for the supply of trace elements to the cell, such as metals. These membrane embedded transporters fulfil their task by interacting with a soluble, high-affinity periplasmic substrate binding protein. The physiological role of prokaryotic ABC exporters is less clear and only few substrates are known. MsbA, an ABC exporter in gram-negative bacteria is a lipid flippase, transporting lipid A and lipopolysaccharides (LPS) from the cytoplasmic side to the periplasmic side of the inner membrane. In addition, ABC exporters have been shown to be associated with multidrug resistance (MDR). In bacteria they were found to be responsible for extrusion of antimicrobial substances (PatAB, LmrCD)(2, 3) and in eukaryotic cells for the export of anticancer drugs (MRP1 and P-glycoprotein (P-gp))(4, 5). Additionally, some ABC exporters are connected to common hereditary diseases like cystic fibrosis (CFTR) or neonatal diabetes (SUR1).

The core of ABC transporters is built up by four domains, two transmembrane domains (TMDs) and two nucleotide binding domains (NBDs). The TMDs are responsible for substrate interaction and translocation and the NBDs provide the energy for the conformational changes within the TMDs necessary for providing alternative access to the substrate cavity. Binding of two ATP molecules to the motor domains (NBDs) leads to their dimerisation. This movement is transmitted to the TMDs via the coupling helices, which orient the TMDs outward-facing. The hydrolysis of ATP and the sequential release of inorganic phosphate (Pi) and ADP reset the TMDs again in an inward-facing conformation. Conserved motifs from both NBDs are responsible for the interaction with the nucleotides in a head-to-tail manner. The A-loop, a conserved aromatic residue makes favourable π-π-stacking interactions with the aromatic adenine ring(6). The Walker A motif of one NBD and the ABC signature motif of the other NBD and vice versa sandwich the γ-phosphate moiety of the nucleotides. A conserved glutamate and histidine from the Walker B and the switch motif, respectively, together constitute a catalytic dyad responsible for ATP hydrolysis. In heterodimeric ABC transporters the Walker B and switch motif sequences often depart from the consensus sequence. This catalytic site is therefore called the degenerate site. In addition, heterodimeric transporters deviate in the signature motif and the D-loop sequence at the degenerate site (Figure 1). The Q-loop glutamine interacts with the γ-phosphate moiety of the nucleotide and links the hydrolysis site with the TMDs via the coupling helices. And last but not least, the D-loop has been proposed to link the two hydrolysis sites of the two NBDs and thus might play a role in interdomain communication(7). We reported previously on the structure of the heterodimeric ABC transporter TM287/288 with one molecule of AMP-PNP bound asymmetrically to the degenerate site. In this inward-facing structure the NBDs remain in close contact which is mainly mediated by D-loop interactions at the degenerate site(8).

Here we present the apo structure of the heterodimeric ABC transporter TM287/288 solved at a resolution of 2.53 Å. The apo TM287/288 structure shows an inward-facing conformation similar to the AMP-PNP bound structure of TM287/288(8). In addition, the model of the nucleotide-bound structure

was refined to a resolution of 2.6 Å. The two high resolution structures of TM287/288 with and without bound nucleotide allow for the first time the comparison of conformational changes occurring in the NBDs upon nucleotide binding in a full-length ABC exporter. This sheds light on the long lasting question regarding rigid-body movements between the α-helical and the RecA-like subdomain in NBDs. Furthermore the structures suggest that complete NBD disengagement is not a prerequisite for nucleotide exchange in ABC exporters. The two structures allow interesting conclusions about the interdomain communication between the two NBDs via both D-loops.

4.2 Materials and Methods

4.2.1 Protein production, purification and crystallization

Production and purification of TM287/288 was performed as described previously for the AMP-PNP structure(8). Well diffracting crystals of TM287/288 in a nucleotide-free (apo) state were obtained by the vapor diffusion method in sitting drops at 20 °C against a reservoir containing 26 % (w/v) polyethylene glycol (PEG) 400, 50 mM Na-cacodylate pH 5.5 and 50 mM $CaCl_2$. The crystallization set-ups were performed in the presence of 2.5 mM ADP and 3 mM $MgCl_2$. Interestingly, ADP binding was not observed in the solved structure. Crystals of TM287/288 were also obtained in the complete absence of nucleotides and $MgCl_2$ and grew against a reservoir containing 25 % PEG 400, 50 mM N-(2-acetamido)iminodiacetic acid (ADA) pH 6.5 and 50 mM Zn-acetate. These crystals diffracted to 3.5 Å and their structure (R_{work}=22.6 % and R_{free}=28.8 %, not deposited) was indistinguishable to the high resolution apo structure presented in this manuscript.

4.2.2 Data collection and processing

All crystals were frozen without further cryo protection. Diffraction data were collected at the protein crystallography beamline X06SA at the Swiss Light Source (SLS) of the Paul Scherrer Institut (PSI) and processed using the program XDS(9). Apo TM287/288 was crystallized in the same space group as the previously solved AMP-PNP bound TM287/288 and the structure was solved by molecular replacement using the program Phaser(10). The diffraction data exhibited strong anisotropy, and was therefore truncated using the online anisotropy server of the University of California Los Angeles using default settings(11), which lead to an improvement of the electron density maps. The density allowed for the building of the entire polypeptide chain with the exception of eight C-terminal residues of TM287 (residues 570-577), nine N-terminal residues of TM288 (residues 1-9) and five C-terminal residues of TM288 (residues 593-597). The AMP-PNP dataset was reprocessed and cut at a resolution of 2.6 Å. Side by side comparison of constant parts of the apo and the nucleotide-bound structures allowed for an iterative improvement of both models. Data collection and refinement statistics are listed in Table 1.

4.2.3 Tilting angles between RecA-like and α-helical subdomain

The type I importer MalFGK (PDBs 2R6G and 3PV0)(12, 13), the type II importer BtuCD (PDBs 4FI3, 1L7V, 2QI9 and 4DBL)(14-17) and the exporter TM287/288 (PDBs …. and ….) were considered for this analysis. The apo structures (moving) were superimposed on the nucleotide-bound structures

(fixed). First the RecA-like subdomains (four segments) were superimposed then the α-helical subdomains (four segments) were used for superimposition to determine the rotation angle between the RecA-like subdomain and the α-helical subdomain. The segments used for the superimposition are listed in Table 2. The program Superpose of the CCP4 Program Suite was utilized.

4.3 Results

4.3.1 Structure determination and superimposition with the AMP-PNP bound TM287/288 structure

The apo crystal structure of the heterodimeric ABC exporter TM287/288 was solved as described in Materials and Methods. Apo TM287/288 was crystallized in the same space group as the AMP-PNP bound form (Table 1). Its structure was refined to 2.53 Å resolution (PBD ...., R_{work}=23.9 % and R_{free}=29.1 %) and shows an inward-facing conformation very similar to the one crystallized together with the non-hydrolysable ATP analogue AMP-PNP. The root-mean-square deviation (rmsd) between the C_α-positions of the TM287/288 structure with bound nucleotide (PDB ...., new 2.6 Å structure, R_{work}=22.68 % and R_{free}=27.06 %) and the 2.53 Å structure without nucleotides is 0.636 Å over residues 1-569 (chain A) and 10-592 (chain B). Figure 2a depicts the full-length nucleotide-bound structure solved at 2.6 Å and highlights residues in red whose C_α-position deviate from the structure of the apo-state by more than 1.1 Å. Figure 2b shows the same analysis as in Figure 2a, but the deviations are highlighted on the 2.53 Å apo structure. Most differences are found in the NBDs and only few are observed in the transmembrane domains of the transporter. In addition, the majority of the deviations cluster at the degenerate nucleotide binding site around the bound nucleotide or at the interface of the two motor domains (Figure 2c). Influences by crystal packing interactions can be excluded, because both structures were crystallized in the same space group with basically identical cell edges. Figure 2d depicts the NBD in the same orientation as in Figure 2c, but instead of the structural deviations, conserved NBD motifs are shown. It is intriguing how well the differences between the two TM287/288 structures and the functionally important motifs co-localize. The analysis of the C_α-differences for NBD287 and NBD288 is additionally plotted as distances in Å vs. amino acid residue in Figure 3.

4.3.2 Nucleotide binding domain 287

The above analysis has shown that almost all differences between the full-length structures of TM287/288 in the two nucleotide states are found at the nucleotide binding domains. Therefore, a more thorough analysis was performed at the NBD level. Figure 4a shows a superimposition of the isolated NBD dimers of the two crystallized states (cyan and pink (AMP-PNP), white and gray (apo)). The root mean square deviation (rmsd) between NBD287 in the two states is 0.952 Å (over residues 330-569). The rmsd of the corresponding two NBD288 is only 0.460 Å (over residues 353-592). Comparing the two NBD287s that provide the Walker A and the switch motif of the degenerate ATPase site in the apo and the nucleotide-bound form reveals structural differences that are strongly associated with conserved NBD motifs (Figure 2c and 2d). The whole loop (Arg340-Asp346) including Tyr341 (A-loop) is undergoing an outward movement of about 1.7 Å to accommodate the adenine moiety of AMP-PNP (Figure 4b and Figure 5a). The Walker A motif (GETGSGK in NBD287) that wraps around the nucleotide(7), shows differences in the C_α-positions of Gly369 and Ser373, which are in close proximity to the functionally important Walker A Lys372. The lysine itself undergoes only a slight rearrangement. More pronounced is the displacement of Leu375 (2.4 Å) and Met376 (2.7 Å), which are part of a α-helix directly following the Walker A motif (Figure 3a and Figure 5b). The Q-loop Gln414, which serves as a hinge between the α-helical and the RecA-like subdomain(18) shows a change in conformation in TM287/288 upon AMP-PNP binding. It flips into hydrogen bonding distance with the γ-phosphate hydroxyl group of the nucleotide (Figure 5c) and is involved in Mg^{2+} coordination. Its involvement in ATP sensing, which triggers inward rotation of the α-helical subdomain with respect to the RecA-like subdomain and more precisely the ATPase active site, respectively, has been suggested(19). Interestingly, this inward rotation of the helical subdomain is only very subtle in full-length TM287/288 upon nucleotide binding (see below). The Walker B motif in NBD287 (VLILDD), deviating from the consensus sequence (ΦΦΦΦDE, Φ = aliphatic amino acid), shows a difference between the apo and nucleotide-bound structures in Asp494 (1.6 Å) and Asp495 (1.7 Å) and especially in the adjacent Cys496 (4.6 Å) (Figure 3a and Figure 5d). But by far the biggest difference upon nucleotide binding can be observed in the D-loop of NBD287 (SSVD), the adjacent Pro502 and the helix (Lys513-Lys517) following the D-loop. Ser498 moves 1.2 Å, Ser499 5.9 Å, Val500 even 7 Å and Asp501 3.3 Å. All these differences are associated with a pronounced conformational change of the D-loop (Figure 5e). In agreement with these observations, the D-loop of NBD287 shows a high B-factor, reflecting its flexibility (Figure 6). However, electron density was sufficiently defined to allow model building. In contrast, in one of the four structures of ABCB10 (PBD 4AYW) the D-loop could not be traced completely, probably due to this high flexibility. A more detailed description of the D-loop of NBD287 and its interactions with the opposite NBD288 is given below in a separate section.

4.3.3 Nucleotide binding domain 288

Next to conformational changes in NBD287, minor changes are observed in NBD288 upon nucleotide binding. Figure 2c, Figure 3b and Figure 4c highlight these differences. A pronounced change two amino acids upstream (Thr438) of the Q-loop Gln436 in NBD288 is visible (Figure 5f). In the ABC-specific signature motif (LSQGQ), which is involved in nucleotide binding in closed NBD dimers, Ser493 undergoes a conformational change upon AMP-PNP binding (Figure 5f). Nucleotide binding to

the degenerate site is responsible for the disruption of a hydrogen bond formed in the apo state between the signature motif Ser493 and the D-loop Asp523 of NBD288. In contrast to the large differences in the D-loop of NBD287 only a minor change in the D-loop of NBD288 (SNVD) in Ser520 is observed (Figure 5f).

4.3.4 Interdomain (nucleotide binding domains) interactions

Nucleotide binding to full-length TM287/288 not only provokes changes within the NBDs, but also influences intermolecular interactions between the NBDs. Yuan *et al.* first described the intermolecular interplay between the signature motif of one NBD and the Walker A of the other NBD(19). In a closed NBD dimer, these two motifs form a composite hydrolysis site sandwiching the nucleotide in a head to tail manner. In the partially open NBD dimer of TM287/288 the signature motif is far apart from the AMP-PNP bound to NBD287. However, the D-loop of NBD288 (SNVD) intimately interacts with the nucleotide binding site of NBD287 and is part of the composite degenerate ATPase site. In the nucleotide-bound TM287/288 structure, the D-loop of NBD288 interacts via an extensive H-bond network with NBD287. The carbonyl oxygen of Ser520 makes a hydrogen bond to the ε-nitrogen of the H-loop Gln526. Gln526 is connected via an additional bond to the D-loop Asn521. Asn521 makes a direct contact to the bound AMP-PNP. Furthermore, Val522 and Thr524 of NBD288 establish each two H-bonds with Thr368 and Glu367, respectively, of the Walker A motif of NBD287 (Figure 7a, left). The removal of the nucleotide from the degenerate hydrolysis site results in a rearrangement of this H-bond network. Ser520 remains connected to Gln526, but the H-bond between Gln526 and Asn521 is broken. Instead, Asn521 now makes a hydrogen bond to the Walker A Thr368. The two hydrogen bonds between Thr524 and Glu367 are preserved. Within NBD288, Asp523 of the D-loop forms an H-bond with Ser493 of the signature motif in the apo form of TM287/288. In summary, the number of hydrogen bonds connecting NBD287 and NBD288 at the degenerate ATPase site is reduced from seven to four upon nucleotide removal (Figure 7b, left). Nevertheless, the NBDs remain in contact even in the absence of nucleotides, strengthening our earlier notion that the degenerate site is preformed to accommodate binding of the first nucleotide to the transporter(8).

Nucleotide binding is associated with a pronounced movement of the D-loop and the connected D-loop helix in NBD287 at the consensus site. It is fascinating to notice that this D-loop (SSVD) is actually more than 19 Å away from the site of nucleotide binding (measured between AMP-PNP γ-phosphate and C_α of Asp501). The structural link between the bound nucleotide and the D-loop is in part established via the Walker B Asp495, which precedes the D-loop, separated by two residues and moves closer to the γ-Pi of AMP-PNP upon nucleotide binding (Figure 8). When AMP-PNP is bound, an interaction between Thr390 (NBD288) and the D-loop Asp501 is established (Figure 7a, right). Thr390 is part of the Walker A motif in NBD288 and is the corresponding residue to Thr368 (NBD287). Asp501 additionally interacts with the backbone nitrogen of Thr368. The switch residue His548 of the consensus ATPase site is too far away from the D-loop to interact in a similar way as the corresponding Q526 at the degenerate site. Nucleotide removal leads to a rearrangement of the D-loop in NBD287 and disrupts the interaction of Asp501 with the Walker A of NBD288 (Figure 7b, right). The involvement of the D-loop in NBD-NBD interdomain communication has been postulated before based on structures of isolated NBDs(7). Here we show asymmetric interactions of the D-loops of

heterodimeric ABC exporters in the context of the full-length transporter structure. Our analysis reveals that the D-loop of the degenerate site plays a key role in the stabilization of the NBD interaction, whereas the D-loop at the consensus site is highly flexible and interacts with the opposite NBD only when a nucleotide is bound to the degenerate site.

4.3.5 Nucleotide binding domain opening in inward-facing ABC exporter structures

Three bacterial structures and five structures of eukaryotic origin in an inward-facing conformation have been deposited. When comparing these different exporter structures the different separation distances between the two NBDs are eye-catching. In the two structures of the *E. coli* and *V. cholerae* MsbA, the NBDs are separated by 61.69 – 68.46 Å (depending on the homodimer in the asymmetric unit) and 32.75 Å, respectively (distances are measured between C_α- positions of residues in the coupling helices, Figure 9 and Table 3). The NBDs of the *Vibrio* protein show an additional rotation of one domain with respect to the other(20). These observed separations of the NBDs in MsbA raised criticism regarding the physiological relevance of such conformations, in particular because the separated NBDs were involved in crystal contacts. However, by using electron spin resonance measurements (EPR) these conformations could be confirmed in solution(21, 22). In addition, two recently published P-gp structures support this conformational flexibility. In the mouse apo P-gp structure the NBDs are 34.77 – 35.90 Å (depending on the chain in the asymmetric unit) away from each other. In the *C. elegans* P-gp structure the motor domains are separated by 46.14 Å. In the ABCB10 structures the NBDs are separated by 29.83 Å, 28.84 Å and 25.1 Å, respectively. All three ABCB10 structures have two nucleotides bound at the NBD-NBD interface. The NBDs of TM287/288 with one AMP-PNP molecule bound are only 29.13 Å apart and are interacting with each other via an extensive H-bonding network between the D-loop of NBD288 and the Walker A and switch motif of NBD287 (Figure 7). Basically the same distance can be observed in TM287/288 crystallized without nucleotide (28.89 Å), although the hydrogen bonding network at the degenerate site appears to be weaker than in the AMP-PNP structure (discussed above). Our analysis suggests that at least in (bacterial) heterodimeric ABC exporters the NBDs do not have to separate completely to exchange a nucleotide and remain in constant contact during cycling.

4.3.6 Rigid body movements of the subdomains in the nucleotide binding domain

Nucleotide binding domains can be divided into two individual subdomains. The larger of these two domains, the RecA-like domain, has a α/β-fold, whereas the smaller α-helical domain contains only alpha helices. The RecA-like domain bears the highly conserved Walker A and Walker B motifs common to all ATPases and the α-helical domain contains the ABC transporter specific ABC signature motif. By comparing isolated NBDs crystallized with and without nucleotides, rigid body rotations between RecA-like and α-helical domains were associated with nucleotide binding. In the full-length transporter context of TM287/288, we for the first time can analyze the structural consequences of nucleotide binding in an ABC exporter. In contrast to isolated NBDs, where rigid body movements up to 30 ° were observed between the RecA-like and the α-helical domain(23, 24), we observed only very

minor tilts of 2 ° upon binding of AMP-PNP to NBD287. Although information on eventual rigid body movements in NBD288 upon binding of the second nucleotide to the consensus site is missing, it is likely that interactions at the NBDs with the coupling helices, which interact with both the RecA-like and the α-helical domain as well as the intimate interdomain communication between the NBDs play a more important role than nucleotide binding with regard to rigid body rotations.

The tilting angles between the RecA-like and the α-helical subdomain for two ABC importers for which crystal structures with and without bound nucleotides exist were calculated in addition, namely for the maltose transporter MalFGK and the vitamin B12 transporter BtuCD. The calculated angles for MalFGK(12, 13), which is a type I ABC transporter, were between 12 and 15 °. The analysis for the type II importer BtuCD(14-17), gave rotation angles between 2 and 3 °, which is as low as in TM287/288. Table 2 summarizes the segments used for the superimposition analysis and lists the angles calculated for the rotation of the α-helical subdomain.

4.4 Discussion

Although progress in the field of membrane protein crystallography is impressive, the amount of structural data of these flexible and relatively instable proteins remains scarce. In addition, often only unrelated proteins within a protein superfamily can be crystallized in different conformational states. Therefore, conclusions regarding the transport mechanism of a class of transporters are often based on rather speculative assumptions or inaccurate homology models. To overcome these limitations, obtaining crystal structures of one single protein in different conformations or in ligand-bound and ligand-free states at high resolution is highly desirable to draw meaningful conclusions regarding the function and mechanism of transporters under study.

Here we present the apo structure of the heterodimeric ABC transporter TM287/288. Together with the recently published AMP-PNP structure of TM287/288, for the first time the consequences of nucleotide binding in one and the same full-length ABC exporter can be analysed. We observed that in the subclass of (bacterial) heterodimeric ABC exporters a full separation of the nucleotide binding domains, as seen for *E. coli* MsbA or P-gp, does not seem to be essential for nucleotide exchange and that the NBDs appear to be held constantly together by an extensive hydrogen bonding network at the degenerate ATPase site even in the absence of nucleotides. In addition, the often described rigid-body rotation in isolated NBDs between the alpha helical subdomain with respect to the RecA-like subdomain associated with nucleotide binding could not be observed. Most interestingly, we were able to gain insight into the mechanism of interdomain communication between the two ATPase sites promoted via the D-loops. The presence of a nucleotide bound to the degenerate site is sensed by residues of the Walker B motif and further transmitted in a long-range conformational change to the D-loop to form two hydrogen bonds between the D-loop Asp501 of NBD287 and Thr390 of the Walker A motif of NBD288. These two H-bonds are disrupted when the nucleotide at the degenerate site dissociates (apo structure). In addition, nucleotide binding to the degenerate site breaks a hydrogen bond between the D-loop Asp523 and the ABC signature Ser493 of NBD288.

This new structure together with the recently solved AMP-PNP structure helps to better understand the mechanism underlying this medically relevant ABC exporter subtype, with eukaryotic representatives like CFTR, SUR1, Tap1/2 or MRP1.

4.5 Bibliography

1. Locher, K.P., *Review. Structure and mechanism of ATP-binding cassette transporters.* Philos Trans R Soc Lond B Biol Sci, 2009. 364(1514): p. 239-45.
2. Garvey, M.I., A.J. Baylay, R.L. Wong, and L.J. Piddock, *Overexpression of patA and patB, which encode ABC transporters, is associated with fluoroquinolone resistance in clinical isolates of Streptococcus pneumoniae.* Antimicrob Agents Chemother, 2011. 55(1): p. 190-6.
3. Lubelski, J., A. de Jong, R. van Merkerk, H. Agustiandari, O.P. Kuipers, J. Kok, and A.J. Driessen, *LmrCD is a major multidrug resistance transporter in Lactococcus lactis.* Mol Microbiol, 2006. 61(3): p. 771-81.
4. Pham, A.N., J. Wang, J. Fang, X. Gao, Y. Zhang, P.E. Blower, W. Sadee, and Y. Huang, *Pharmacogenomics approach reveals MRP1 (ABCC1)-mediated resistance to geldanamycins.* Pharm Res, 2009. 26(4): p. 936-45.
5. Ganguly, A., K. Banerjee, P. Chakraborty, S. Das, A. Sarkar, A. Hazra, M. Banerjee, A. Maity, M. Chatterjee, N.B. Mondal, and S.K. Choudhuri, *Overcoming multidrug resistance (MDR) in cancer in vitro and in vivo by a quinoline derivative.* Biomed Pharmacother, 2011. 65(6): p. 387-94.
6. Kim, I.W., X.H. Peng, Z.E. Sauna, P.C. FitzGerald, D. Xia, M. Müller, K. Nandigama, and S.V. Ambudkar, *The conserved tyrosine residues 401 and 1044 in ATP sites of human P-glycoprotein are critical for ATP binding and hydrolysis: evidence for a conserved subdomain, the A-loop in the ATP-binding cassette.* Biochemistry, 2006. 45(24): p. 7605-16.
7. Zaitseva, J., S. Jenewein, T. Jumpertz, I.B. Holland, and L. Schmitt, *H662 is the linchpin of ATP hydrolysis in the nucleotide-binding domain of the ABC transporter HlyB.* Embo J, 2005. 24(11): p. 1901-10.
8. Hohl, M., C. Briand, M.G. Grütter, and M.A. Seeger, *Crystal structure of a heterodimeric ABC transporter in its inward-facing conformation.* Nat Struct Mol Biol, 2012. 19(4): p. 395-402.
9. Kabsch, W., *Xds.* Acta Crystallogr D Biol Crystallogr, 2010. 66(Pt 2): p. 125-32.
10. McCoy, A.J., R.W. Grosse-Kunstleve, P.D. Adams, M.D. Winn, L.C. Storoni, and R.J. Read, *Phaser crystallographic software.* J Appl Crystallogr, 2007. 40(Pt 4): p. 658-674.
11. Strong, M., M.R. Sawaya, S. Wang, M. Phillips, D. Cascio, and D. Eisenberg, *Toward the structural genomics of complexes: crystal structure of a PE/PPE protein complex from Mycobacterium tuberculosis.* Proc Natl Acad Sci U S A, 2006. 103(21): p. 8060-5.

12. Oldham, M.L., D. Khare, F.A. Quiocho, A.L. Davidson, and J. Chen, *Crystal structure of a catalytic intermediate of the maltose transporter.* Nature, 2007. 450(7169): p. 515-21.

13. Oldham, M.L. and J. Chen, *Crystal structure of the maltose transporter in a pretranslocation intermediate state.* Science, 2011. 332(6034): p. 1202-5.

14. Korkhov, V.M., S.A. Mireku, and K.P. Locher, *Structure of AMP-PNP-bound vitamin B12 transporter BtuCD-F.* Nature, 2012. 490(7420): p. 367-72.

15. Locher, K.P., A.T. Lee, and D.C. Rees, *The E. coli BtuCD structure: a framework for ABC transporter architecture and mechanism.* Science, 2002. 296(5570): p. 1091-8.

16. Hvorup, R.N., B.A. Goetz, M. Niederer, K. Hollenstein, E. Perozo, and K.P. Locher, *Asymmetry in the structure of the ABC transporter-binding protein complex BtuCD-BtuF.* Science, 2007. 317(5843): p. 1387-90.

17. Korkhov, V.M., S.A. Mireku, R.N. Hvorup, and K.P. Locher, *Asymmetric states of vitamin B(1)(2) transporter BtuCD are not discriminated by its cognate substrate binding protein BtuF.* FEBS Lett, 2012. 586(7): p. 972-6.

18. Ramaen, O., N. Leulliot, C. Sizun, N. Ulryck, O. Pamlard, J.Y. Lallemand, H. Tilbeurgh, and E. Jacquet, *Structure of the human multidrug resistance protein 1 nucleotide binding domain 1 bound to Mg2+/ATP reveals a non-productive catalytic site.* J Mol Biol, 2006. 359(4): p. 940-9.

19. Yuan, Y.R., S. Blecker, O. Martsinkevich, L. Millen, P.J. Thomas, and J.F. Hunt, *The crystal structure of the MJ0796 ATP-binding cassette. Implications for the structural consequences of ATP hydrolysis in the active site of an ABC transporter.* J Biol Chem, 2001. 276(34): p. 32313-21.

20. Ward, A., C.L. Reyes, J. Yu, C.B. Roth, and G. Chang, *Flexibility in the ABC transporter MsbA: Alternating access with a twist.* Proc Natl Acad Sci U S A, 2007. 104(48): p. 19005-10.

21. Mittal, A., S. Bohm, M.G. Grütter, E. Bordignon, and M.A. Seeger, *Asymmetry in the homodimeric ABC transporter MsbA recognized by a DARPin.* J Biol Chem, 2012. 287(24): p. 20395-406.

22. Borbat, P.P., K. Surendhran, M. Bortolus, P. Zou, J.H. Freed, and H.S. McHaourab, *Conformational motion of the ABC transporter MsbA induced by ATP hydrolysis.* PLoS Biol, 2007. 5(10): p. e271.

23. Diederichs, K., J. Diez, G. Greller, C. Müller, J. Breed, C. Schnell, C. Vonrhein, W. Boos, and W. Welte, *Crystal structure of MalK, the ATPase subunit of the trehalose/maltose ABC transporter of the archaeon Thermococcus litoralis.* Embo J, 2000. 19(22): p. 5951-61.

24. Hopfner, K.P., A. Karcher, D.S. Shin, L. Craig, L.M. Arthur, J.P. Carney, and J.A. Tainer, *Structural biology of Rad50 ATPase: ATP-driven conformational control in DNA double-strand break repair and the ABC-ATPase superfamily.* Cell, 2000. 101(7): p. 789-800.

Figure 1

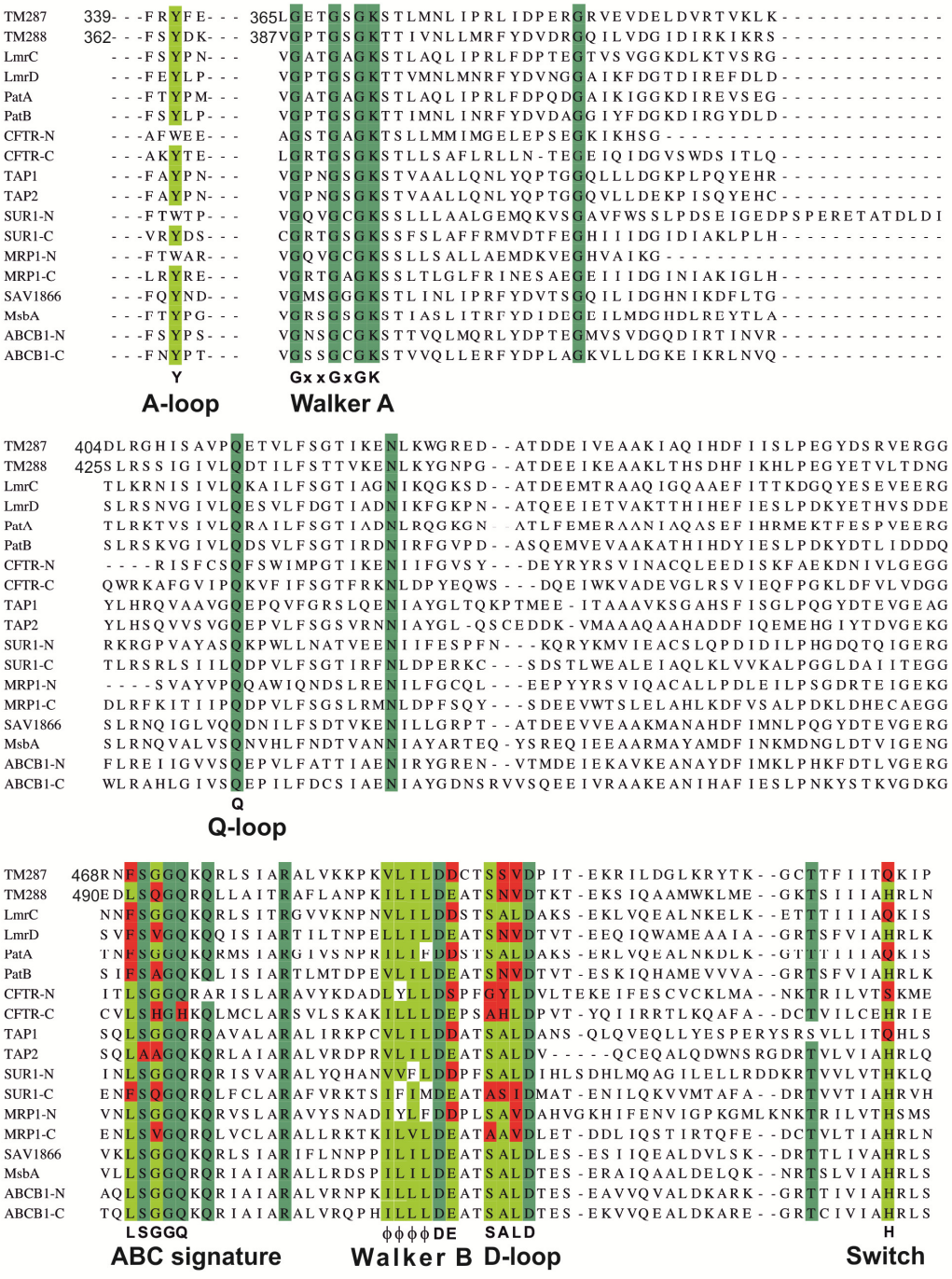

Figure 1:
Alignment of selected ABC exporter NBD sequences. The consensus sequence of described structural motifs is given at the bottom of the alignment (Φ stands for an aliphatic amino acid). Positions in which the sequences deviate from consensus are highlighted in red.

Figure 2

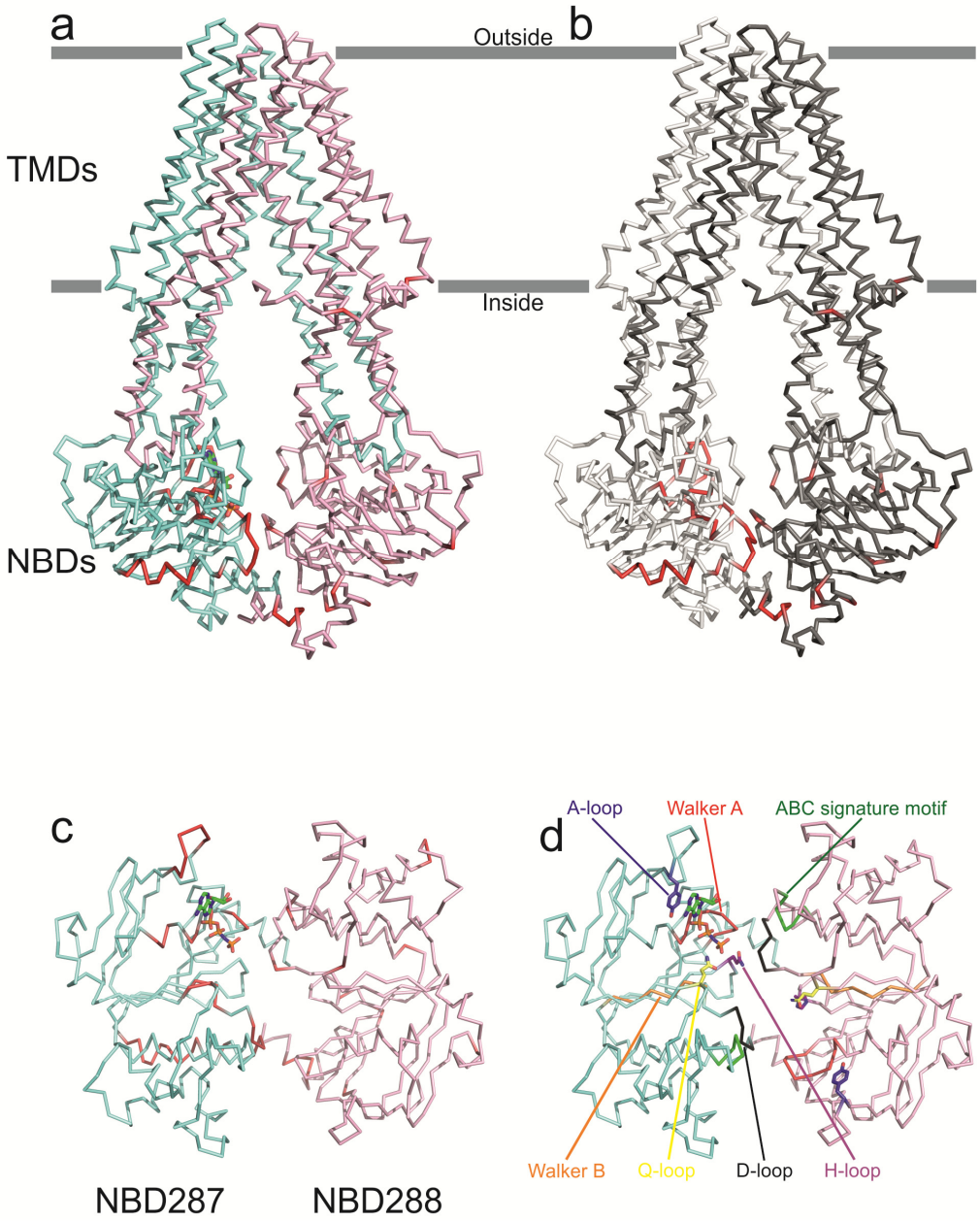

Figure 2:
Structural differences between the apo and the nucleotide-bound TM287/288 structures. (a) Side view of the nucleotide-bound TM287/288 structure colored in cyan (TM287) and pink (TM288). AMP-PNP is shown as sticks. C_α-positions deviating more that 1.1 Å between the nucleotide-bound and the apo structure are highlighted in red. Membrane boundaries are indicated in gray. (b) The same analysis as in (a) is shown, but the differences are highlighted on the apo structure. TM287 is shown in white and TM288 in dark gray. (c) Top view on the NBD dimer alone (NBD287: Gly330-Phe569, NBD288: Gly353-Leu593) with bound AMP-PNP with the same differences accentuated as in (a). (d) NBD dimer in the same orientation as in (c) with conserved motifs highlighted in colors. A-loop (blue), Walker A (red), Q-loop (yellow), ABC signature motif (green), Walker B (orange), D-loop (black) and H-loop (magenta).

Figure 3

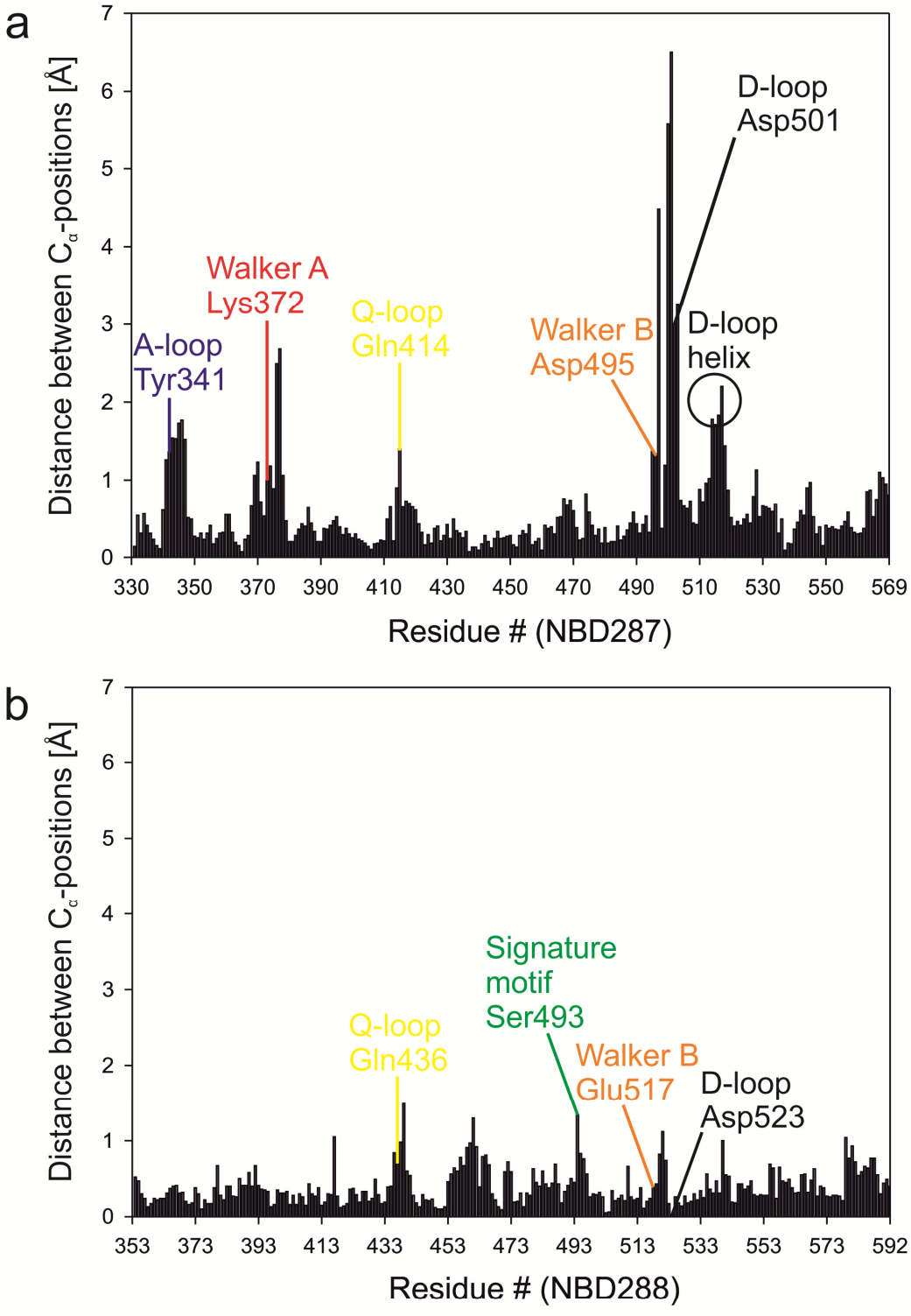

Figure 3:
Superimposition analysis of the nucleotide-bound and the apo TM287/288 structures at the level of the NBDs. The backbone carbon distances between each residue (in Å) of the nucleotide-bound and apo states of NBD287 (a) and NBD288 (b) is plotted against the residue number. Key residues of conserved NBD motifs are labeled.

Figure 4

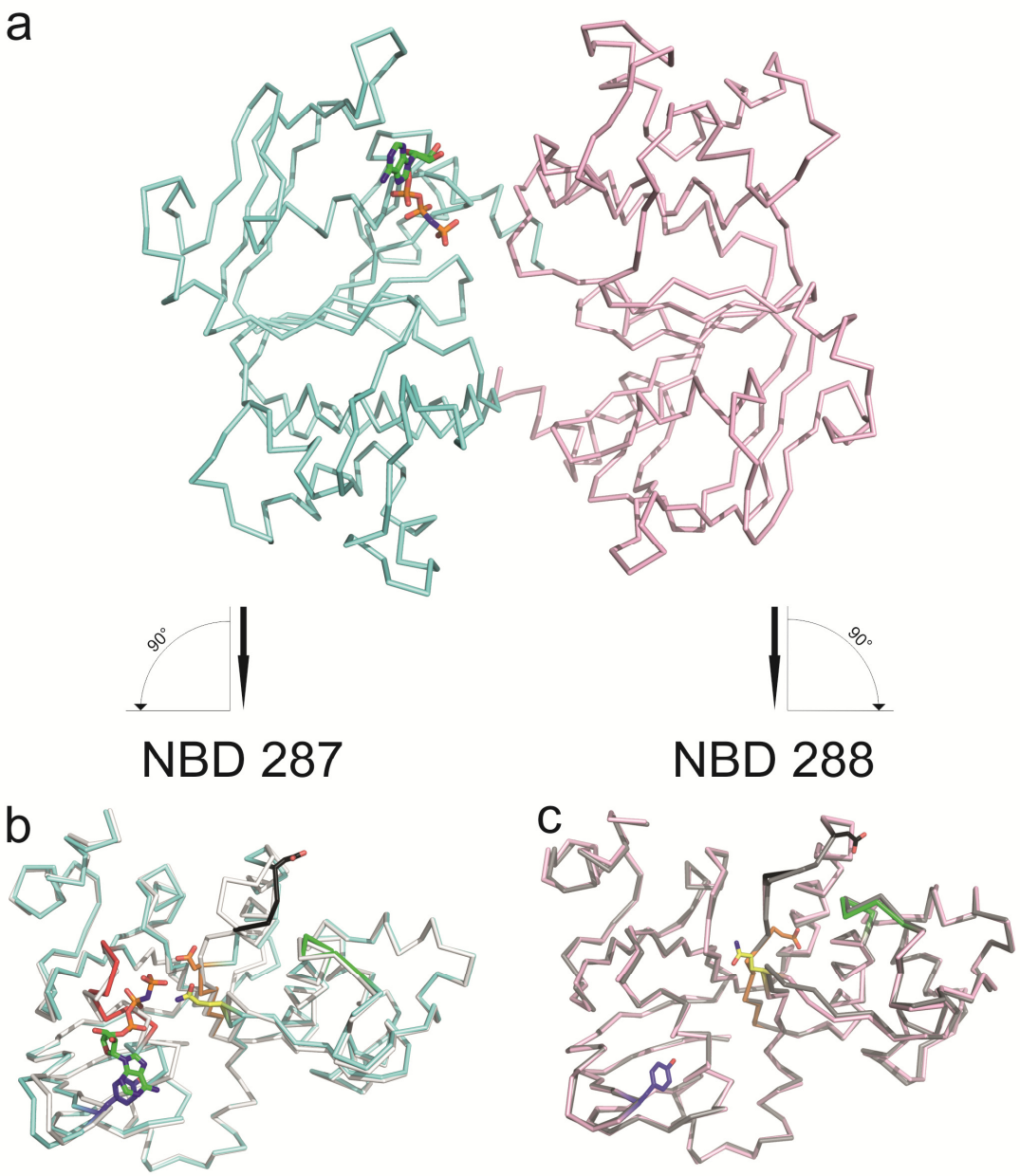

Figure 4:
Superimposition of individual NBDs. (a) The NBD dimer (cyan/pink) of the AMP-PNP structure is shown as an overview. AMP-PNP is shown as sticks. (b) Superimposition of the individual NBD287s in the apo (white/dark gray) and the AMP-PNP bound states. (c) Superimposition of NDB288. A-loop (blue), Walker A (red), Q-loop (yellow), ABC signature motif (green), Walker B (orange), D-loop (black).

Figure 5

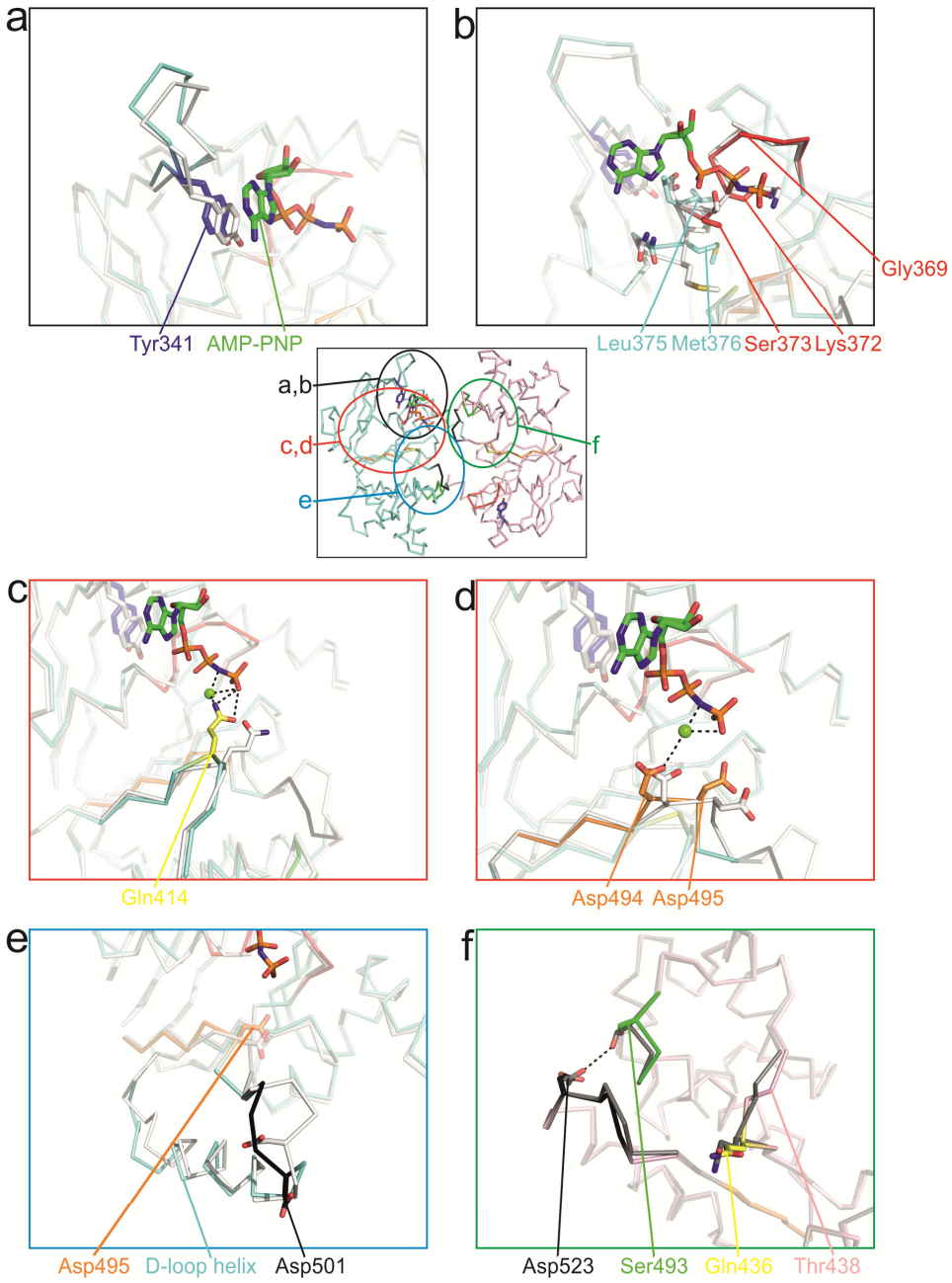

Figure 5:
Close-up views highlighting local differences seen between the nucleotide-bound (cyan/pink) and the apo structure (white/dark gray). The smaller picture in the second line is given as an overview. For clarity, conserved motifs and highlighted side chains are only colored in the AMP-PNP structure. AMP-PNP is shown as sticks in a-e, Mg^{2+} as a green sphere in c and d. (a) Structural changes in the A-loop (blue) of NBD287. Tyr341 of the A-loop is highlighted as sticks. (b) Differences of the Walker A motif (red) in NBD287 and residues following Walker A are shown. Walker A Lys372, Ser372, Leu375 and Met376 are shown as sticks. (c) The Q-loop Gln414 (yellow) is shown in stick representation. It moves towards the bound nucleotide in the AMP-PNP structure. (d) Deviations seen in the Walker B motif (orange) upon AMP-PNP binding. Asp494 and Asp495 of the degenerate site are shown. (e) Large changes in conformation are seen in the D-loop (black) of NBD287. Asp501 is highlighted as sticks. (f) Changes seen in NBD288 associated with nucleotide binding to NBD287. The signature motif is colored in green (Ser493), the D-loop in black (Asp523) and the Q-loop in yellow (Gln436). The H-bond between Ser493 and Asp523 that is formed only in absence of a nucleotide at the degenerate site is highlighted.

Figure 6

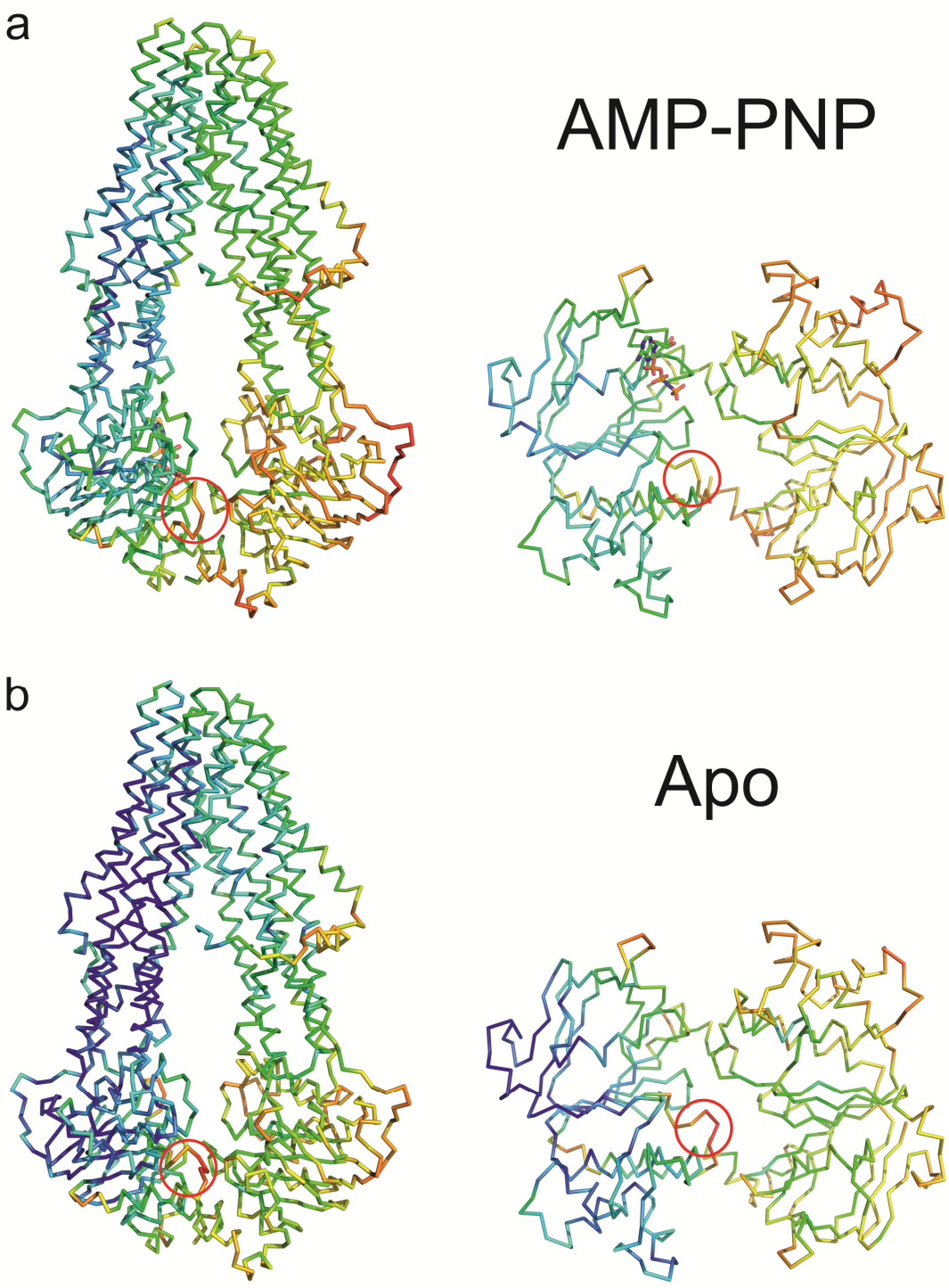

Figure 6:
B-factor analysis of the apo and AMP-PNP TM287/288 structures. (a) Shown are B-factors of the nucleotide-bound structure of TM287/288 viewed from the side (left) and on top of the NBD dimer (right). (b) Same analysis as in (a) of the apo TM287/288 structure, full-length (left) and isolated NBD dimer (right). The D-loop of NBD287 is highlighted with a red circle.

Figure 7

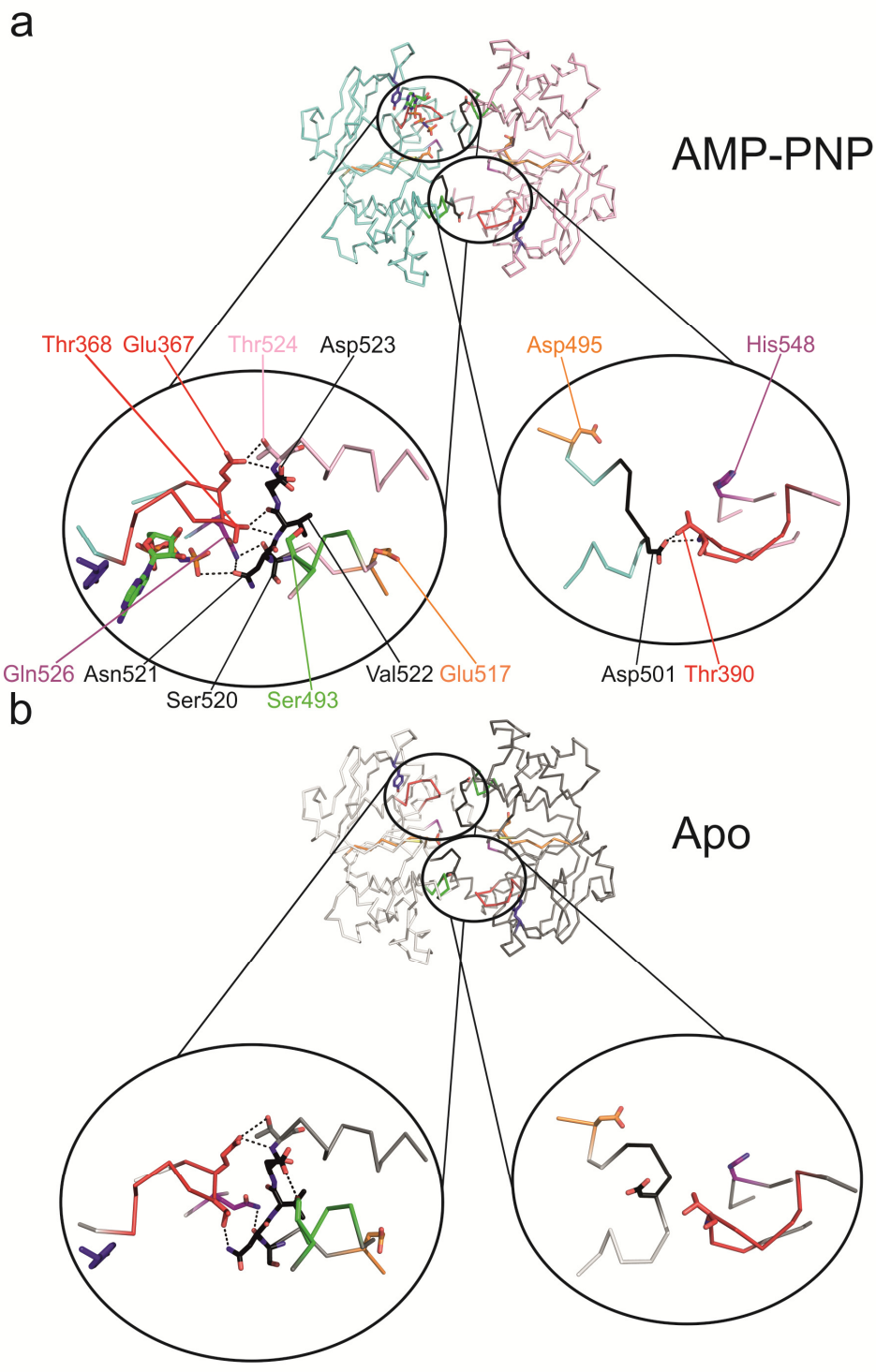

Figure 7:
Interdomain interaction and conformational changes in the D-loops. (a) Left panel: Hydrogen-bonding network (≤3.6 Å) between the D-loop (Ser520, Asn521, Val522 and Asp523, black) and Thr524 of NBD288 and the switch Gln526 (purple) and Walker A Glu367 and Thr368 (both red) of NBD287 in the nucleotide-bound structure. AMP-PNP is shown as sticks. Right panel: Hydrogen bonds of the consensus site. The D-loop (Asp501 of NBD287, black) and the Walker A (Thr390 of NBD288, red) are in hydrogen bonding distance. (b) Same analysis as in (a) shown for the apo-state.

Figure 8

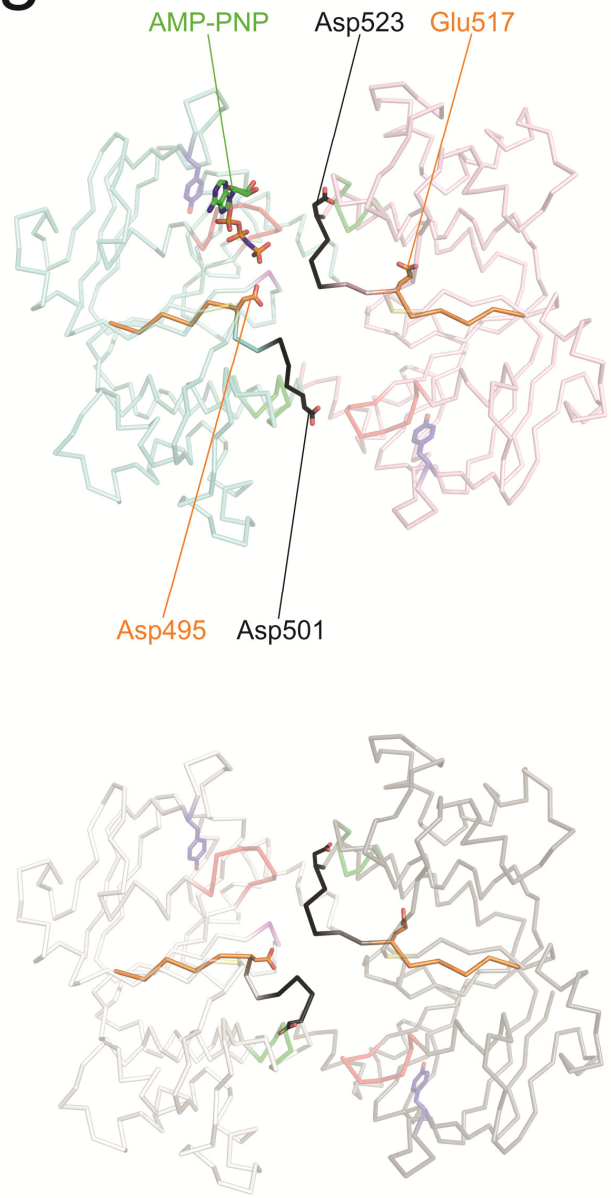

Figure 8:
Long-range intradomain communication in the asymmetric NBD dimer. The D-loop of NBD287 including Asp501 (black) is flexible and undergoes large conformational changes in response to nucleotide binding (upper versus lower panel). AMP-PNP is shown as sticks. The Walker B catalytic residue in NBD288, Glu517 (orange) is shown. The corresponding Walker B Asp495 is as well highlighted. Asp523 of the D-loop of NBD288 is colored in black.

Figure 9

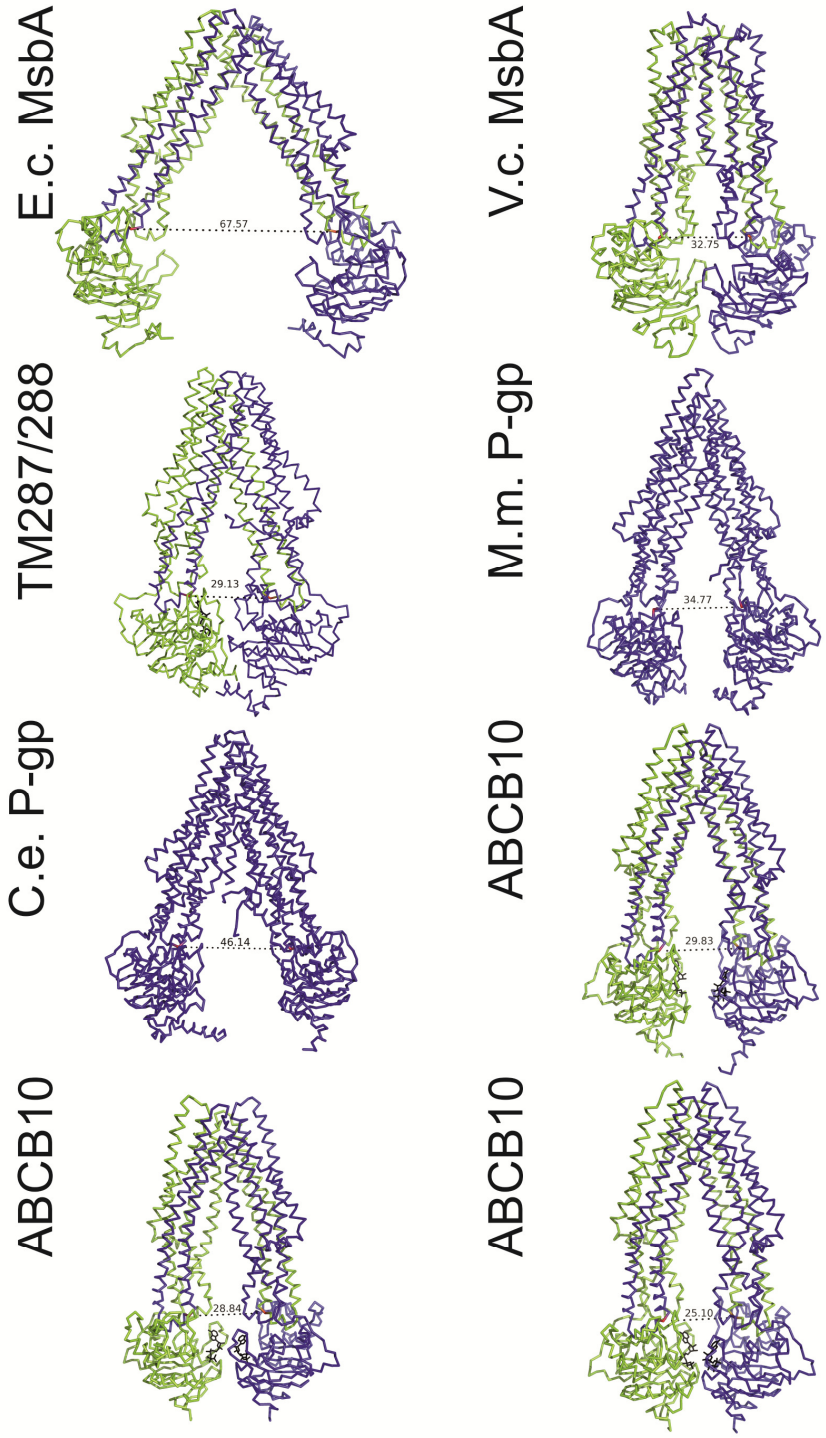

Figure 9:
Inter-NBD distances of all deposited inward-facing full-length exporter structures. The c_α-positions between which the distances were measured are highlighted in red. Bound nucleotides are shown in black as sticks (for TM287/288 one; for ABCB10 two each). For *Escherichia coli* (E.c.) MsbA and *Mus musculus* (M.m.) P-gp only a representative dimer of the asymmetric unit is shown. The measured distances are summarized in Table 2. *Vibrio cholerae* (V.c.), *Caenorhabditis elegans* (C.e.)

TABLE 1 | DATA COLLECTION AND REFINEMENT STATISTICS

	Apo structure[b)]	Apo structure[c)]	AMP-PNP structure
Data Collection			
Space group	C2	C2	C2
Cell dimensions			
a, b, c (Å)	214.64	214.64	216.33
	84.01	84.01	84.31
	114.11	114.11	115.78
α, β, γ (º)	90.000	90.000	90.000
	93.268	93.268	91.923
	90.000	90.000	90.000
Resolution[a)] (Å)	2.60 (2.67-2.60)	2.53 (2.59-2.53)	2.6 (2.67-2.60)
R_{merge} (%)	5.3 (109.8)	5.3 (67.9)	6.2 (205.0)
I/σI	23.15 (1.32)	23.81 (1.66)	17.65 (1.36)
Completeness (%)	93.1 (64.6)	87.3 (25.6)	99.5 (99.4)
Redundancy	3.8 (2.5)	3.8 (2.0)	6.8 (7.0)
Refinement			
Resolution (Å)		30-2.53	25-2.6
No. reflections (work/test)		59481/3003	63492/3181
R_{work}/ R_{free}		23.85/29.06	22.68/27.06
No. atoms			
Protein		9126	9134
AMP-PNP		-	31
Mg^{2+}		-	1
Water		12	-
B-factors			
Protein		109	123
Ligand		-	112
Ion		-	112

Water	67	-
R.m.s deviations		
Bond lengths (Å)	0.004	0.004
Bond angles (º)	0.856	0.862

[a)] Highest resolution shell is shown in parenthesis.

[b)] Conventionally scaled data using XSCALE.

[c)] Ellipsoidal truncation and anisotropy scaling was performed using the UCLA MBI Diffraction Anisotropy server(11).

TABLE 2 | CALCULATIONS OF RIGID BODY ROTATION IN FULL-LENGTH ABC TRANSPORTERS

Type I importer

	fixed	moving	---------- Segment 1	Rec A-like Segment 2	domain Segment 3	---------- Segment 4	---------- Segment 1	Helical Segment 2	domain Segment 3	---------- Segment 4	Rigid body rotation angle [°]
MalFGK	2R6G_Chain A	3PV0_Chain A	29-43	154-158	186-190	204-207	88-97	107-118	121-125	135-149	12.633
	2R6G_Chain A	3PV0_Chain B	29-43	154-158	186-190	204-207	88-97	107-118	121-125	135-149	13.113
	2R6G_Chain B	3PV0_Chain A	29-43	154-158	186-190	204-207	88-97	107-118	121-125	135-149	14.441
	2R6G_Chain B	3PV0_Chain B	29-43	154-158	186-190	204-207	88-97	107-118	121-125	135-149	14.914

Type II importer

	fixed	moving	---------- Segment 1	Rec A-like Segment 2	domain Segment 3	---------- Segment 4	---------- Segment 1	Helical Segment 2	domain Segment 3	---------- Segment 4	Rigid body rotation angle [°]
BtuCD	4FI3_Chain C	1L7V_Chain C	26-40	154-158	185-189	204-207	88-97	105-114	120-122	126-143	2.556
	4FI3_Chain C	1L7V_Chain D	26-40	154-158	185-189	204-207	88-97	105-114	120-122	126-143	2.556
	4FI3_Chain D	1L7V_Chain C	26-40	154-158	185-189	204-207	88-97	105-114	120-122	126-143	2.484
	4FI3_Chain D	1L7V_Chain D	26-40	154-158	185-189	204-207	88-97	105-114	120-122	126-143	2.478
	4FI3_Chain C	2QI9_Chain C	26-40	154-158	185-189	204-207	88-97	105-114	120-122	126-143	2.882
	4FI3_Chain C	2QI9_Chain D	26-40	154-158	185-189	204-207	88-97	105-114	120-122	126-143	2.871
	4FI3_Chain D	2QI9_Chain C	26-40	154-158	185-189	204-207	88-97	105-114	120-122	126-143	2.795
	4FI3_Chain D	2QI9_Chain D	26-40	154-158	185-189	204-207	88-97	105-114	120-122	126-143	2.79
	4FI3_Chain C	4DBL_Chain C	26-40	154-158	185-189	204-207	88-97	105-114	120-122	126-143	2.955
	4FI3_Chain C	4DBL_Chain D	26-40	154-158	185-189	204-207	88-97	105-114	120-122	126-143	2.933
	4FI3_Chain C	4DBL_Chain H	26-40	154-158	185-189	204-207	88-97	105-114	120-122	126-143	2.95
	4FI3_Chain C	4DBL_Chain I	26-40	154-158	185-189	204-207	88-97	105-114	120-122	126-143	2.933
	4FI3_Chain D	4DBL_Chain C	26-40	154-158	185-189	204-207	88-97	105-114	120-122	126-143	2.877
	4FI3_Chain D	4DBL_Chain D	26-40	154-158	185-189	204-207	88-97	105-114	120-122	126-143	2.854
	4FI3_Chain D	4DBL_Chain H	26-40	154-158	185-189	204-207	88-97	105-114	120-122	126-143	2.871
	4FI3_Chain D	4DBL_Chain I	26-40	154-158	185-189	204-207	88-97	105-114	120-122	126-143	2.854

Exporter

	fixed	moving	---------- Segment 1	Rec A-like Segment 2	domain Segment 3	---------- Segment 4	---------- Segment 1	Helical Segment 2	domain Segment 3	---------- Segment 4	Rigid body rotation angle [°]
TM287/288	...._Chain A	...._Chain A	359-373	490-494	520-524	538-541	421-430	437-446	459-461	469-486	2.105

TABLE 3 | NBD SEPARATION IN INWARD-FACING ABC EXPORTERS

Protein (PDB, Chain)	Nucleotide(s)/Metal(s)	Residue 1	Residue 1	Distance (Å)
EcMsbA (3B5W, Chains A + B)	—	G213	G213	67.57
EcMsbA (3B5W, Chains C + D)	—	G213	G213	68.46
EcMsbA (3B5W, Chains E + F)	—	G213	G213	61.69
EcMsbA (3B5W, Chains G + H)	—	G213	G213	62.19
VcMsbA (3B5X, Chains A + B)	—	G213	G213	32.75
TM287/288 (…., Chains A + B)	AMP-PNP/Mg^{2+}	G201 (TM287)	G225 (TM288)	29.13
TM287/288 (…., Chains A + B)	—	G201 (TM287)	G225 (TM288)	28.89
Pgp (3G5U, Chain A)	—	A256	F900	34.77
Pgp (3G5U, Chain B)	—	A256	F900	35.90
Pgp (4F4C)	—	S284	N944	46.14
ABCB10 (4AYT)	2 AMP-PCP/2 Mg^{2+}	N360	N360	25.10
ABCB10 (4AYW)	2 AMP-PNP	N360	N360	28.84
ABCB10 (4AYX)	2 AMP-PCP/2 Mg^{2+}	N360	N360	29.83

5 Subdomain flexibility in the nucleotide binding domains of the heterodimeric ABC exporter TM287/288

Subdomain flexibility in the nucleotide binding domains of the heterodimeric ABC exporter TM287/288

Magdalena A. Bukowska*, Michael Hohl*, Markus A. Seeger** and Markus G. Grütter**

Manuscript in preparation

* contributed equally

**corresponding authors

References for the following manuscript are numbered separately and are listed directly at the end of this section.

5.1 Abstract

ATP binding cassette transporters shuttle various compounds across the lipid bilayer. The transport is energized by ATP binding and hydrolysis at two cytosolic ATPase sites. Numerous heterodimeric ABC exporters are characterized by the presence of functionally non-equivalent catalytic sites. Recently, the first full-length structure of the heterodimeric ABC exporter TM287/288 was determined [1]. Although the protein was captured in an inward-facing conformation, the nucleotide binding domains (NBDs) remained in a partial contact. Here we report a detailed description of the behavior of the isolated TM287/288 NBDs in solution. In addition we solved crystal structures of the individual NBDs and analyzed structural differences between the domains in isolation and in the context of the full-length transporter. Our findings highlight the importance of conformational flexibility for the function of the NBDs.

5.2 Introduction

ATP binding cassette (ABC) transporters constitute one of the largest protein families and are abundantly represented in all kingdoms of life. These multi-domain integral membrane proteins utilize the energy of ATP hydrolysis to drive translocation of various compounds across cellular membranes. ABC transporters are crucial for diverse physiological processes such as the uptake of nutrients, homeostasis maintenance, resistance to toxins or antigen processing [2]. When impaired, the ABC transporters can cause hereditary diseases in humans, including cystic fibrosis [3], Stargardt disease [4] or adrenoleukodystrophy [5]. In addition, the ABC transporters are notorious for causing multidrug resistance of bacteria and tumor cells resulting in a chemotherapy failure.

5.2.1 NBDs and their functional asymmetry

All ABC transporters share a canonical architecture comprising two transmembrane domains (TMDs) and two cytosolic nucleotide binding domains (NBDs). While transmembrane domains of the ABC transporters differ significantly, the NBDs show a high degree of similarity. A number of monomeric [6-10] and homodimeric [11-14] NBD structures were determined, providing valuable insights into the general fold, mode of the nucleotide binding and the functional dimeric arrangement, which were subsequently validated by structures of the full-length transporters [15-17]. The NBD encompasses several conserved motifs involved in nucleotide binding and hydrolysis, such as a Walker A motif that interacts with the α- and β-phosphates of nucleotides, a Walker B that contains a catalytic glutamate, an H-loop (or a switch region) with a conserved histidine and an ABC signature motif that contacts the γ-phosphate of the ATP. The functional NBD dimer contains two composite ATPase sites with both NBDs contributing to each of them. The Walker A, Walker B and the H-loop of one NBD are complemented with the signature motif of the second NBD so that nucleotides become sandwiched between the two NBDs [11, 18, 19]. Many of the heterodimeric ABC exporters, including the medically relevant examples TAP1/2, CFTR or SUR1 exhibit an intriguing asymmetry in the NBDs. These transporters contain substitutions in the conserved ATPase motifs. Typically NBD1 has an aspartate in place of a conserved glutamate in the Walker B and the histidine of the H-loop is substituted with a glutamine. The NBD2 has a non-canonical signature motif. Upon the NBD heterodimerization, the

divergent motifs align to form a non-canonical ATPase site, while the other site consists of consensus motifs. The consensus site has been demonstrated to be largely or solely responsible for the necessary ATPase activity and for the NBD closure [13]. In contrast, the non-canonical site is suggested to be catalytically incompetent. To date the reasons for this functional asymmetry remain unclear. A hypothesis of functional non-equivalence of the ATPase sites in ABC transporters has emerged from biochemical [20, 21] as well as from structural studies [22, 23]. In a recent study of Mittal *et al*. [24] the homodimeric ABC exporter MsbA was trapped in an asymmetric state using conformation-sensitive DARPin binders.

5.2.2 The TM287/288 structure

Recently, the first high resolution full-length structure of a heterodimeric ABC exporter, TM287/288 was determined [1]. The transporter was captured in its inward-facing conformation. The structure revealed that the NBDs are only partially disegaged. So far all ABC exporters crystallized in an inward-facing conformation were homodimeric and showed a complete separation of the NBDs with varying distances between them [17, 25, 26]. Although, the presence of the conformation with distantly spaced NBDs in solution was additionally confirmed by spectroscopic methods [27, 28], some studies argue whether the large NBD separation is necessary for drug binding and ATP hydrolysis [29]. It is also plausible that the heterodimeric ABC exporters undergo different conformational changes than the homodimeric counterparts and that a partial NBD opening (as opposed to complete separation) might be common to all heterodimeric exporters, however this hypothesis needs to be supported by additional studies.

To date, the attempts to stabilize the TM287/288 in an outward-facing conformation for structure determination were not successful and assumptions made by comparisons with the outward-facing models of homodimeric exporters may be misleading. To gain more insight into the structural basis of the functional asymmetry in the heterodimeric ABC exporters we perfomed detailed functional and structural studies of both consensus and non-consensus NBDs of TM287/288 in isolation.

5.3 Results and Discussion

5.3.1 Protein purification and biochemical characterization

The nucleotide binding domains of the heterodimeric ABC exporter TM287/288 are termed NBD287 and NBD288 for NBD1 and NBD2, respectively. The NBD287 (residues 330-577) was expressed in *E. coli*, fused at the N-terminus to the His-tagged SUMO3 tag protein. After Ni-chelating chromatography purification, the SUMO3 tag was cleaved off using SUMO protease and the NBD287 devoid of tags was used for crystallization. The NBD288 (residues 353-592) was expressed with a C-terminal avi-tag followed by a His-tagged GFP. The GFP tag was cleaved off using 3C protease, leaving the avi-tag at the C-terminus of the domain. Despite the presence of the avi-tag, the domain migrated as a monodisperse species in size exclusion chromatography.

Analytical size exclusion chromatography and analytical ultracentrifugation analyses showed that both domains are monomeric in solution and no ATP-induced dimerization could be observed (Figure 1).

The avi-tag does not affect the oligomeric state of NBD288, as the same migration behavior was also observed for a NBD288 construct devoid of tags (not shown). The domains alone or mixed have no detectable affinity for ATP and show no ATPase activity (data not shown), while under similar conditions the full-length transporter binds and hydrolyzes ATP [1].

5.3.2 Structural analysis

NBD287 was crystallized at 1.95 Å resolution and solved by molecular replacement using NBD1 from the TM287/288 structure (PDB code 3QF4) as a search model. The final model was refined to 23.7 % (R_{free}=25.76 %) and includes the residues 353-366, 409-569. The NBD288 crystals diffracted to 2.3 Å. The structure was solved by molecular replacement using NBD2 of the TM287/288 structure as a search model (PDB code 3QF4) and refined to 19.13 % (R_{free}=23.89 %). The final model encompasses residues 353-519 and 523-592 of the domain. In addition, the model contains an N-terminal serine (cloning artifact) and 17 residues of the C-terminal avi-tag. The data collection and refinement details are summarized in Table 1.

5.3.3 Domain architecture

The fold of the ATP binding cassette has been established by numerous previously reported structures of isolated NBDs (over 50 NBD structures are listed in [9]) and full-length ABC transporters [15-17, 25, 26, 30-36]. The NBD fold consists of a catalytic and a helical domain. The catalytic domain can be further subdivided into two subdomains: the RecA-like (or F1) [37] and an ABC-specific β [38]. The catalytic domain, common to all P-loop ATPases, contains 2 β-sheets flanked by helices and harbors the conserved motives which form a nucleotide binding site: the Walker A, the Walker B, the switch (H-loop), the D-loop and the A-loop. The helical domain is a bundle of four α-helices typical for ABC transporters and contains the ABC signature motif. The topology scheme with the boundaries of the secondary structure elements and the location of the conserved elements is shown in Figure 2.

The NBD287 structure

Our model of the NBD287 encompasses the helical domain and most of the RecA-like subdomain but lacks the ABC-β subdomain, the loop-helix motif containing the Walker A and eight C-terminal residues. The absence of the electron density, despite the high diffraction quality, suggests that the missing portion of the domain is inherently flexible. The other functionally relevant motifs including the non-canonical ABC signature, Walker B, D-loop and the switch motives are well ordered. Interestingly, the very same structures were independently obtained from three different protein constructs: NBD287 with the N-terminal avi-tag (pBXNAC3GH_NBD287), NBD287 expressed with the cleavable N-terminal SUMO protein tag (pET11M-SUMO-FX-NBD287) and NBD287 with the cleavable N-terminal 10xHis-tag (pBXNH3_NBD287). Mass spectrometry analysis of the dissolved crystals did not reveal protein fragmentation that would correspond to the portion seen in the structure (data not shown).

5.3.4 Comparison with the corresponding domain of the full-length TM287/288 transporter

The full-length TM287/288 exporter was crystallized in the nucleotide-bound [1] and nucleotide-free (Hohl *et al.*, in preparation) states. In both cases the transporter is trapped in an inward-facing conformation with the NBDs in a partially disengaged arrangement. In contrast to other inward-facing ABC transporter structures, where the NBDs are fully separated, in the case of TM287/288 the NBDs remain sealed together at the degenerate ATPase site, irrespectively of whether it is nucleotide-bound or nucleotide-free. The availability of the NBD structures from the same system in isolation and in the full-length context provides the unique opportunity to describe the structural plasticity of the NBDs. In the context of the full-length transporter, the NBDs form extensive inter- and intrachain interactions. Isolated domain structures allow for a better interpretation of the extent of conformational adjustments necessary to form a functional molecular complex. And this, in turn, gives valuable insight into the mechanistic features of the ATP hydrolysis and transport.

Superimposition of the structured part of the NBD287 in isolation with its counterpart NBD1 of the full-length TM287/288 structures results in an RMSD of about 1 Å (backbone carbon alignment with nucleotide-bound NBD1 along 158 atoms, with nucleotide-free NBD1 along 155 atoms) (Figure 3a and 3b). The secondary structure element matching (SSM) results in a slightly higher RMSD of around 1.4 Å over 168 residues. When secondary structure elements of the catalytic domain are used for superimposition, the relative rotation of the helical domain becomes apparent. In the isolated domain, the bundle of helices rotates away from the core beta sheet by 10 degrees relative to the nucleotide-bound and 11 degrees relative to the nucleotide-free structure (Figure 3c and 3d). This high degree of flexibility of the helical domain in NBDs has been described before [7, 9, 38-40]. The flexibility of this region is not unanticipated as it is extensively involved in interchain interactions in the intact protein. In the full-length transporter the helical domain accommodates the intracellular loops extending from the transmembrane portion of the transporter and its signature motif complements the composite ATPase site in the dimerized NBD state. We also compared the relative positions of the conserved motives of our structure in relation to the full-length protein (Figure 4). Unexpectedly, the arrangement of the Walker B, H-loop and the D-loop resembles the nucleotide-bound NBD1 of the intact TM transporter. The hydrogen bond network of the aspartate 495 (corresponding to the canonical general base glutamate) in the isolated domain is slightly altered with respect to the nucleotide-bound intact transporter. Here the aspartate 495 points towards the H-loop and makes a hydrogen bond with the glutamine 526 that substitutes the canonical histidine of the catalytic dyad (Figure 5a). In the full-length structure with the AMP-PNP bound, the aspartate 495 was locked in a hydrogen bond network with serine 498 of the D-loop (Figure 5b). In both structures the Q-loop is beyond the hydrogen bonding distance to aspartate 495. The situation in the nucleotide-free full-length structure is significantly different, as the aspartate 495 is withdrawn from the interaction with the H-loop but it interacts extensively with the remodeled D-loop via hydrogen bonds with serines 498 and 499. It is also close enough to the Q-loop to form a hydrogen bond with the conserved glutamine 414 (Figure 5c). In summary, the positioning of the Walker B, the H-loop and of the D-loop is similar to the nucleotide-bound NBD1 of the full-length TM287/288 structure. Incapability of the isolated NBD287 to bind ATP

might result from the flexibility of domain portion that harbors the Walker A motif and that was not structured in our model.

The ABCβ-subdomain of the isolated NBD287 is flexible when taken out of the context of the full-length transporter

In the full-length TM287/288 structure, the ABCβ-subdomain of NBD287 forms one side of the binding groove for the intracellular loop 4 (ICL4) that protrudes from the TM288 polypeptide. The ICL4 contains a coupling helix – a conserved element that stabilizes interchain and interdomain interactions. Several residues of the coupling helix make direct contacts with the ABCβ-subdomain stabilizing its position (Figure 6). Furthermore, the Walker A motif, that directly precedes the ABCβ region, is interacting with the D-loop and D-loop helix (a helix that immediately follows the D-loop) of the neighboring NBD288 contributing to the composite ATPase site. Therefore, it is likely that in the absence of the TM288 (its NBD and coupling helix) the conformational freedom of the ABCβ subdomain and of the loop that harbors the WalkerA motif is increased. This would explain the lack of electron density corresponding to this part of the NBD287.

The NBD288 structure

Current structural knowledge of the NBD2 is very limited. Apart from full-length TM287/288, the only NBD2 structure deposited comes from the multidrug resistance protein 2 of Plasmodium yoelli (PDB code 2GHI) published by a Structural Genomics Consortium [41]. Our model covers the whole domain with the exception of three residues corresponding to the D-loop. The overall structure is similar to the one observed in the intact transporter. When compared with the nucleotide-bound full-length structure, the superimposition of the C_α atoms results in a RMSD of 1.3 Å (over 215 atoms) and secondary structure matching – in a RMSD of 1.5 Å (Figure 7a). Comparison with the nucleotide-free TM287/288 structure results in an even closer match of a RMSD = 1.28 Å over 220 C_α atoms and a RMSD of 1.45 Å for secondary structure matching. The relative position of the catalytic and helical domain is quite different from the one seen in the domains of the intact transporter. When the models are superimposed using secondary structure elements of the catalytic domain, the relative displacement of the helical domain is emphasized (Figure 7b). Similarly as seen in the NBD287, the helical domain rotates outwards from the RecA core by 11 and 10 degrees when compared to the nucleotide-bound and the nucleotide-free TM287/288 structures, respectively. Interestingly, we observe a significant displacement of the D-loop helix which tilts along its long axis away from the RecA β-sheet by 12 and 11 degrees with respect to its position in the nucleotide-bound and nucleotide-free intact transporter structure, respectively (Figure 7c). This rotation seems to be of functional importance as the position of this helix is sensitive to the conformation of the D-loop and contacts the Walker A of the neighboring NBD, and therefore is important for coordination of the events taking place in the two ATPase sites. The full-length TM287/288 structures, our isolated NBD288 and the MRP2 NBD2 structures were crystallized devoid of nucleotides. However, the generally accepted hypothesis is that NBD2 is predominantly responsible for ATP hydrolysis in heterodimeric ABC exporters. In the context of the full-length protein (irrespectively of whether a nucleotide in the degenerate site is bound or not) the catalytic base (glutamate 517) following the Walker B motif adopts a very unusual position, pointing its

side chain away from the active site (Figure 9b). In the NBD288 structure, the active site is rearranged when compared to the intact transporter structure. The catalytic glutamate is flipped and points more towards the active site but still is locked in a state incompetent for catalysis. It interacts with the backbone amide of the histidine 548 and with the following residues of the H-loop. The interactions with the residues following the H-loop distort the alpha helical geometry of the 551-556 helix, which in our structure adopts a 3_{10} geometry (Figure 9a). The glutamate – H-loop backbone interaction has been seen before in the structure of the isolated HlyB-NBD where the histidine was substituted by an alanine [12]. Such positioning of the catalytic base does not allow polarization of the attacking water necessary for catalysis. The thorough structural analysis of the maltose transporter in different states of catalysis showed that in the presence of the nucleotide the catalytic base is expected to interact with the imidazole ring of the H-loop histidine that orients it toward the γ-phosphate of the ATP where it is in a suitable distance to deprotonate the attacking water molecule [30]. The same is true for the ABC exporter Sav1866 [42]. The active site of the AMP-PNP bound Sav1866 is shown in Figure 9c.

The C-terminal avi-tag of NBD288 mediates crystal contacts

Inspection of the NBD288 crystal packing revealed an intriguing feature of the crystal lattice. The NBD288 molecules are arranged as beads along the filament formed by protruding C-terminal avi-tags (Figure 10). The avi-tag peptides specifically interact forming extended antiparallel beta sheets that fit in the unoccupied ATP-binding groove of the symmetry related NBD288 molecule. The filaments are spatially separated resulting in a high solvent content of the asymmetric unit of >63 %.

The interfacial areas of the degenerate ATPase site are inherently more flexible

The electron density maps for both the NBD287 and the NBD288 allow fitting of only parts of the sequence of the domains. This means that certain areas of the NBDs must be flexible. When the partial structural models of NBD287 and NBD288 are oriented as they would face each other in the full-length protein, we see a striking correlation of the disordered areas with the location of the degenerate ATPase site. The parts that are missing in our models (the Walker A and the ABC-specific β subdomain of NBD1 and the D-loop of the NBD2) are parts of the composite interface in the intact transporter (Figure 11). In addition, an analysis of the temperature factor distribution along the isolated NBDs suggests that this area is relatively more fexible than the region harboring the consensus site (Figure 11b). Previous studies on the CFTR showed that during the functional cycle, the degenerate site most likely stays connected for most of the time and only the second ATPase site (consensus site) undergoes partial opening allowing for nucleotide exchange [43]. Analysis of the full-length TM287/288 transporter structure supports the hypothesis of only partial disengagement of the NBDs during the catalytic cycle. Our structural analysis emphasizes higher flexibility/stability of this area and suggests that upon disengagement, the separated halves of the degenerate site are highly flexible.

5.4 Conclusions

The comparison of the structures of the intact transporter with the isolated NBDs of the same protein provides an unprecedented insight into the mechanism and mechanics involved in ATPase hydrolysis and transport. In addition, to our best knowledge, this is the first report in which both NBD structures of a heterodimeric transporter are described.

The isolated NBDs of TM287/288 are unable to hydrolyze ATP and they do not dimerize. This clearly suggests that a productive dimerization can only take place in the full-length protein. It has been proposed that a nucleotide acts as molecular glue keeping the degenerate site together. However, this seems unlikely since the TM287/288 structure without nucleotide (Hohl *et al*., Chapter 4) shows the same NBD arrangement with the NBDs in contact at the degenerate site.

The isolated NBD structures revealed that the domains exhibit remarkable plasticity that is necessary to support inter- and intrachain interactions in the full-length structure and conformational changes during the catalytic cycle. The helical subdomains of both NBDs possess certain autonomy that is necessary to accommodate the intracellular loops protruding from the transmembrane portion and containing the coupling helices. The stability of the ABCβ subdomain in NBD287 is compromised in the absence of TM288. In the full-length structure the ABCβ subdomain is supported by the interaction with the TM288 coupling helix and with the D-loop of the NBD288. The interfacial areas that build the canonical ATPase site (Walker A, Walker B and H-loop of NBD288 and D-loop and ABC signature of NBD287) seem to be rather stable and the catalytic site remains preformed even outside the context of the full-length protein and in the absence of nucleotides. In contrast, the elements that build the degenerate ATPase site could not be resolved in the isolated structures. This suggests that this area is not preformed and only becomes structured in the heterodimeric arrangement of the intact transporter. Therefore our analysis emphasizes the structural asymmetry of the system by identifying the degenerate composite ATP-binding interface as a region of higher inherent flexibility.

5.5 Experimental Procedures

5.5.1 Cloning of the TM287/288 NBDs

The two NBDs of the heterodimeric ABC transporter TM287/288 were amplified from the FX-vector pBXNH3_TM287/288 [44] used for the structure determination of the full-length transporter [1]. For each NBD, ten SapI-restriction enzyme based FX-vectors were constructed for test expressions. Cloning was performed as described in [44]. The primers NBD287_for, NBD287_rev, NBD288_for and NBD288_rev (sequences see below) were used to amplify the two soluble domains, both starting with a conserved glycine residue (Gly330 (NBD1) and Gly353 (NBD2) of the full-length transporter). The inserts were cloned into the FX-expression vectors pBXNH3, pBXC3H [44] and pBXC3GH (Geertsma *et al*., unpublished). Additionally, both inserts were ligated into the FX-avi-tag vectors pBXNH3A, pBXNH3CA, pBXNAC3H, pBXNAC3GH, pBXCA3H and pBXCA3GH (Geertsma *et al*., unpublished). Table 2 illustrates the nomenclature used for the vector annotation. The six avi-constructs were both used for crystallization attempts as well as for immobilization- and selection purposes (Hohl *et al*., unpublished). The vector pETM11-SUMO3GFP [45] was used as the only pET-based vector for test expressions. For this purpose the vector was modified to make it available for FX-cloning, with the exception that this resulting vector does not contain a ccdB-cassette and therefore has to be predigested with SapI and separated from its insert via agarose gel. An undesirable SapI site on pETM11-SUMO3GFP was removed by QuickChange mutagenesis using the primers pET11M_SUMO_delSapI_for and pET11M_SUMO_delSapI_rev (sequences see below). This SapI-free pET11M-SUMO3GFP vector was then cleaved with the restriction enzymes AgeI and HindIII and ligated with the two annealed oligonucleotides pETM11_FX_for and pETM11_FX_rev (sequences see below). pETM11_FX_for together with pETM11_FX_rev form overhangs compatible with AgeI and HindIII. This resulted in the SapI-based pET11M-SUMO-FX expression vector.

NBD287_for: 5’-ATATGCTCTTCTAGTGGGAGCGTTTCCTTCGAAAATGTC-3’

NBD287_rev: 5’-TATAGCTCTTCATGCGGCATCGTTCATCACCCCGTTTCC-3’

NBD288_for: 5’-ATATGCTCTTCTAGTGGAGAAATCGAGTTCAAGAATGTC-3’

NBD288_rev: 5’-TATAGCTCTTCATGCTGCTTCTTTTTCTACAACGAGACC-3’

pET11M_SUMO_delSapI_for: 5’-GAGGAAGCGGATGAGCGCCTG-3’

pET11M_SUMO_delSapI_rev: 5’-CAGGCGCTCATCCGCTTCCTC-3’

pETM11_FX_for: 5’-CCGGTGGAAGTAGAAGAGCATATGCTCTTCTGCATAATA-3’

pETM11_FX_rev: 5’-AGCTTATTATGCAGAAGAGCATATGCTCTTCTACTTCCA-3’

5.5.2 Test expression of the NBD287 and NBD288

E. coli MC1061 (for pBX vectors) and BL21 (DE3) cells (for pET vectors) transformed with the desired vectors were used to produce the NBDs in shaking flasks containing 100 ml LB media, 100 µg/ml ampicillin (pBX) or 50 µg/ml kanamycin (pET) at 30 °C. Protein production was induced with 0.0025 % L-arabinose (pBX) or with 0.5 mM IPTG (pET) at an OD_{600} = 1 for about four hours. The cells were then spun down at 5000 x g and frozen at -20 °C. After resuspension in 20 mM Tris-HCl pH 8.0, 200 mM NaCl, 3 mM $MgCl_2$ and the addition of DNase I the cells were treated by sonication. To get rid of unopened cells and cell fragments the suspension was centrifuged again for half an hour at 15'000 x g. The supernatant was subsequently loaded on a Ni-NTA column, washed with 50 mM imidazole pH 7.5, 200 mM NaCl and 10 % glycerol. Elution from the column was performed with 200 mM imidazole pH 7.5, 200 mM NaCl and 10 % glycerol. Collected fractions were analyzed for expression yield via SDS-PAGE. The best expressing constructs were further analyzed by size exclusion chromatography for their monodispersity. The best behaving constructs are further described in the part expression, purification and crystallization and an additional rating is given in Table 3.

5.5.3 Protein expression and purification

The NBD287 structure was determined for the protein expressed from pET11M-SUMO-FX_NBD287 construct. For overexpression freshly transformed BL21 *E. coli* cells were cultured in LB medium at 37 °C in the presence of kanamycin (50 µg/mL) until optical density (OD_{600}) reached 0.8. The culture was then induced by IPTG (0.1 mM final) and the expression was carried out for 4 hours at 30 °C. For the cell lysis, the pellet was resuspended in a lysis buffer (20 mM Tris-HCl pH 8.0, 200 mM NaCl, 10 mM imidazole, 2 mM $MgCl_2$, EDTA-free protease inhibitor cocktail (Roche), 1 mM PMSF, 10 µg/mL DNaseI). Upon disruption, the lysate was cleared by centrifugation for 30 min at 20'000 rpm at 4 °C and applied onto a gravity flow Ni-NTA column equilibrated with 20 mM Tris-HCl pH 8.0, 200 mM NaCl, 10 mM imidazole, 10% glycerol. Unbound proteins were washed by applying a buffer containing 40 mM imidazole. The SUMO3-NBD287 fusion was eluted in buffer containing 200 mM imidazole. For buffer exchange, the protein was applied onto a PD-10 desalting column (GE Healthcare) prior to an overnight proteolytic cleavage of the SUMO3-tag using the SenP2 protease (at 1:500 of the SenP2:SUMO3-fusion w/w ratio). The SUMO and the SenP2 were re-bound to the nickel resin. Directly before crystallization of NBD287, devoid of tags, it was subjected to size exclusion chromatography on a Superdex 75 column (10/300 GL, GE Healthcare) with 20 mM Tris-HCl pH 7.5, 150 mM NaCl as a running buffer, and concentrated to around 12 mg/mL (MWCO=10 kDa).

The NBD288 expression construct spans positions 353-598 of the TM0288 polypeptide followed by an avi-tag, 3C cleavage site, GFP and 10-His tag. For protein overexpression, freshly transformed MC1061 *E. coli* cells were grown in 2YT medium supplemented with ampicillin (100 µg/mL) to OD_{600} between 0.9 to 1 and then induced by adding L-Arabinose (final concentration 0.0025% w/v). The expression was carried out for 5 hours at 30 °C. Harvested cells were disrupted in lysis buffer: 20 mM Tris-HCl pH 8.0, 200 mM NaCl, 5 mM $MgCl_2$, EDTA-free protease inhibitor cocktail, 1 mM PMSF, 10 µg/mL DNaseI. The lysate was cleared by centrifugation at 20'000rpm for 30 minutes at 4 °C and applied onto a gravity flow column with Ni-NTA resin equilibrated with 20 mM Tris-HCl pH 8.0, 200 mM NaCl. Unbound proteins were washed with a buffer containing 40 mM imidazole. The protein was eluted using buffer containing 200 mM imidazole. In order to remove imidazole, the protein was applied onto a PD-10 desalting column. The GFP-His tag was removed by an overnight enzymatic cleavage using a His-tagged 3C protease at a 1:20 ratio (w/w) enzyme to fusion protein. The cleaved tags and the protease were re-bound to the Ni-NTA agarose and the NBD288-avi protein. Directly before crystallization the NBD288-avi was subjected to size exclusion chromatography on the Superdex 75 column (GE Healthcare) equilibrated with 20 mM Tris-HCl, 150 mM NaCl, pH 7.5 and concentrated to around 10 mg/mL (MWCO=10 kDa).

5.5.4 Analytical size exclusion and ultracentrifugation

Analytical size exclusion chromatography was performed on the HPLC system (Agilent 1200 series, Agilent Technologies) using a Superdex 200 column (5/150, GE Healthcare). For the runs without nucleotides the column was equilibrated with 20 mM Tris-HCl pH 7.5, 150 mM NaCl and samples were incubated with 1 mM EDTA in order to exclude potential effects caused by any contaminating magnesium. For the analysis in the presence of ATP, the column was equilibrated with at least three

column volumes of the same buffer with addition of 1 mM $MgCl_2$ and 1 mM ATP and the protein samples were incubated with 1-5 mM MgATP prior to injections. The NBD mixture was prepared by mixing equimolar amounts of NBDs. In addition, we performed the separation runs in the absence of magnesium which did not reveal any different migration behavior of the domains (not shown).

Sedimentation velocity analytical ultracentrifugation was performed using an Optima XL-1 centrifuge (Beckman Coulter) using epoxy counter pieces with sapphire windows. After size exclusion, the protein samples were diluted to an appropriate concentration to reach A_{280nm}~0.7. The NBD mixture was prepared by mixing NBDs at equimolar concentration and addition of 1 mM $MgCl_2$ and 1 mM ATP. The centrifugation was carried out at 4 °C and at 40'000 rpm. 300 absorption scans were collected and the data were analyzed using the SedFit software [46].

5.5.5 Crystallization and structure determination

NBD287 and NBD288 were subjected to vapour diffusion crystallization. Initial crystal screening was done with the use of a nanoliter drop robotic dispenser of the NCCR high-throughput crystallization facility. NBD287 crystallized at 20 °C in hanging drops. The protein was mixed at 1:1 ratio with reservoir solution containing 100 mM Tris pH 7.8, 100 mM sodium acetate, 25 % (w/v) PEG 2000 MME. The crystals were transferred to the cryo solution containing 30 % PEG 2000 MME prior to cryo-cooling in liquid nitrogen. Several conditions yielded crystals for the NBD288-avi construct and the final data was collected from a crystal grown at 20 °C in sitting drops containing a 1:1 mixture of protein and reservoir solution: 100 mM sodium acetate pH 5.5, 6 % (w/v) PEG 550 MME, 6 % (w/v) PEG 20'000, 200 mM $MgCl_2$. The crystals were transferred into the cryo solution containing 25 % ethylene glycol and cryo-cooled in liquid nitrogen. Diffraction data were collected at beamline X06SA of the Swiss Light Source (SLS, Villigen, Switzerland) equipped with PILATUS detector (Dectris). Data were indexed with XDS [47] and scaled with XSCALE of the CCP4 package [48]. The free R factor (R_{free}) was calculated from 5 % of randomly chosen reflections. The phases were obtained by molecular replacement in PHASER [49] using a model derived from the full-length TM287/288 transporter structure (PDB code 3QF4). The structure was built into the electron density using COOT [50] and refined with PHENIX [51].

5.5.6 Mass spectrometry analysis of the dissolved NBD287 crystals

The NBD287 crystals were extensively washed in the reservoir solution and dissolved in distilled water. The MALDI-MS analysis was performed at the Functional Genomics Center Zurich (FGCZ) of the University of Zurich and ETH Zurich.

5.6 Acknowledgements

We would like to thank Dr. Eric Geertsma for providing vectors for the FX-cloning, Beat Blattmann and Céline Stutz-Ducommun of the NCCR HT crystallization facility for performing the crystallization screening, Dr. Christophe Briand and the SLS X06SA beamline staff for their assistance in diffraction data collection and Dr. Serge Chesnov from FGCZ for mass spectrometry analysis of the NBD287 crystals. This work was supported by the Swiss National Center of Competence in Research (NCCR)

Structural Biology, an Ambizione grant of the Swiss National Science Foundation (to M.A.S.). M.A.B. and M.H. are affiliated with the PhD program in Biomolecular Structure and Mechanism of the Life Science Zurich Graduate School.

5.7 Bibliography

1. Hohl, M., C. Briand, M.G. Grütter, and M.A. Seeger, Crystal structure of a heterodimeric ABC transporter in its inward-facing conformation. Nature structural & molecular biology, 2012. 19(4): p. 395-402.

2. Holland, I.B., ABC transporters, mechanisms and biology: an overview. Essays in biochemistry, 2011. 50(1): p. 1-17.

3. Riordan, J.R., J.M. Rommens, B. Kerem, N. Alon, R. Rozmahel, Z. Grzelczak, J. Zielenski, S. Lok, N. Plavsic, J.L. Chou, and et al., Identification of the cystic fibrosis gene: cloning and characterization of complementary DNA. Science, 1989. 245(4922): p. 1066-73.

4. Allikmets, R., N.F. Shroyer, N. Singh, J.M. Seddon, R.A. Lewis, P.S. Bernstein, A. Peiffer, N.A. Zabriskie, Y. Li, A. Hutchinson, M. Dean, J.R. Lupski, and M. Leppert, Mutation of the Stargardt disease gene (ABCR) in age-related macular degeneration. Science, 1997. 277(5333): p. 1805-7.

5. Mosser, J., Y. Lutz, M.E. Stoeckel, C.O. Sarde, C. Kretz, A.M. Douar, J. Lopez, P. Aubourg, and J.L. Mandel, The gene responsible for adrenoleukodystrophy encodes a peroxisomal membrane protein. Human molecular genetics, 1994. 3(2): p. 265-71.

6. Hung, L.W., I.X. Wang, K. Nikaido, P.Q. Liu, G.F. Ames, and S.H. Kim, Crystal structure of the ATP-binding subunit of an ABC transporter. Nature, 1998. 396(6712): p. 703-7.

7. Gaudet, R. and D.C. Wiley, Structure of the ABC ATPase domain of human TAP1, the transporter associated with antigen processing. The EMBO journal, 2001. 20(17): p. 4964-72.

8. Verdon, G., S.V. Albers, B.W. Dijkstra, A.J. Driessen, and A.M. Thunnissen, Crystal structures of the ATPase subunit of the glucose ABC transporter from Sulfolobus solfataricus: nucleotide-free and nucleotide-bound conformations. Journal of molecular biology, 2003. 330(2): p. 343-58.

9. Haffke, M., A. Menzel, Y. Carius, D. Jahn, and D.W. Heinz, Structures of the nucleotide-binding domain of the human ABCB6 transporter and its complexes with nucleotides. Acta crystallographica. Section D, Biological crystallography, 2010. 66(Pt 9): p. 979-87.

10. Lewis, H.A., S.G. Buchanan, S.K. Burley, K. Conners, M. Dickey, M. Dorwart, R. Fowler, X. Gao, W.B. Guggino, W.A. Hendrickson, J.F. Hunt, M.C. Kearins, D. Lorimer, P.C. Maloney, K.W. Post, K.R. Rajashankar, M.E. Rutter, J.M. Sauder, S. Shriver, P.H. Thibodeau, P.J. Thomas, M. Zhang, X. Zhao, and S. Emtage, Structure of nucleotide-binding domain 1 of the cystic fibrosis transmembrane conductance regulator. The EMBO journal, 2004. 23(2): p. 282-93.

11. Smith, P.C., N. Karpowich, L. Millen, J.E. Moody, J. Rosen, P.J. Thomas, and J.F. Hunt, ATP binding to the motor domain from an ABC transporter drives formation of a nucleotide sandwich dimer. Molecular cell, 2002. 10(1): p. 139-49.

12. Zaitseva, J., S. Jenewein, T. Jumpertz, I.B. Holland, and L. Schmitt, H662 is the linchpin of ATP hydrolysis in the nucleotide-binding domain of the ABC transporter HlyB. The EMBO journal, 2005. 24(11): p. 1901-10.

13. Procko, E., I. Ferrin-O'Connell, S.L. Ng, and R. Gaudet, Distinct structural and functional properties of the ATPase sites in an asymmetric ABC transporter. Molecular cell, 2006. 24(1): p. 51-62.

14. Chen, J., G. Lu, J. Lin, A.L. Davidson, and F.A. Quiocho, A tweezers-like motion of the ATP-binding cassette dimer in an ABC transport cycle. Molecular cell, 2003. 12(3): p. 651-61.

15. Dawson, R.J. and K.P. Locher, Structure of a bacterial multidrug ABC transporter. Nature, 2006. 443(7108): p. 180-5.

16. Oldham, M.L., D. Khare, F.A. Quiocho, A.L. Davidson, and J. Chen, Crystal structure of a catalytic intermediate of the maltose transporter. Nature, 2007. 450(7169): p. 515-21.

17. Ward, A., C.L. Reyes, J. Yu, C.B. Roth, and G. Chang, Flexibility in the ABC transporter MsbA: Alternating access with a twist. Proceedings of the National Academy of Sciences of the United States of America, 2007. 104(48): p. 19005-10.

18. Hopfner, K.P., A. Karcher, D.S. Shin, L. Craig, L.M. Arthur, J.P. Carney, and J.A. Tainer, Structural biology of Rad50 ATPase: ATP-driven conformational control in DNA double-strand break repair and the ABC-ATPase superfamily. Cell, 2000. 101(7): p. 789-800.

19. Jones, P.M. and A.M. George, Subunit interactions in ABC transporters: towards a functional architecture. FEMS microbiology letters, 1999. 179(2): p. 187-202.

20. Urbatsch, I.L., B. Sankaran, J. Weber, and A.E. Senior, P-glycoprotein is stably inhibited by vanadate-induced trapping of nucleotide at a single catalytic site. The Journal of biological chemistry, 1995. 270(33): p. 19383-90.

21. Orelle, C., O. Dalmas, P. Gros, A. Di Pietro, and J.M. Jault, The conserved glutamate residue adjacent to the Walker-B motif is the catalytic base for ATP hydrolysis in the ATP-binding cassette transporter BmrA. The Journal of biological chemistry, 2003. 278(47): p. 47002-8.

22. Zaitseva, J., C. Oswald, T. Jumpertz, S. Jenewein, A. Wiedenmann, I.B. Holland, and L. Schmitt, A structural analysis of asymmetry required for catalytic activity of an ABC-ATPase domain dimer. The EMBO journal, 2006. 25(14): p. 3432-43.

23. Aittoniemi, J., H. de Wet, F.M. Ashcroft, and M.S. Sansom, Asymmetric switching in a homodimeric ABC transporter: a simulation study. PLoS computational biology, 2010. 6(4): p. e1000762.

24. Mittal, A., S. Bohm, M.G. Grütter, E. Bordignon, and M.A. Seeger, Asymmetry in the homodimeric ABC transporter MsbA recognized by a DARPin. The Journal of biological chemistry, 2012. 287(24): p. 20395-406.

25. Aller, S.G., J. Yu, A. Ward, Y. Weng, S. Chittaboina, R. Zhuo, P.M. Harrell, Y.T. Trinh, Q. Zhang, I.L. Urbatsch, and G. Chang, Structure of P-glycoprotein reveals a molecular basis for poly-specific drug binding. Science, 2009. 323(5922): p. 1718-22.

26. Jin, M.S., M.L. Oldham, Q. Zhang, and J. Chen, Crystal structure of the multidrug transporter P-glycoprotein from Caenorhabditis elegans. Nature, 2012. 490(7421): p. 566-9.

27. Zoghbi, M.E., S. Krishnan, and G.A. Altenberg, Dissociation of ATP-binding cassette nucleotide-binding domain dimers into monomers during the hydrolysis cycle. The Journal of biological chemistry, 2012. 287(18): p. 14994-5000.

28. Verhalen, B., S. Ernst, M. Borsch, and S. Wilkens, Dynamic ligand-induced conformational rearrangements in P-glycoprotein as probed by fluorescence resonance energy transfer spectroscopy. The Journal of biological chemistry, 2012. 287(2): p. 1112-27.

29. Verhalen, B. and S. Wilkens, P-glycoprotein retains drug-stimulated ATPase activity upon covalent linkage of the two nucleotide binding domains at their C-terminal ends. The Journal of biological chemistry, 2011. 286(12): p. 10476-82.

30. Oldham, M.L. and J. Chen, Snapshots of the maltose transporter during ATP hydrolysis. Proceedings of the National Academy of Sciences of the United States of America, 2011. 108(37): p. 15152-6.

31. Locher, K.P., A.T. Lee, and D.C. Rees, The E. coli BtuCD structure: a framework for ABC transporter architecture and mechanism. Science, 2002. 296(5570): p. 1091-8.

32. Hollenstein, K., D.C. Frei, and K.P. Locher, Structure of an ABC transporter in complex with its binding protein. Nature, 2007. 446(7132): p. 213-6.

33. Gerber, S., M. Comellas-Bigler, B.A. Goetz, and K.P. Locher, Structural basis of trans-inhibition in a molybdate/tungstate ABC transporter. Science, 2008. 321(5886): p. 246-50.

34. Pinkett, H.W., A.T. Lee, P. Lum, K.P. Locher, and D.C. Rees, An inward-facing conformation of a putative metal-chelate-type ABC transporter. Science, 2007. 315(5810): p. 373-7.

35. Kadaba, N.S., J.T. Kaiser, E. Johnson, A. Lee, and D.C. Rees, The high-affinity E. coli methionine ABC transporter: structure and allosteric regulation. Science, 2008. 321(5886): p. 250-3.

36. Woo, J.S., A. Zeltina, B.A. Goetz, and K.P. Locher, X-ray structure of the Yersinia pestis heme transporter HmuUV. Nature structural & molecular biology, 2012. 19(12): p. 1310-5.

37. Story, R.M. and T.A. Steitz, Structure of the recA protein-ADP complex. Nature, 1992. 355(6358): p. 374-6.

38. Karpowich, N., O. Martsinkevich, L. Millen, Y.R. Yuan, P.L. Dai, K. MacVey, P.J. Thomas, and J.F. Hunt, Crystal structures of the MJ1267 ATP binding cassette reveal an induced-fit effect at the ATPase active site of an ABC transporter. Structure, 2001. 9(7): p. 571-86.

39. Diederichs, K., J. Diez, G. Greller, C. Müller, J. Breed, C. Schnell, C. Vonrhein, W. Boos, and W. Welte, Crystal structure of MalK, the ATPase subunit of the trehalose/maltose ABC transporter of the archaeon Thermococcus litoralis. The EMBO journal, 2000. 19(22): p. 5951-61.

40. Zaitseva, J., S. Jenewein, A. Wiedenmann, H. Benabdelhak, I.B. Holland, and L. Schmitt, Functional characterization and ATP-induced dimerization of the isolated ABC-domain of the haemolysin B transporter. Biochemistry, 2005. 44(28): p. 9680-90.

41. Vedadi, M., J. Lew, J. Artz, M. Amani, Y. Zhao, A. Dong, G.A. Wasney, M. Gao, T. Hills, S. Brokx, W. Qiu, S. Sharma, A. Diassiti, Z. Alam, M. Melone, A. Mulichak, A. Wernimont, J. Bray, P. Loppnau, O. Plotnikova, K. Newberry, E. Sundararajan, S. Houston, J. Walker, W. Tempel, A. Bochkarev, I. Kozieradzki, A. Edwards, C. Arrowsmith, D. Roos, K. Kain, and R. Hui, Genome-scale protein expression and structural biology of Plasmodium falciparum and related Apicomplexan organisms. Molecular and biochemical parasitology, 2007. 151(1): p. 100-10.

42. Dawson, R.J. and K.P. Locher, Structure of the multidrug ABC transporter Sav1866 from Staphylococcus aureus in complex with AMP-PNP. FEBS letters, 2007. 581(5): p. 935-8.

43. Tsai, M.F., M. Li, and T.C. Hwang, Stable ATP binding mediated by a partial NBD dimer of the CFTR chloride channel. The Journal of general physiology, 2010. 135(5): p. 399-414.

44. Geertsma, E.R. and R. Dutzler, A versatile and efficient high-throughput cloning tool for structural biology. Biochemistry, 2011. 50(15): p. 3272-8.

45. Costa, S.J., A. Almeida, A. Castro, L. Domingues, and H. Besir, The novel Fh8 and H fusion partners for soluble protein expression in Escherichia coli: a comparison with the traditional gene fusion technology. Applied microbiology and biotechnology, 2012.

46. Brown, P.H. and P. Schuck, A new adaptive grid-size algorithm for the simulation of sedimentation velocity profiles in analytical ultracentrifugation. Computer physics communications, 2008. 178(2): p. 105-120.

47. Kabsch, W., Xds. Acta crystallographica. Section D, Biological crystallography, 2010. 66(Pt 2): p. 125-32.

48. Collaborative Computational Project, N., The CCP4 suite: programs for protein crystallography. Acta crystallographica. Section D, Biological crystallography, 1994. 50(Pt 5): p. 760-3.

49. McCoy, A.J., R.W. Grosse-Kunstleve, P.D. Adams, M.D. Winn, L.C. Storoni, and R.J. Read, Phaser crystallographic software. Journal of applied crystallography, 2007. 40(Pt 4): p. 658-674.

50. Emsley, P., B. Lohkamp, W.G. Scott, and K. Cowtan, Features and development of Coot. Acta crystallographica. Section D, Biological crystallography, 2010. 66(Pt 4): p. 486-501.

51. Adams, P.D., R.W. Grosse-Kunstleve, L.W. Hung, T.R. Ioerger, A.J. McCoy, N.W. Moriarty, R.J. Read, J.C. Sacchettini, N.K. Sauter, and T.C. Terwilliger, PHENIX: building new software for automated crystallographic structure determination. Acta crystallographica. Section D, Biological crystallography, 2002. 58(Pt 11): p. 1948-54.

Table 1. Data collection and refinement statistics.

	NBD287	**NBD288**
Data collection		
Beamline	X06SA	X06SA
Space group	$P6_522$	$P3_221$
Cell dimensions		
a, b, c (Å)	80.15, 80.15, 129.55	58.3, 58.3, 208.69
α, β, γ (°)	90, 90, 120	90, 90, 120
Resolution (Å)	47.35 -1.95	49.07-2.3
R_{meas} (%)	4.7 (67.3)	9.3 (96.7)
$I/\sigma I$	30.19 (4.35)	19.94 (3.31)
Completeness (%)	100 (100)	99.99 (100)
Refinement		
Resolution (Å)	1.95	2.3
Number of reflections	18606	19132
R_{work}/R_{free} (%)	23.71/25.76	19.13/23.89
No. of atoms		
Protein	1376	2053
Solvent	76	139
Average *B*-factors (Å^2)		
Protein	23.0	69.9
Solvent	19.9	70.1
R.M.S. deviations		
Bond lengths (Å)	0.008	0.009
Bond angles (°)	1.139	1.149
Ramachandran plot (%)		
Favoured	98.84	98.04
Allowed	1.16	1.96

Values in parenthesis correspond to the highest resolution shell.

Table 2. The NBD construct annotation

pBXNH3	10His-3C-NBD
pBXC3H	NBD-3C-10His
pBXC3GH	NBD-3C-GFP-10His
pBXNH3A	10His-3C-AviTag-NBD
pBXNH3CA	10His-3C-NBD-AviTag
pBXNAC3H	AviTag-NBD-3C-10His
pBXNAC3GH	AviTag-NBD-3C-GFP-10His
pBXCA3H	NBD-AviTag-3C-10His
pBXCA3GH	NBD-AviTag-3C-GFP-10His

Table 3. Analysis of the expression yield and oligomeric behavior of the various NBD constructs.

	NBD287		NBD288	
Vector	Yield	SEC peak	Yield	SEC peak
pBXNH3	++	monodisperse	++	shoulder
pBXC3H	++	n.d.	++	monodisperse
pBXC3GH	++	n.d.	+	monodisperse
pBXNH3A	+++	shoulder	+	n.d.
pBXNH3CA	-	n.d.	+	n.d.
pBXNAC3H	+	n.d.	+	n.d.
pBXNAC3GH	+++	monodisperse	++	n.d.
pBXCA3H	++	n.d.	+++	shoulder
pBXCA3GH	++	n.d.	++	monodisperse
pET11M-SUMO-FX	+++	monodisperse	+++	insoluble

Figure 1

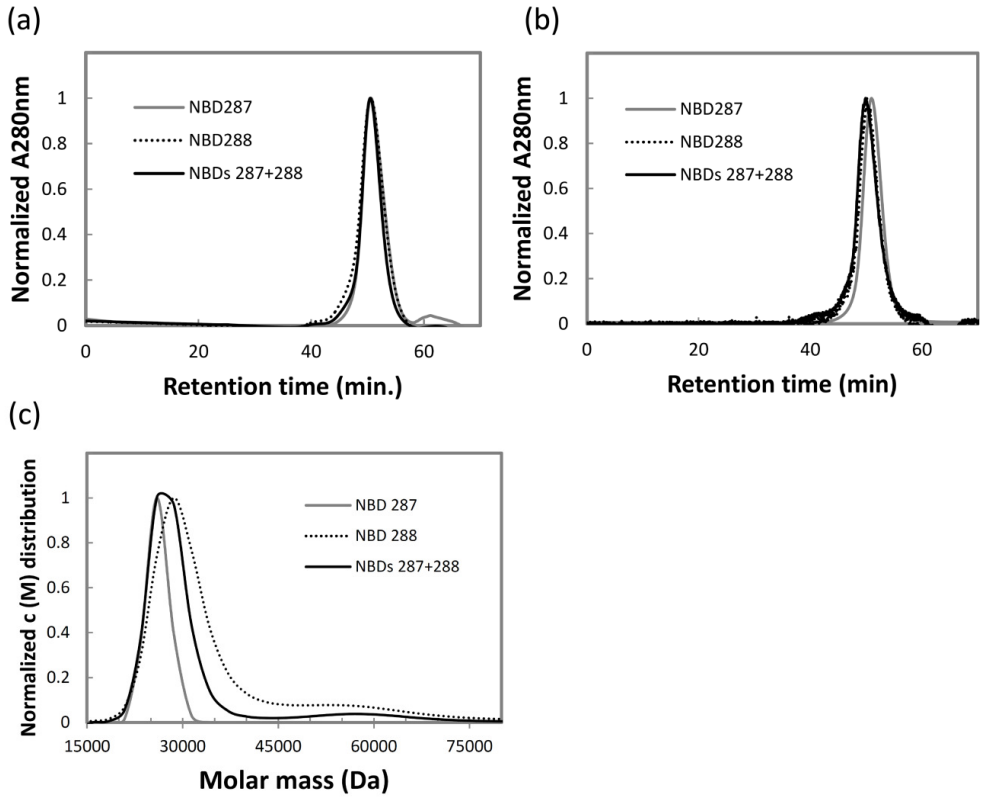

Figure 1 Oligomeric behavior of the NBDs and their mixture

(a) Analytical size exclusion chromatography of the NBDs in the absence of nucleotides. (b) Analytical size exclusion chromatography of the NBDs in the presence of MgATP. (c) Analytical ultracentrifugation of NBDs and their mixture in the presence of MgATP.

Figure 2

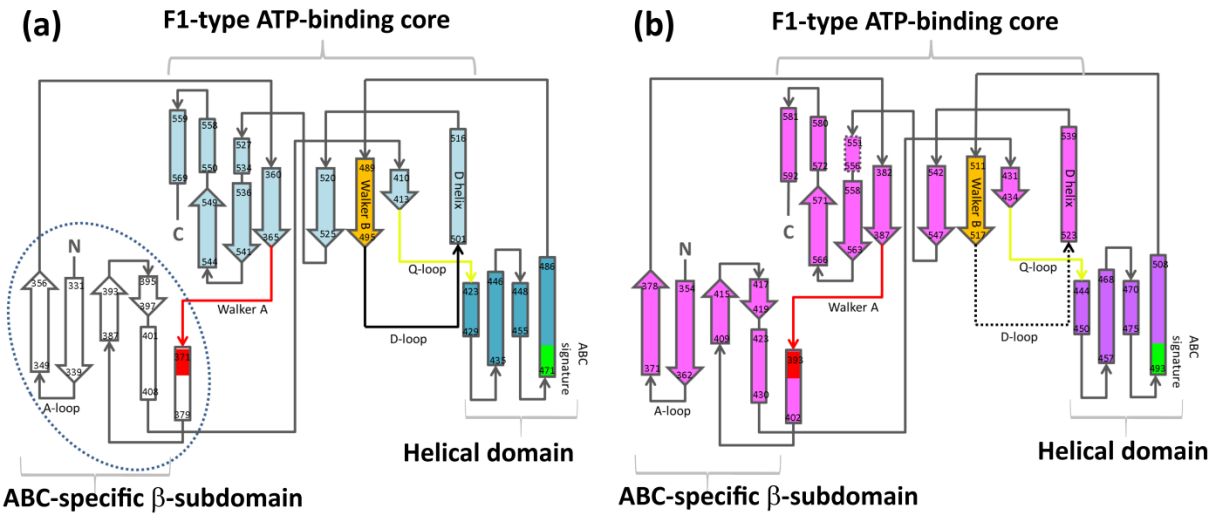

Figure 2 Topology schemes of the NBDs indicating subdomain organization and position of the conserved elements.

The Walker A is depicted in red, the Walker B - in orange, the ABC signature - in green, the Q-loop - in yellow. The dotted line indicates areas not resolved in the structures. (a) The NBD287 (b) The NBD288.

Figure 3

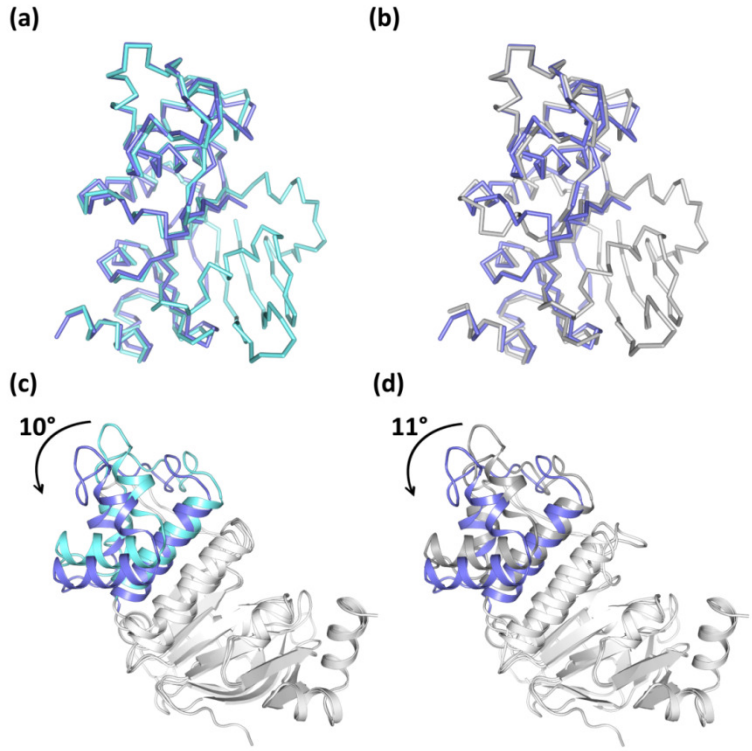

Figure 3 The NBD287 structure in isolation and in the context of the full-length.

Alignment of the C_α atoms of the isolated NBD287 with the NBD1 of nucleotide-bound TM287/288 (a), and with NBD1 of nucleotide-free TM287/288 (b). Rotation of the helical domain in the isolated NBD287 (slate blue) with respect to its position in NBD1 of nucleotide-bound TM287/288 (aquamarine) (c), and in NBD1 of nucleotide-free TM287/288 (light gray) (d).

Figure 4

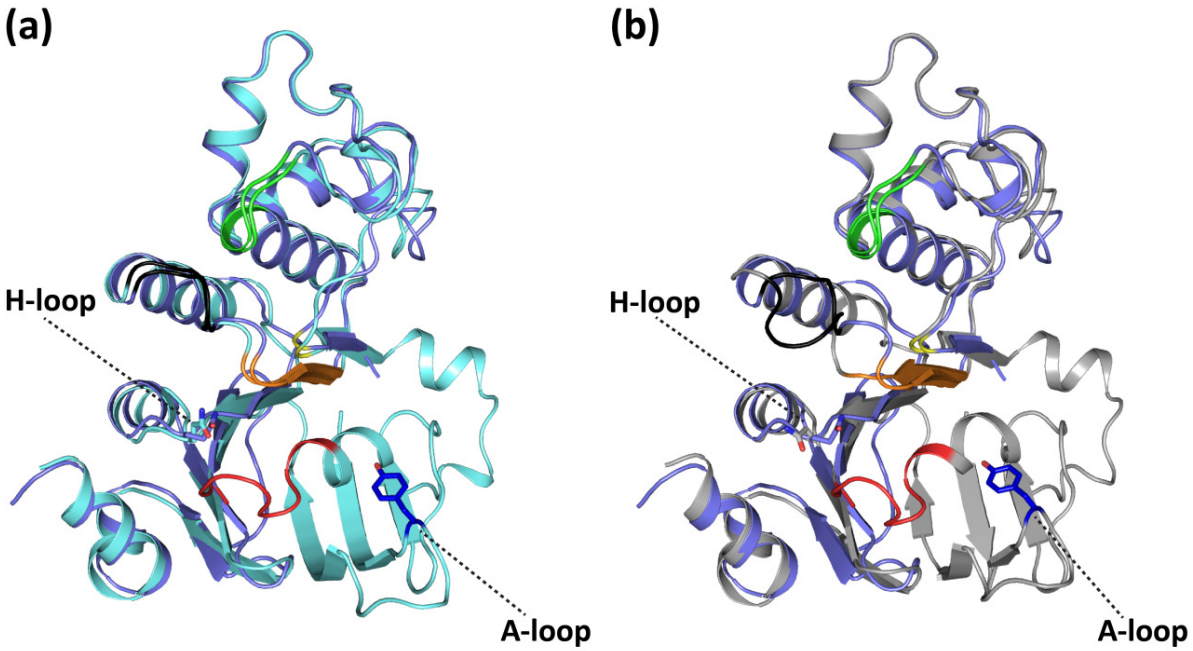

Figure 4 Location of the conserved motifs of the NBD287 in isolation and in the context of the full-length protein.

The isolated NBD287 (slate blue) was superimposed on the NBD287 from the nucleotide-bound full-length structure (aquamarine) (c) and on the NBD287 from the nucleotide-free full-length structure (light gray) (b). The conserved motifs were depicted as following: the Walker B - in orange, the Q-loop - in yellow, the D-loop - in black, the H-loop - in dark blue, the Walker A - in red. The tyrosine of the A-loop and the noncanonical glutamine of the H-loop are depicted as sticks.

Figure 5

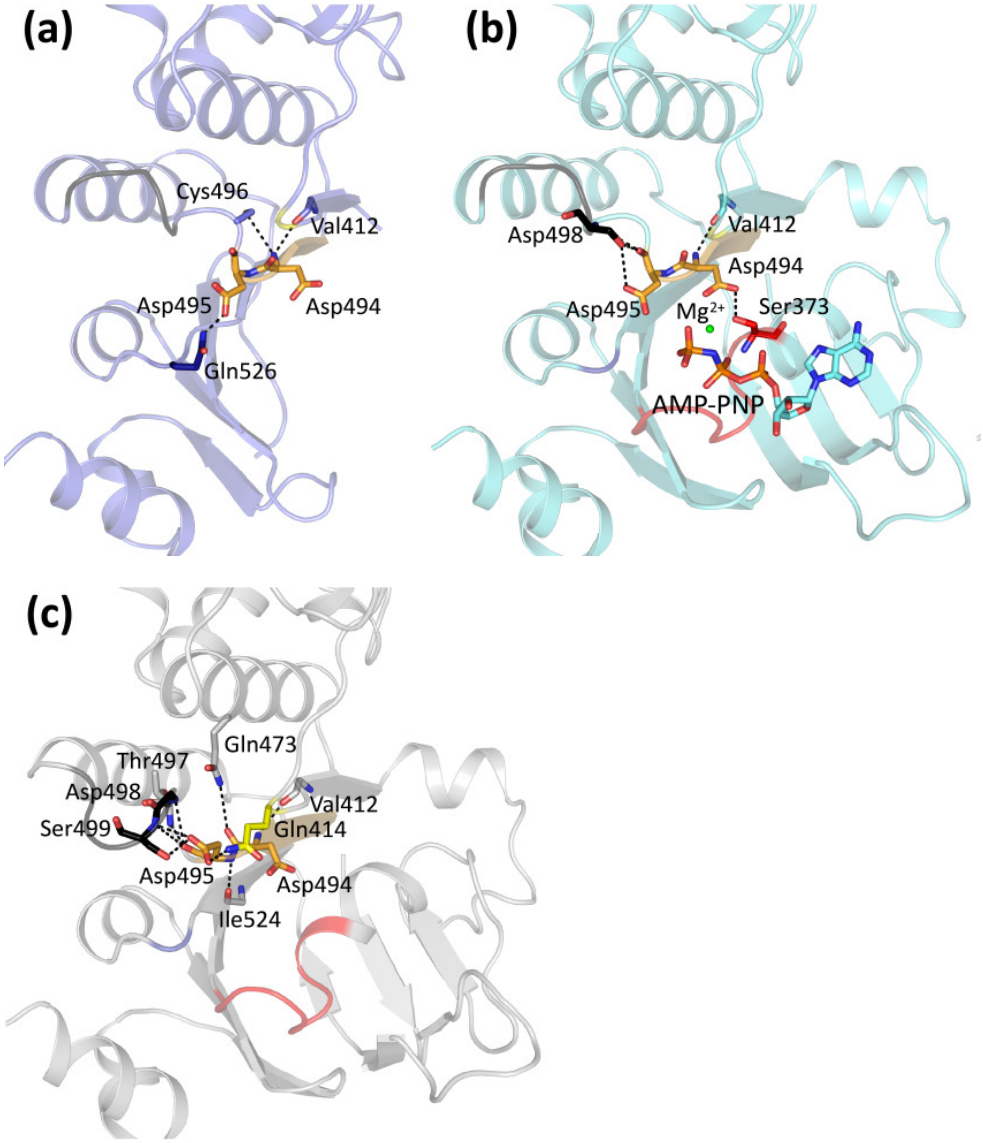

Figure 5 Catalytic site of the NBD287.

The catalytic site of: the isolated NBD287 (a), the nucleotide-bound NBD287 from the full-length TM287/288 structure (PDB code 3FQ4) and the nucleotide-free TM287/288 full-length structure (c). The conserved asparagine (Asp494) and non-canonical asparagine (Asp495) residues of the Walker B (orange) and residues within the hydrogen bonding distance to them are depicted as sticks. The residues which belong to the coserved motifs are colored according to the same coding as before. For orientation the protein context of the catalytic site is shown as cartoon and the conserved elements are colored as before. Additionally, in (b) the AMP-PNP molecule and magnesium ion are depicted as sticks and green sphere. Hydrogen bonds are depicted as black dashed lines.

Figure 6

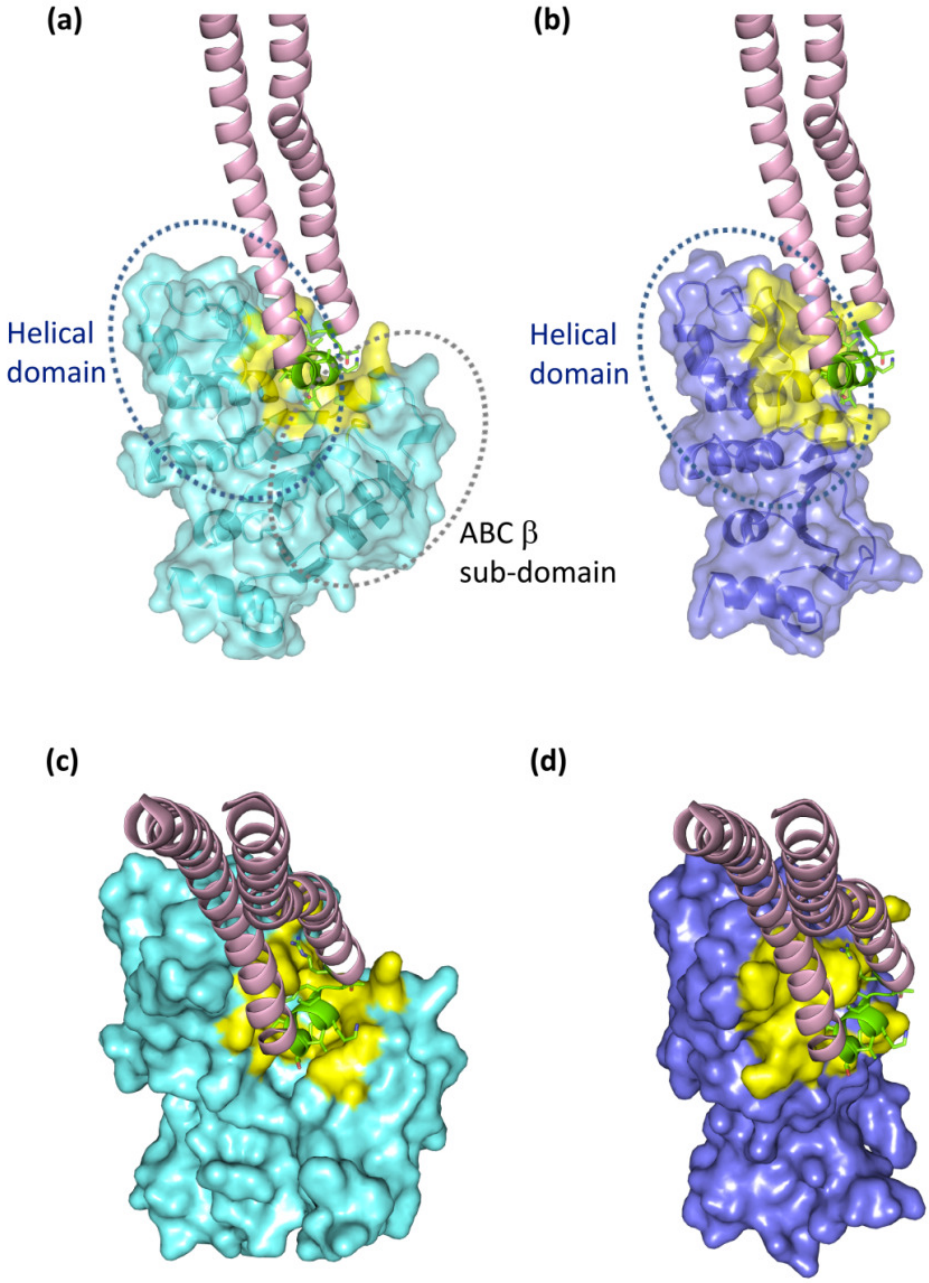

Figure 6 The ABCβ subdomain of NBD287 forms a binding groove for the coupling helix from TM288.

Side (a) and top (c) view on the intracellular loop 4 (ICL4) (light pink) containing the coupling helix (green). The coupling helix lies in the binding groove created between the helical (blue dashed line) and ABCβ subdomains (gray dashed line) of the NBD287 in the full-length TM287/288 structure. Side (b) and top (d) view on the ICL4 superimposed on the incomplete isolated NBD287 structure. The NBD287 residues in a close proximity to the coupling helix (within 5 Å) are colored in yellow.

Figure 7

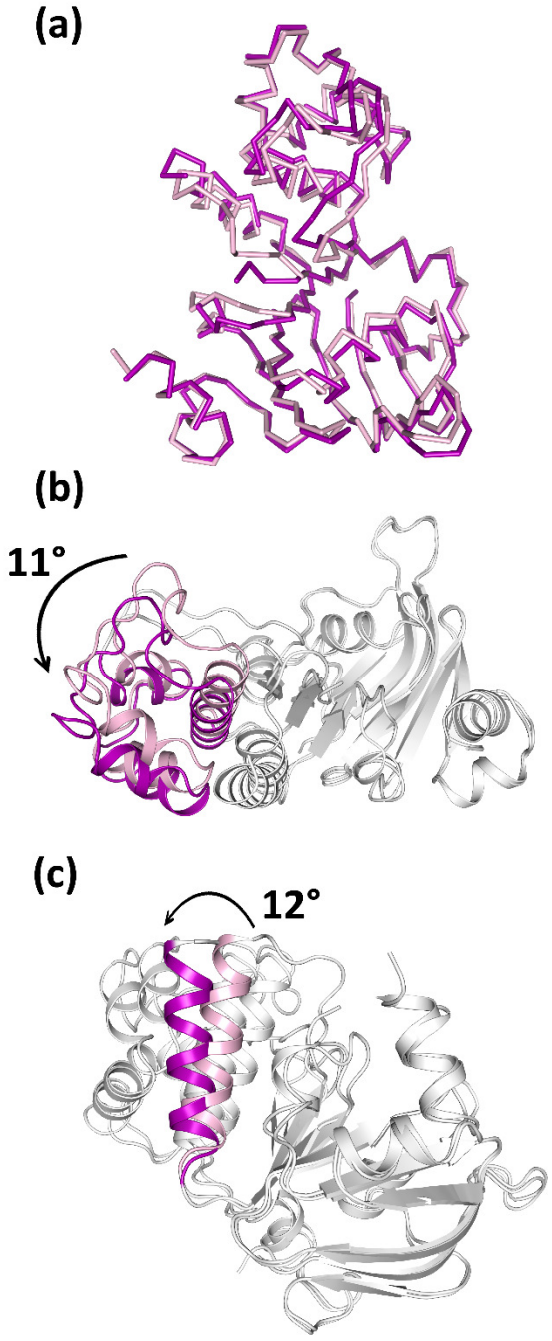

Figure 7 The NBD288 structure in isolation and in the context of the full-length.

The C_α atom alignment of the isolated NBD288 (purple) with the NBD2 of nucleotide-bound TM287/288 – light pink (a). Rotation of the helical domain in the isolated NBD288 (purple) with respect to its position in the NBD2 of the nucleotide-bound TM287/288 – light pink (b). The D-loop helix tilting in the isolated NBD288 structure (purple) in relation to its position in the NBD2 of nucleotide-bound TM287/288 – light pink (c).

Figure 8

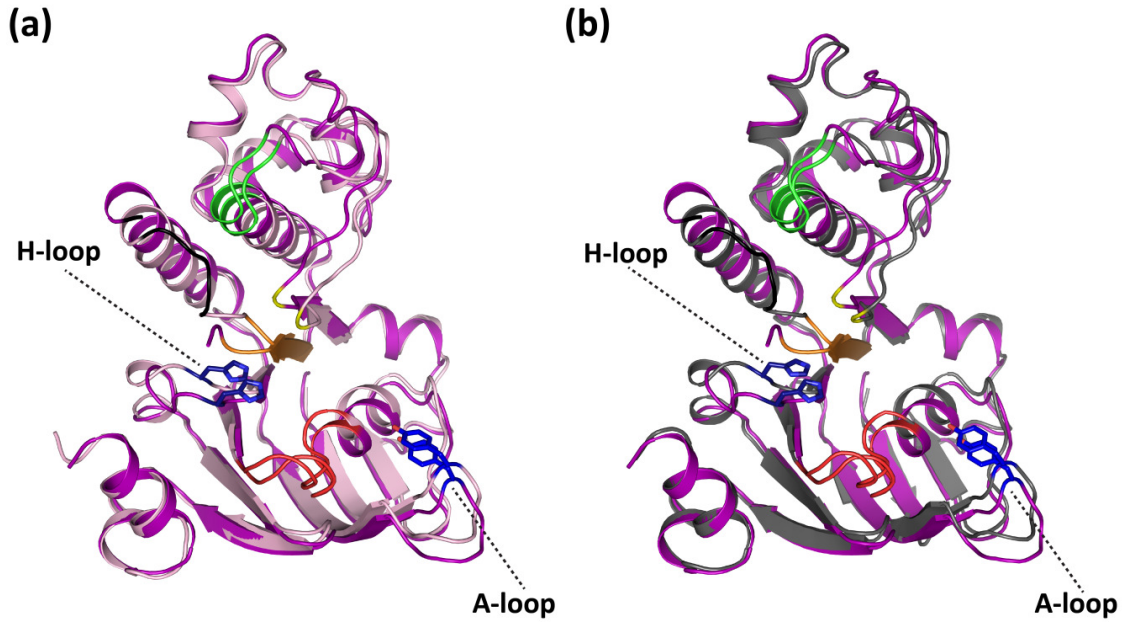

Figure 8 Location of the conserved motifs of the NBD288 in isolation and in the context of the full-length transporter.

The isolated NBD288 (purple) was superimposed on the NBD288 from the nucleotide-bound full-length structure (light pink) (c) and on the NBD288 from the nucleotide-free full-length structure (dark gray) (b). The conserved motifs were depicted as following: the Walker B - in orange, the Q-loop - in yellow, the D-loop - in black, the H-loop - in dark blue, the Walker A - in red. The tyrosine of the A-loop and the histidine of the H-loop are depicted as dark blue sticks.

Figure 9

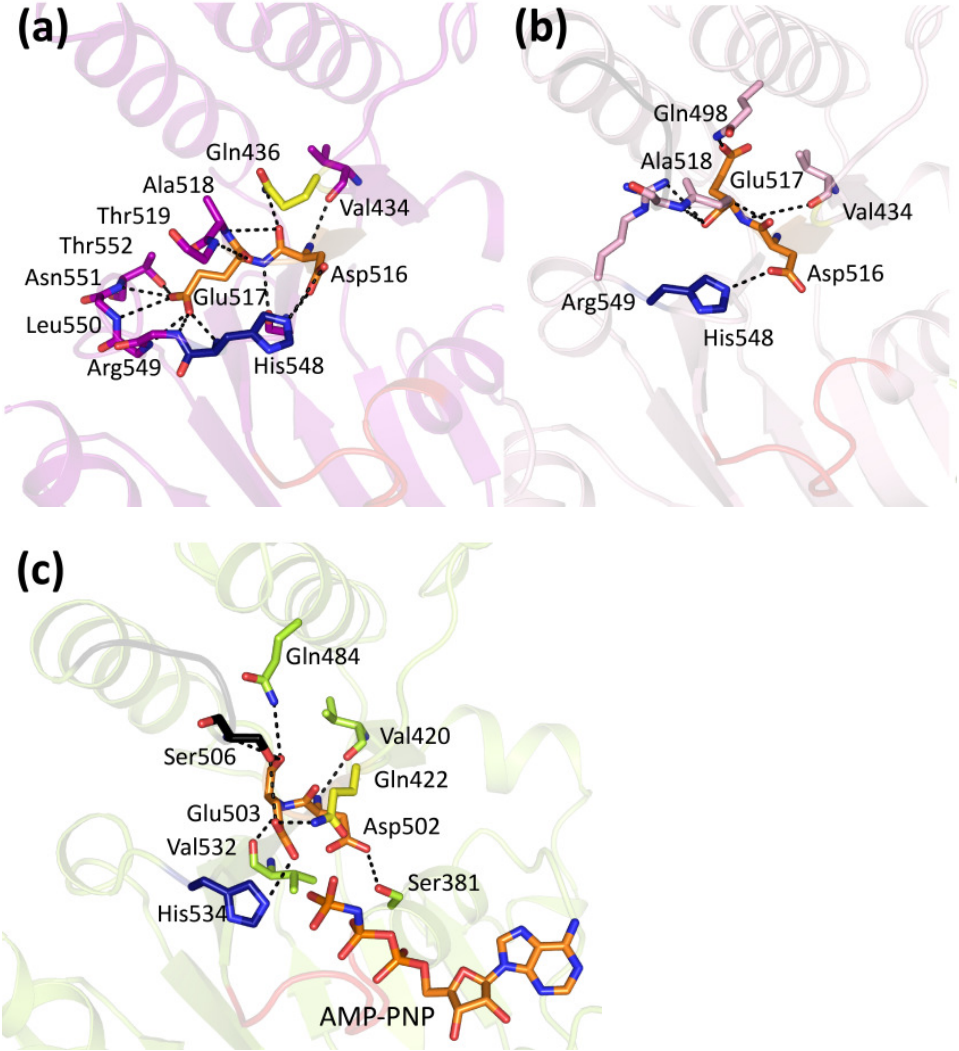

Figure 9 Catalytic site of the NBD2

The catalytic site of: the isolated NBD288 (a), the NBD288 from the full-length TM287/288 protein (PDB code 3FQ4) and the nucleotide-bound Sav1866 full-length structure (PDB code: 2ONJ) (c). The conserved asparagine (Asp516 in TM287/288 and Asp502 in Sav1866) and glutamine (Glu517 in TM287/288 and Glu503 in Sav1866) residues of the Walker B (orange) and residues within the hydrogen bonding distance to them are depicted as sticks. The residues which belong to the coserved motifs are colored according to the same coding as before. The histidine of the H-loop (His548 in TM287/288 and His534 in Sav1866) is depicted in dark blue. The glutamine of the Q loop (Gln436 in TM287/288 and Gln422 in Sav1866) is depicted in yellow. Additionaly in (c) the AMP-PNP molecule is depicted as sticks. For orientation the protein context of the catalytic site is shown as cartoon and the conserved elements are colored as before. Hydrogen bonds are depicted as black dashed lines.

Figure 10

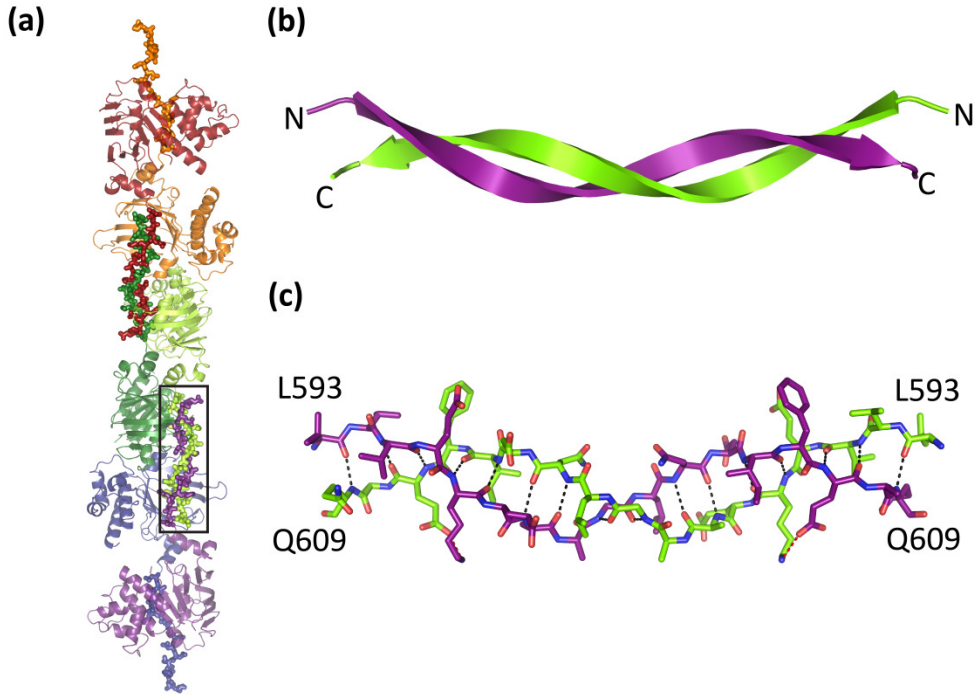

Figure 10 C-terminal avi-tag of the NBD288 mediates crystal contacts

(a) Fragment of the crystal lattice showing the filament-like organization of the NBD288 along the dimerized peptide linkers. Each symmetry-related NBD288 is depicted as cartoon in different color. The C-terminal tags are depicted as sticks and colored according to the color of the domain they come from. (b) cartoon representation of two C-terminal tags from symmetry-related NBD288s. (c) stick representation of two interacting C-terminal tags with polar interactions depicted with dashed lines.

Figure 11

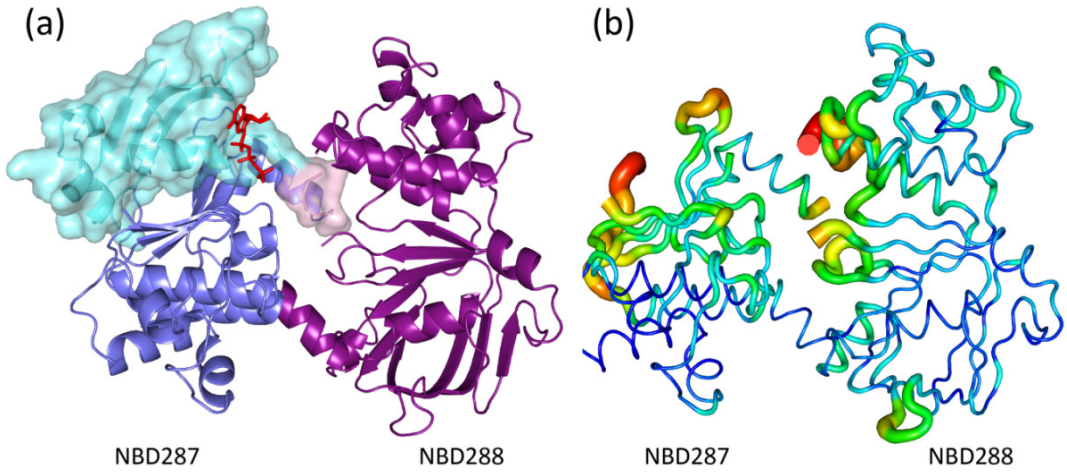

Figure 11 Flexibility of the degenerate ATPase site.

(a) The isolated NBDs were superimposed on the full-length TM287/288 structure using their helical sub-domains. The parts of the intact transporter corresponding to the missing elements of the isolated domains are depicted as surface. AMP-PNP molecule is depicted as red sticks. (b) The isolated domains in the worm-like representation are oriented as in (a) and colored according to the B factor. The worm thickness is proportional to the backbone B-factor.

Acknowledgement

I would like to thank different people who have helped me through the completion of this thesis. The first person to thank is Prof. Dr. Markus Grütter who gave me the opportunity to work on this very fascinating and challenging project after initially suggesting me some other, in my opinion, less attractive topics. In addition, I am very thankful that he allowed me to use such a broad set of methodologies.

I am very thankful to the Professors who kindly agreed to take part in my PhD committee: Prof. Dr. Raimund Dutzler and Prof. Dr. Ulrich Baumann (University of Cologne). In addition, I am very thankful to Raimund Dutzler for several interesting discussion and advices he gave me during the course of this thesis.

I am infinitely thankful to Dr. Markus Seeger, my supervisor. We had a very great and productive time together. We have sat out many long night or weekend shifts at the SLS of the Paul Scherrer Institute, we had good and inspiring discussions about possible transport mechanisms and about future projects sometimes with or without a stimulating cold beer in our hands. It was as well a pleasure to write all the manuscripts and the PhD thesis together with you. Thank you so much! I am looking forward working with you as a post-doc on the new fascinating project and in the “new” Institute.

I wish to thank Dr. Christophe Briand for the good collaboration on the project “Crystal structure of a heterodimeric ABC transporter in its inward-facing conformation” and the nice advises he gave me during data collection and data processing and for sharing boiled eggs with me at the SLS.

I am very thankful to other collaborators and colleagues: Magdalena Bukowska, Lea Hürlimann, Simon Böhm (ETH Zurich), Jendrik Schoeppe and Dr. Enrica Bordignon (ETH Zurich). It was nice working together with you! Magdalena for sharing the successful project “Sub-domain flexibility in the nucleotide binding cassettes of the heterodimeric ABC exporter TM287/288”. Lea for her commitment during her Master’s thesis and the collaboration on the project “Interdomain communication between nucleotide binding sites of ABC transporters is promoted via the D-loops”. Simon, Jendrik and Enrica in addition contributed substantially to the success of the project entitled “Interdomain communication between nucleotide binding sites of ABC transporters is promoted via the D-loops”.

I would like to thank Prof. Ben Schuler and Dr. Andrea Soranno for their interest and help in measuring FRET with our transporters. It was very interesting to have some insight into this nice technique.

I am very grateful to Céline Stutz-Ducommun and Beat Blattmann from the NCCR crystallization facility. They do a fantastic job and always were so patient with me even though they often had to fulfill special wishes.

I thank Dr. Anshumali Mittal for his advice and the helpful discussions at the beginning of my PhD and the nice time we spent together on other occasions, especially when eating some nice Indian meals, like Palak Paneer or Aloo Gobi. I wish you all the best for you post-doc in Salt Lake City.

I would like to thank all the former and current members of the Grütter lab that provided a very nice working and discussion atmosphere. These are Christopher, Damien, Georg, Andi, Heidi, Peter, Sara, Reto, Thilo, Franziska, Frank Thomas, Sibylle, Nicole, Mareike, Jana, Martin, Peer, Chaithanya, Florence and Tobi. Reto and Heidi I would like to thank in addition for introducing me to the Ribosome display technology.

I wish to thank Salome Rittmeyer who kept the “stable” running and always had an open ear for my problems and needs.

Furthermore, I would like to acknowledge everybody of the Biochemistry Institute Staff, from the workshop Sascha and Adrian, from the IT Steve and Stefan. In addition, Sibylle, Regula and Simone, responsible for logistics and administration.

A big thank as well to all the members of the other research groups, especially the people from the Dutzler and the Plückthun lab, former and present members. Thanks to Iwan, Janine, Carlo, Stephan, Eric, Yvonne, Sibylle, Novandy, Adrian, Juan… and to Peter, Birgit, Ykelien, Mane, Niki, Anja, Christian, Alexander, Dirk, Sven, Andrea, Pascal, Matthias, Lutz, Christian, Karola, Mark, Marco, Mareike, Gabriela, Stefanie…

I spent a great time sitting as an “intruder” in the J-floor. It was a nice atmosphere working in the lab next to all the nice immunology people from the lab of Christian Münz and Burkhard Becher. Especially, I would like to mention Miguel, Kathrin, Johannes, Heike, Christian, Anne, Isaak, Christina, Patrick, Kristina, Ana, Felix, Sara, Sabine, Patrick, Stas, Carol, Olga, Vanessa, Bettina and many others I have not listed here.

A big thanks goes as well to all my nice friends from Zurich and Solothurn. I am sorry for all the lab stories and explanations about my projects I was bothering you with.

A very special thank goes to Eva, mi tesoro. I am very happy to have you at my side. Besos y abrazos.

Last but not least I would like to thank my parents Erwin and Rosmarie and my brother Daniel for their constant support during my studies as well as for the support during my PhD. Without you it would not have been possible. You are the best parents one could imagine. Happy 60th anniversary again to my father.

Curriculum Vitae

Name	**Michael Hohl**
Date of birth	March 4th, 1980
Place of birth	Krefeld, Germany
Nationality	Swiss

Education

2009-now	**University of Zurich, Switzerland** PhD program in Biomolecular Structure and Mechanism of the Life Science Zurich Graduate School
Currently	PhD Thesis: **"Structural and Functional Investigations of Prokaryotic Heterodimeric ABC Exporters".** Supervision by Dr. Markus Seeger (Group Prof. Dr. Markus Grütter)
2006-2008	**University of Zurich, Switzerland** Master of Science (M.Sc.) studies in Biochemistry (Biophysics track)
September 2008	M.Sc. Thesis: **"Designed Ankyrin Repeat Protein-RNase 1 fusion".** Supervision by Dr. Birgit Dreier (Group Prof. Dr. Andreas Plückthun)
2002-2006	**University of Zurich, Switzerland** Bachelor of Science (B.Sc.) studies in Biochemistry (Biophysics track)
July 2006	B.Sc. Thesis: **"Heading for Fluorescent Phages: Site-directed Mutagenesis of Three Auto Fluorescent Proteins (AFPs)".** Supervision by Dr. Peter Lindner (Group Prof. Dr. Andreas Plückthun)
2001	**Federal Institute of Technology (ETH) Zurich, Switzerland** "Biologie chemische Richtung"
1996-2001	**Kantonsschule Solothurn, Switzerland** Profile: "Wirtschaft und Recht (Typus E)"
February 2001	Matura Typus E

Publications

Subdomain flexibility in the nucleotide binding domains of the heterodimeric ABC exporter TM287/288

Magdalena A. Bukowska*, **Michael Hohl***, Markus A. Seeger, and Markus G. Grütter

Manuscript in preparation

* Equal contribution

Interdomain communication between nucleotide binding sites of ABC transporters is promoted via the D-loops

Michael Hohl, Markus G. Grütter, and Markus A. Seeger

Manuscript in preparation

X-Ray Structure of a Heterodimeric ABC Transporter Crystallized in its Inward-Facing Conformation

Michael Hohl, Markus G. Grütter, and Markus A. Seeger

Chimia (Aarau). 2012 October; 66(10):802

Tuning the drug efflux activity of an ABC transporter in vivo by in vitro selected DARPin binders

Seeger A Markus, Anshumali Mittal, Saroj Velamakanni, **Michael Hohl**, Ihsene Salaa, Markus G Grütter, and Hendrik W van Veen

PLoS One 2012 June 4; 7(6)

Crystal structure of a heterodimeric ABC transporter in its inward-facing conformation

Michael Hohl, Christophe Briand, Markus G. Grütter and Markus A. Seeger

Nat. Struct. Mol. Biol. 2012 March 25; 19(4):395-402.

Binding of 9-Methylguanine to [cis-Ru(2,2'-bpy)2]2+: First X-ray Structure of a cis-Bis Purine Complex of Ruthenium

Fabio Zobi, **Michael Hohl***, Iwan Zimmermann*, and Roger Alberto

Inorg. Chem. 2004 May 3; 43(9):2771-2.

* Equal contribution

Conferences and PhD Retreats

August 29-30, 2012	10th NCCR Symposium on Trends in Structural Biology ETH Zurich, Zurich, Switzerland Poster presentation
August 17-19, 2012	5th Annual Retreat of the PhD program in Biomolecular Structure and Mechanism of the Life Science Zurich Graduate School Swiss Youth and Education Center, Einsiedeln, Switzerland Poster presentation
July 1-6, 2012	Gordon Research Conference on Membrane Transport Proteins Les Diablerets Conference Center, Les Diablerets, Switzerland Poster presentation
September 1-2, 2011	9th International NCCR Symposium on New Trends in Structural Biology University of Zurich, Zurich, Switzerland Poster presentation
July 1-2, 2011	4th Annual Retreat of the PhD program in Biomolecular Structure and Mechanism of the Life Science Zurich Graduate School Lungern, Switzerland Oral presentation: Crystal structure of a heterodimeric ATP binding cassette (ABC) transporter in its inward-facing conformation
June 19-24, 2011	Gordon Research Conference on Mechanisms of Membrane Transport University of New England, Biddeford ME, USA Poster presentation
September 2-3, 2010	8th International NCCR Symposium on New Trend in Structural Biology ETH Zurich, Zurich, Switzerland Poster presentation
August 13-15, 2010	3rd Annual Retreat of the PhD program in Biomolecular Structure and Mechanism (BSM) of the Life Science Zurich Graduate School Aarbergerhus, Ligerz, Switzerland Poster presentation
September 7-8, 2009	7th International NCCR Symposium on New Trends in Structural Biology ETH Zurich, Zurich, Switzerland